National Library of Canada
Bibliothèque nationale du Canada

Canadian Theses Service
Service des thèses canadiennes

Ottawa, Canada
K1A 0N4

NOTICE

The quality of this microform is heavily dependent upon the quality of the original thesis submitted for microfilming. Every effort has been made to ensure the highest quality of reproduction possible.

If pages are missing, contact the university which granted the degree.

Some pages may have indistinct print especially if the original pages were typed with a poor typewriter ribbon or if the university sent us an inferior photocopy.

Reproduction in full or in part of this microform is governed by the Canadian Copyright Act, R.S.C. 1970, c. C-30, and subsequent amendments.

AVIS

La qualité de cette microforme dépend grandement de la qualité de la thèse soumise au microfilmage. Nous avons tout fait pour assurer une qualité supérieure de reproduction.

S'il manque des pages, veuillez communiquer avec l'université qui a conféré le grade.

La qualité d'impression de certaines pages peut laisser à désirer, surtout si les pages originales ont été dactylographiées à l'aide d'un ruban usé ou si l'université nous a fait parvenir une photocopie de qualité inférieure.

La reproduction, même partielle, de cette microforme est soumise à la Loi canadienne sur le droit d'auteur, SRC 1970, c. C-30, et ses amendements subséquents.

NL-339 (r. 88/04) c

Canada

UNIVERSITY OF ALBERTA

PRESSURE TRANSIENT BEHAVIOUR FOR A WELL IN A MULTI-LAYERED COMPOSITE RESERVOIR WITH AN INCLINED FRONT

BY

© IRUNGU KIOME

A THESIS

SUBMITTED TO THE FACULTY OF GRADUATE STUDIES AND RESEARCH IN PARTIAL FULFILLMENT OF THE REQUIREMENTS FOR THE DEGREE OF

MASTER OF SCIENCE

IN

PETROLEUM ENGINEERING

DEPARTMENT OF MINING, METALLURGICAL AND PETROLEUM ENGINEERING

EDMONTON, ALBERTA

FALL, 1991

National Library of Canada
Bibliothèque nationale du Canada

Canadian Theses Service
Service des thèses canadiennes

Ottawa, Canada
K1A 0N4

The author has granted an irrevocable non-exclusive licence allowing the National Library of Canada to reproduce, loan, distribute or sell copies of his/her thesis by any means and in any form or format, making this thesis available to interested persons.

L'auteur a accordé une licence irrévocable et non exclusive permettant à la Bibliothèque nationale du Canada de reproduire, prêter, distribuer ou vendre des copies de sa thèse de quelque manière et sous quelque forme que ce soit pour mettre des exemplaires de cette thèse à la disposition des personnes intéressées.

The author retains ownership of the copyright in his/her thesis. Neither the thesis nor substantial extracts from it may be printed or otherwise reproduced without his/her permission.

L'auteur conserve la propriété du droit d'auteur qui protège sa thèse. Ni la thèse ni des extraits substantiels de celle-ci ne doivent être imprimés ou autrement reproduits sans son autorisation.

ISBN 0-315-70164-1

Canada

UNIVERSITY OF ALBERTA

RELEASE FORM

NAME OF AUTHOR	Irungu Kiome
TITLE OF THESIS	Pressure Transient Behaviour for a Well in a multi-layered Composite Reservoir With an Inclined Front
DEGREE FOR WHICH THESIS WAS PRESENTED:	MASTER OF SCIENCE
YEAR THE DEGREE WAS GRANTED	FALL, 1991

Permission is hereby granted to the UNIVERSITY OF ALBERTA LIBRARY to reproduce single copies of this thesis and to lend or sell such copies for private, scholarly or scientific research purposes only.

The author reserves other publication rights, and neither the thesis nor extensive extracts from it may be printed or otherwise reproduced without the author's written permission.

(SIGNED) Kiūmū Wa Maina

PERMANENT ADDRESS:
P.O. BOX 236
MUKURWE-INI, KENYA

DATED: July 31, 1991

THE UNIVERSITY OF ALBERTA

FACULTY OF GRADUATE STUDIES AND RESEARCH

The undersigned certify that they have read, and recommend to the Faculty of Graduate Studies and Research for acceptance, a thesis entitled "PRESSURE TRANSIENT BEHAVIOUR FOR A WELL IN A MULTI-LAYERED COMPOSITE RESERVOIR WITH AN INCLINED FRONT" submitted by IRUNGU KIOME in partial fulfillment of the requirements for the degree of MASTER OF SCIENCE in PETROLEUM ENGINEERING.

A.K. Ambastha (Supervisor)

J. M. Whiting

R.G. Bentsen

K. Nandakumar

DATED: MARCH 28 , 1991

DEDICATION

Dedicated to Gikuyu na Mumbi, Maitu na Awa na mbari ya Maina, Matemo Waciuri, Wathiiha wa Maina, Dr. Yossef A. A. ben Jochannan, Dr. Cheikh Anta Diop, Marcus Garvey, Enjeri Kihooto, na nduka ciothe cia andu airu.

THAI, THATHAIYA NGAI, THAAI.

ABSTRACT

During an enhanced oil recovery project, e.g. steam or CO_2 flooding, a circular region surrounding the injection well develops wherein fluid and/or rock properties are different from those of the unaltered (or unswept) outer region of the reservoir. These two regions have different hydraulic diffusivities. This type of reservoir is called a composite reservoir.

Single-layer composite reservoir models have been used successfully to analyze well-tests from various recovery projects, including geothermal reservoirs. Such models have a sharp (90°) front at the discontinuity. However, gravity or fingering effects may cause a front to be tilted, or change the shape of the front associated with the swept volume. A multilayered composite reservoir model has been used to study the effects of a tilted front on well-test analysis. This is achieved by assigning an appropriate value of front radius to each layer of the model to obtain a step approximation of the desired front shape such that the volumes of the swept region in both the multilayer and the tilted front models are the same.

This study considers the effects of front angle on dimensionless pressure derivative responses for drawdown and buildup tests. An analytical solution for a multilayered composite reservoir is employed to generate transient pressure responses. Limitations of the sharp front (90°) models to properly analyze recovery projects with extreme override (10°) have been presented. The validity of using a sharp front model to analyze well-test data from a reservoir with a tilted front configuration is also studied. Producing (or injection) time must be long enough to properly analyze well test data from composite

reservoirs having a tilted front. If individual layer properties (e.g. permeabilities and skin factors) are different, the pressure transient responses may be different also. Effects of complex front shapes on pressure transient responses are also considered.

ACKNOWLEDGEMENTS

Sincere gratitude is due to Professor A.K. Ambastha for his guidance and support throughout this study. The author feels he has gained invaluable advice and patience from Professor Ambastha, without whom this study would not have been as rewarding. The encouragement of Mr. A. M'Imanyara (Ministry of Energy, Nairobi, Kenya) to pursue this field of study is greatly apppreciated. Financial support for this work and my graduate studies was provided by the Government of Kenya through the Canadian International Development Agency (C.I.D.A) and a grant from CRF-NSERC, administered through the University of Alberta. I am indebted to my wife, Erima (Nyina wa Wambura), and Insaka Alkebu-lan, for their support during my studies.

TABLE OF CONTENTS

Page

ABSTRACT v

ACKNOWLEDGEMENTS vii

TABLE OF CONTENTS viii

LIST OF TABLES x

LIST OF FIGURES xi

NOMENCLATURE xvi

1. INTRODUCTION 1

2. LITERATURE REVIEW 3

3. PROBLEM STATEMENT 14

4. MATHEMATICAL MODEL FOR A MULTI-LAYERED COMPOSITE RESERVOIR 15

   4.1 Mathematical Development 16

   4.2 Model Validation 26

5. RESULTS AND DISCUSSION 34

   5.1 Calculation of Front Radii Values for the Model 36

   5.2 Drawdown Response 39

   5.2.1 Effect of Number of Layers 40

   5.2.2 Correlating Parameter 44

   5.2.3 Effect of Front Angle 48

   5.2.4 Effect of Mobility and Storativity Ratios 53

   5.2.5 Determination of Front Radius 58

   5.2.6 Validity of using an Average Radius 60

5.2.7 Pseudosteady State Analysis 62
5.2.8 Sensitivity Studies 74
5.2.9 Wellbore Storage Effects 80
5.2.10 Effects of Complex Front Shapes 83
5.3 Buildup Response 93
6. CONCLUSIONS AND RECOMMENDATIONS 109
6.1 Conclusions 109
6.2 Recommendations 110
REFERENCES 111
APPENDIX A: Computer programs 116
APPENDIX B: Sample input data for the computer program 129
Front Radii for Reservoirs with 2,3,6, and 10 Layers 130

LIST OF TABLES

Page

Table 4.1: Example input data for the computer program (Appendix A1).....27

Table 4.2: Values of parameters for Figure 4.6 33

Table 5.1: Front radii for a five-layer reservoir for different front angles.....39

Table 5.2: Mobility increasing from 'top to bottom'.....75

Table 5.3: Mobility increasing from 'bottom to top'.....75

Table 5.4: 'Random pattern' mobility among the layers.....76

Table 5.5: Front Radii for Cases A, B, C and D.....86

Table B1: Sample Input values for the Computer Program ($\theta = 60°$, F = 100).....129

Table B2: Sample Input values for the Computer Program ($\theta = 30°$, F = 1000).....129

Table B3: Front radii for a two-layer model for various front angles 130

Table B4: Front radii for a three-layer model for various front angles.....130

Table B5: Front radii for a six-layer model for various front angles 131

Table B6: Front radii for a ten-layer model for various angles.....132

LIST OF FIGURES

Page

Figure 4.1: Dimensionless pressure response for a 1-layer homogeneous reservoir....29

Figure 4.2: Dimensionless pressure response for a 3-layer homogeneous reservoir....29

Figure 4.3: Dimensionless pressure response for a 2-layer heterogeneous reservoir....30

Figure 4.4: Pressure derivative response for a single-layer composite reservoir. 30

Figure 4.5: Pressure transient response for a two-layer composite reservoir.....32

Figure 4.6: Drawdown pressure derivative type-curve....32

Figure 5.1: Schematic diagram of a two-region multilayer composite reservoir..35

Figure 5.2: Schematic diagram of a reservoir with a tilted front....36

Figure 5.3: A schematic of a front-view of a reservoir with a tilted front.....37

Figure 5.4: Effect of number of layers on pressure derivative (front angle = 10°)....41

Figure 5.5: Effect of number of layers on pressure derivative (front angle = 30°)....41

Figure 5.6: Effect of number of layers on pressure derivative (front angle = 45°)....42

Figure 5.7: Effect of number of layers on pressure derivative (front angle = 60°)....42

Figure 5.8: Effect of number of layers on pressure derivative (R_{Dmin} = 2000)....43

Figure 5.9: Effect of minimum front radius on pressure derivative (front angle = 10°)....45

Figure 5.10: Effect of minimum front radius on pressure derivative (front angle = 30°)....45

Figure 5.11: Effect of minimum front radius on pressure derivative (front angle = 45°)....46

Figure 5.12: Effect of minimum front radius on pressure derivative (front angle = 60°) 46

Figure 5.13: Effect of minimum front radius on pressure derivative (front angle = 90°) 47

Figure 5.14: Effect of front angle on pressure derivative (M = 10, F = 100) 49

Figure 5.15: Effect of front angle on pressure derivative (M = 1000, F = 100) 49

Figure 5.16: Effect of front angle on pressure derivative (M = 10, F = 1000) 50

Figure 5.17: Effect of layering and front angle on pressure derivative (M = 1000) 51

Figure 5.18: Effect of layering and front angle on pressure derivative (M = 100) 51

Figure 5.19: Effect of layering and front angle on pressure derivative (M = 10) 52

Figure 5.20: Effect of mobility ratio on pressure derivative (front angle = 10°) 54

Figure 5.21: Effect of mobility ratio on pressure derivative (front angle = 30°) 54

Figure 5.22: Effect of mobility ratio on pressure derivative (front angle = 45°, 60°, and 90°) 55

Figure 5.23: Effect of storativity ratio on pressure derivative (front angle = 10°) 56

Figure 5.24: Effect of storativity ratio on pressure derivative (front angle = 30°) 56

Figure 5.25: Effect of storativity ratio on pressure derivative (front angle = 45°, 60° and 90°°) 57

Figure 5.26: Validity of using R_{Davg} for tilted front (front angle = 10°) 63

Figure 5.27: Validity of using R_{Davg} for tilted front (front angle = 30°) 63

Figure 5.28: Validity of using R_{Davg} for tilted front (front angle = 60°) 64

Figure 5.29: Validity of using R_{Davg} for tilted front (R_{Dmin} = 2000, front angle = 10°) 64

Figure 5.30: Effect of number of layers on Cartesian derivative (front angle = 60°) 65

Figure 5.31: Effect of minimum front radius on Cartesian derivative (front angle = 10°) 67

Figure 5.32: Effect of minimum front radius on Cartesian derivative (front angle = 20°) 67

Figure 5.33: Effect of minimum front radius on Cartesian derivative (front angle = 30°) 68

Figure 5.34: Effect of minimum front radius on Cartesian derivative (front angle = 45°) 68

Figure 5.35: Effect of minimum front radius on Cartesian derivative (front angle = 60°) 69

Figure 5.36: Effect of mobility ratio on Cartesian derivative 70

Figure 5.37: Effect of storativity ratio on Cartesian derivative 70

Figure 5.38: Effect of front angle on Cartesian derivative (front angle = 10°) 72

Figure 5.39: Effect of front angle on Cartesian derivative (front angle = 20°) 72

Figure 5.40: Effect of front angle on Cartesian derivative (front angle = 30° and 90°) 73

Figure 5.41: Effect of different patterns of layer mobilities on pressure derivative (front angle = 10°) 77

Figure 5.42: Effect of different patterns of layer mobilities on pressure derivative (front angle = 60°) 77

Figure 5.43: Effect of skin factors on pressure derivative 79

Figure 5.44: C_De^{2s} as a correlation parameter 81

Figure 5.45: Effect of C_De^{2s} on pressure derivative (front angle = 60°) 82

Figure 5.46: Effect of C_De^{2s} on pressure derivative (front angle = 45°) 82

Figure 5.47: A schematic diagram for case A of Table 5.5 84

Figure 5.48: A schematic diagram for case B of Table 5.5 84

Figure 5.49: A schematic diagram for case C of Table 5.5 85

Figure 5.50: A schematic diagram for case D of Table 5.5 85

Figure 5.51: Effect of a steam chest on pressure derivative 87

Figure 5.52: Effect of a steam chest on Cartesian derivative 87

Figure 5.53: A schematic diagram for cases E and F 89

Figure 5.54: A schematic diagram for case G 89

Figure 5.55: Effect of front shapes on Cartesian derivative 90

Figure 5.56: Effect of front angle on pressure derivative (front angles = 10° and 170°) 90

Figure 5.57: Effect of storativity variation on Cartesian derivative 91

Figure 5.58: Effect of number of layers on Agarwal slope 95

Figure 5.59: Effect of minimum front radius on MDH slope 96

Figure 5.60: Effect of minimum front radius on Agarwal slope (front angle = 10°) 96

Figure 5.61: Effect of minimum front radius on Agarwal slope (front angle = 30°) 98

Figure 5.62: Effect of minimum front radius on Agarwal slope (front angle = 60°) 98

Figure 5.63: Effect of minimum front radius on Agarwal slope (front angle = 90°) 99

Figure 5.64: Effect of front angle on Agarwal slope (10°, 20°, 30°, 45°, 60° and 90°) 100

Figure 5.65: Effect of front angle on Agarwal slope (10°, 20° and 30°) 100

Figure 5.66: Effect of front angle on Agarwal slope (45°, 60° and 90°) 101

Figure 5.67: Effect of front angle on Agarwal slope ($t_{pD}/R^2_{Dmin} = 10^4$) 102

Figure 5.68: Effect of t_{pD} on Agarwal slope ($t_{pD}/R^2_{Dmin} \geq 1.0$) 104

Figure 5.69: Effect of mobility ratio on Agarwal slope ($t_{pD}/R^2_{Dmin} = 0.1$) 104

Figure 5.70: Effect of mobility ratio on Agarwal slope ($t_{pD}/R^2_{Dmin} = 100$) 105

Figure 5.71: Effect of mobility ratio on Agarwal slope ($t_{pD}/R^2_{Dmin} = 10^4$ and drawdown response) 105

Figure 5.72: Effect of storativity ratio on Agarwal slope ($t_{pD}/R^2_{Dmin} = 0.1$) 107

Figure 5.73: Effect of front angle on Agarwal slope ($t_{pD}/R^2_{Dmin} = 100$) 107

Figure 5.74: Effect of storativity ratio on Agarwal slope ($t_{pD}/R^2_{Dmin} = 10^4$) 108

NOMENCLATURE

A	=	Area, πR^2
A_j	=	Arbitrary constant
B	=	Formation volume factor
B_j	=	Arbitrary constant
C	=	Wellbore storage coefficient, m^3 / Pa
c_t	=	Total system compressibility, Pa^{-1}
C_A	=	Shape factor
C_j	=	Arbitrary constant
D_j	=	Arbitrary constant
F	=	Storativity ratio
h	=	Formation thickness, m
I_0	=	Modified Bessel function of first kind of order zero
I_1	=	Modified Bessel function of first kind of order one
K_0	=	Modified Bessel function of second kind of order zero
K_1	=	Modified Bessel function of second kind of order one
k	=	Permeability, m^2
l	=	Laplace variable
M	=	Mobility ratio
m_c	=	Slope of Cartesian straight line, Pa/s
n	=	Total number of layers
p	=	Pressure, Pa
$\bar{p}_{wD}$	=	Dimensionless wellbore pressure in Laplace space
q	=	Flow rate , m^3 / s
r	=	Radius, m

R	=	Discontinuity radius (or Front radius)
$\overline{R}$	=	Average discontinuity radius
s	=	Skin effect at the wellbore
$\bar{s}$	=	Average skin factor
t	=	Time, sec
t_{DA}	=	Dimensionless time based on area, A
t_{De}	=	Dimensionless time based on R
t_{Dpss}	=	Time to the onset of pseudosteady state
$(t_{De})_{end}$	=	Dimensionless deviation time
$(t_{De})_{II}$	=	Dimensionless time of the start of the second semi-log line
$(t_{De})_{max}$	=	Dimensionless time for maximum semi-log slope
t_{end}	=	Deviation time, hrs
V_s	=	Swept volume

GREEK SYMBOLS

α	=	Coefficients in Eqs. 4.39 through 4.42
∂	=	Partial
δ	=	Expression given by Eq. 4.63 or 4.68
Δp_{skin}	=	Pressure drop across skin, Pa
Δt	=	Shut-in time, sec.
η	=	Diffusivity ratio,
γ	=	Expression given by Eq. 4.65
λ	=	Relative mobility
μ	=	Viscosity, Pa.s
ω	=	Relative storativity

ϕ	=	Porosity, fraction
θ	=	Front angle, degrees

SUBSCRIPTS

avg	=	Average
D	=	Dimensionless
e	=	Exterior or Equivalent
eff	=	Effective
f	=	Flowing
h	=	Horizontal
i	=	Initial
j	=	Layer number
m	=	Region number
max	=	Maximum
min	=	Minimum
p	=	Producing (or injection)
pss	=	Pseudosteady state
r	=	Ratio
s	=	Swept or shut-in
t	=	Total
v	=	Vertical
w	=	Wellbore
1	=	Inner Region
2	=	Outer Region

1. INTRODUCTION

A two-region composite reservoir may occur naturally or may be artificially created. Each region is characterised by its distinct fluid and/or rock properties. The radial distance to the discontinuity is referred to as the front (or discontinuity) radius. The discontinuity may be due to the presence of a phase change, drastic temperature variation or significant permeability change of the reservoir rock. Also, enhanced oil recovery (EOR) projects create conditions within the reservoir that can be modeled as a two-region composite system. The inner region contains the injected fluid and is surrounded by the unaltered (or unswept) region of the reservoir. The progress of CO_2 flooding and in-situ combustion projects has been analyzed successfully using the composite reservoir model. Temperature differences in non-isothermal reservoirs may show well-test characteristics similar to those of reservoirs having a high mobility contrast at the discontinuity.

The important parameter sought in well-test studies of reservoirs having a composite system configuration is the front radius (or swept volume). Knowledge of the swept volume is necessary to evaluate the effectiveness of a recovery project. In the case of a steam flood, gravity override effects may contribute to the development of a tilted front. It is more realistic to refer to a swept volume than to a front radius in such EOR projects. Some researchers have studied the effects of a tilted front on well-test analysis by using a multi-layered composite reservoir model. By assigning a different front radius to each layer, various front shapes may be modeled.

This study further investigates the effects of an inclined front on dimensionless pressure derivative responses. A single well in an infinitely-large reservoir producing at a constant rate is considered. Section 2 presents a literature survey. The problem statement is presented in Section 3. A mathematical model for a multi-layered composite reservoir is developed in Section 4. Section 5 presents drawdown and buildup responses for reservoirs with various front shapes and front angle values. Limitations of applying the design equations of a single-layer composite model to analyze data for reservoirs with an inclined front are also discussed. Finally, Section 6 presents conclusions and recommendations for further studies.

2. LITERATURE REVIEW

2.1 Drawdown

"Often, the first significant transient event at a production well is the initial production period that results in pressure drawdown at the formation face. It is thus logical to learn about the well and reservoir from pressure drawdown data."[1] The three flow regimes from a drawdown test are: infinite-acting, transition, and pseudosteady state, all of which may be analyzed for reservoir information[2]. This section reviews research in drawdown analysis by different authors. The scope of reservoir configurations considered is limited to the multilayered reservoir with or without crossflow; and the composite reservoir, single or multilayered, without crossflow.

2.1.1 Multilayered Reservoirs

A number of investigators have studied the behaviour of a well producing from two or more layers. The layering may be caused by the existence of shale barriers separating the different strata of an oil reservoir. In the case of an impermeable shale, the layers communicate only at the wellbore. A reservoir in which there is no vertical flow of fluid from one layer to another within the reservoir is referred to as a "commingled" system. If interlayer communication of fluid occurs, the reservoir is called a "layered system with crossflow". In a reservoir "without crossflow", the vertical permeability across layer bounderies is zero. A study of the behaviour of commingled reservoirs by Lefkovits *et al.*[3] considered an arbitrary number of layers, each with distinct properties, including thickness, permeability, skin and porosity. In their analytical model, they presented both

pressure and layer flowrate transient responses for analyzing bounded reservoir characteristics.

Tempelaar-Lietz[4] studied the pressure behaviour of a constant rate, two-layered, bounded reservoir. Javandel and Witherspoon[5] studied infinite and bounded multi-layered reservoirs with and without crossflow, for both constant-pressure and constant rate cases, by applying the finite-element technique. Russell and Prats[6] used a two-layer reservoir without crossflow for a constant-rate production. Woods[7] also studied a two-layer commingled reservoir using a line-source solution, for the constant-pressure outer boundary and infinite reservoir cases. Cobb *et al.*[8] similarly studied a multi-layered reservoir with no crossflow, by using an analytical model which utilized the Laplace transform. They incorporated the presence of skin at the wellbore for a no-flow outer boundary and a constant rate production at the well. Earlougher *et al.*[9] examined the general characteristics of the pressure-response curve in a multilayer reservoir. Reference 9 concluded that under certain conditions, multi-layered systems will behave like a single-layer reservoir. Most of the analyses in Refs. 3 through 9 consider a two-layer system without skin at the wellbore. Initial pressure at the sandface is assumed equal for both layers. A constant production rate of a fluid with a small but constant compressibility is also assumed. However, Refs. 3, 8 and 9 study the effects of multiple layers. An "effective-wellbore-radius" may incorporate the skin factor by the following relation:

$$r_{wa} = r_w e^{-s}. \tag{2.1}$$

A summary of the significant results of Refs. 3 through 9 as presented in Ref. 10 follows:

1. For a constant production rate, a multilayered reservoir has a pressure drawdown response curve that is similar to that of a single-layer reservoir. There are three flow

regimes: infinite-acting, transition and pseudosteady state. The thickness-averaged flow capacity of the reservoir can be determined from the early-transient flow data.

2. The major difference between the multilayer and single-layer systems is that the late-transient period for a multilayer system is much longer than that of a single-layer system.[3,8,11]
3. Conventional semi-log methods[12-14] may be used to calculate the thickness-averaged flow capacity of the formation.
4. Average reservoir pressure can be calculated using the Matthews-Brons-Hazebroek[15] (MBH) functions.[8,10] An "average" skin factor of the reservoir may also be determined.
5. The rate of production from each individual layer will be different, but the total production rate is constant.[3]

During the late transient period, the production rate from each layer changes from that of the early transient period, except when the diffusivity ratio, $\eta_r = (\eta_1 / \eta_2)$, is unity. The changing production rate accounts for the long late-transition period. This phenomenon is known as differential depletion.[10]

For the commingled system, the model development was extended by Tariq and Ramey[16] who studied the behaviour of multilayered reservoirs including the presence of skin and wellbore storage. Reference 16 developed an analytical solution of the transient pressure behaviour using the Laplace transform. An algorithm proposed by Stehfest[17] was used to invert the solution into real space. This algorithm has since been used in numerous well test studies, including this work. The major findings by Tariq and Ramey[16] were as follows:

1. For high permeability contrast among the layers, and a thin highly permeable layer, false wellbore storage effects may appear.
2. For a two-layered reservoir with different values of r_e for each layer, two semi-log straight lines may appear. The first slope corresponds to the permeability-thickness of the whole system and the second slope corresponds to the permeability-thickness of the larger radius layer.
3. The duration of the late transient period is a function of permeability ratio, skin, and pore volume ratio, and is much longer for multi-layered reservoirs compared to a single-layer reservoir.
4. Any layered reservoir can be analyzed as a single-layer reservoir if appropriate average properties, $\bar{k}$, $\bar{h}$, $\bar{\phi}$, $\bar{\mu}$, and $\bar{A}$, are substituted for k, h, ϕ, μ, and A.[9]
5. During the early transition period, effects of the number of layers and thicknesses of the layers are negligible. These parameters affect the pseudosteady-state and late-transient periods only.
6. Variation in skin among layers can be approximated by an average skin factor, $\bar{s}$, defined as:

$$\bar{s} = \frac{\sum_{j=1}^{n} s_j k_j h_j}{\sum_{j=1}^{n} k_j h_j} \qquad (2.2)$$

Other investigators[10,18-20] have also shown that reservoir parameters for multilayered reservoirs, with or without crossflow, usually cannot be estimated uniquely from the conventional drawdown or buildup tests using only wellbore pressure data. Larsen[18] and Kucuk *et al.*[19] show that layer permeabilities and skin factors can be estimated uniquely from simultaneously measured wellbore pressure and flow rate data. Flowrate

data may be obtained directly by actual measurements from each layer[19], or by analytical methods.[10,18,20] References 9,16 and 18 propose analytical methods to determine estimates of individual layer properties by using wellbore pressure and total flowrate data. The presence of skin in multilayer reservoirs may affect the appearance of conventional semi-log straight lines.[18] An analytical solution for the general problem of n-homogenous layers, with or without crossflow, including wellbore storage, skin, and other properties has been developed.[20] References 10, 18 and 20 demonstrate that the combination of wellbore pressure and layer flowrates provides sufficient information for determination of the complete layered reservoir description. The interpretation procedures presented in Ref. 20 provide a means for solution of the inverse problem that consists of determining layer permeabilities from pressure and layer flowrate transients resulting from a change in the surface flowrate. Methods to predict future performance in stratified (or layered) reservoirs have also been documented, including a summary of the characteristics of such wells.[10]

2.1.2 Composite Reservoirs

A two-region composite reservoir consists of a circular zone surrounding the well in which the fluid and/or rock properties are similar, but are different from properties in the concentric region outside this inner zone. The inner zone is called the "altered" or swept region, and the outer region is referred to as the unaltered or unswept zone (or region). When two or more layers form the reservoir, each layer will have both zones. The radial distance to the discontinuity in each layer is referred to as the "front radius", and may be different for each layer, in the case of a "tilted front", or it may be equal for each layer, in which case the front is considered "sharp". The existence of this altered zone may be due to enhanced oil recovery methods, for example, or it may occur naturally. The

multilayered composite reservoir model, therefore, lends itself to the study of many possible configurations which reservoirs can have.

An early work in the area of composite systems was presented by Kazemi.[21] In his model, he considered the effect of temperature on the thermodynamic properties of reservoir fluids. Kazemi[21] introduced the use of pressure falloff data to approximate the location of a burning front in an in-situ combustion process. Eggenschwiler *et al.*[22] used the composite system model to represent the burned region adjacent to the injection well in an in-situ combustion project. Reference 22 used an analytical solution to obtain an expression in Laplace space for the pressure transient response at a well. A numerical inversion procedure developed by Stehfest[17] was used to obtain dimensionless pressures at the wellbore at any dimensionless time. An examination of the pressure transient data indicates:[22]

1. A short duration wellbore storage effect, which dies in a few minutes.
2. A semi-log straight line develops, whose slope is related to the mobility of the swept volume.
3. A pseudosteady-state (PSS) follows, which is characteristic of the swept volume.
4. A second semi-log straight line characteristic of the unswept region mobility follows.

The major finding was the occurrence of PSS behaviour due to the existence of mobility contrast in the model. Da Prat *et al.*[23] validated the use of the model developed by Eggenschwiler *et al.*[22] for a one-layer composite reservoir in finding the distance to the burning front. The duration required to observe the second semi-log line is quite long.[23] A Cartesian plot used to estimate the volume of the swept region was found to be reliable.[23] Satman *et al.*[24] and Tang[25] showed that a plot of $p_{wD} - \ln(R_D/500)$ vs t_{De} applies for all values of a sharp front radius, R_D, where:

$$t_{De} = \frac{(k/\mu)_1 \; t}{(\phi c_t)_1 \, R^2} = \frac{t_D}{R_D^2} \qquad (2.3)$$

and where $(k/\mu)_1$ and $(\phi c_t)_1$ are properties of the swept region. Their analyses did not include wellbore storage or skin.

Brown[26] investigated the behaviour of pressure derivative curves for composite reservoirs, and presented equations for calculating front radius and skin using well test data. By using mobility and storativity ratios in the range of 0.4 to 2.0 and 0.3 to 30, respectively, he found that the storativity ratio only affects the timing and shape of the transition region between the two semi-log straight lines. The mobility ratio also affects the shape of the transition zone, and the presence of wellbore storage makes accurate analysis of the composite reservoir difficult.[26]

Satman[27] presented an analytical study of interference in a composite reservoir and considered skin and wellbore storage at the active well. Olarewaju and Lee[28] developed a one-layer composite reservoir model to analyze wells with high negative skin. They used both dimensionless pressure and pressure derivative to obtain fracture length or average front radius for three field examples. A type-curve analysis of composite reservoir pressure data requires several type-curves because of the number of parameters involved.[28] The combined effects of wellbore storage and phase redistribution on pressure behaviour in composite reservoirs was studied by Olarewaju and Lee.[29] Phase redistribution causes a "hump" in the early pressure data. Not recognizing phase redistribution at the well can result in misinterpretation of pressure data.[29]

To study the effects of a tilted front, various investigators[30,31,32] extended the single-layer composite model to a multilayer composite system. Front radii in the layers

may be located at different positions away from the well. The resulting front shape can be used to model many forms of discontinuities that occur in reservoirs. Where the front radii are different in each layer, the deviation time method provides an estimate of the distance to the nearest discontinuity from the wellbore. This is possible when a high mobility contrast exists between the inner and outer regions.[30] The pore volume of the swept (inner) region can be calculated. It is independent of the shape of the front.[30] An average front radius is used to obtain the pore volume. This can be calculated by:

$$\bar{R} = \frac{R_1 + R_2}{2} \tag{2.4}$$

for a two-layer reservoir.[30] In the presence of unequal skin among the layers, the first semi-log straight line does not have the correct slope. The skin obscures this semi-log line.[30] Anbarci *et al.*[31] presented a pressure transient interpretation method for multilayer composite reservoirs with or without crossflow. A graphical method to determine front location in layers by use of pressure transient analysis is proposed.[31] Hatzignatiou *et al.*[32] developed analytical solutions for studying the interference pressure behaviour in a multilayered composite reservoir model. Their model examines the effects of wellbore storage, skin, mobility and diffusivity ratios, permeability ratio and interlayer crossflow on pressure response at the active well. The interference tests could be used to determine reservoir characteristics.[32] Satman and Oskay[33] studied the effects of a tilted front on well test analysis by using a multilayered composite reservoir. A step approximation consisting of different values of front radius for each layer was used to model analytically a tilted front. Both buildup and drawdown responses for a well in an infinite reservoir were considered. An important finding of the Satman and Oskay[33] study was that curve-matching procedures should be preferred in analyzing projects with gravity segregation or a tilted front.

2.2 Buildup

The pressure buildup (or falloff) test has been studied and applied by many investigators. For a multilayered system, the time to the onset of pseudosteady state, t_{Dpss}, is longer for systems with no crossflow (commingled) than for an equivalent system with crossflow. For a two-layered system, t_{Dpss} is influenced significantly by the ratio of permeabilities of the two layers. Buildup test results can be used to estimate the permeability ratio between layers. By studying the effects of layer thickness using a two-layer reservoir model, Raghavan *et al.*[11] found that the dimensionless deviation time on a graph of p_{wD} versus log t_D, is a function of layer thickness ratio. For multilayer buildup curves, the semi-log straight line ends at about the same time that it would if the layer with the smallest value of $\phi\mu c_t / k$ acted alone. The preceding observations are valid for tests on a single well located in the centre of a circular, closed, two-layer system with constant and equal layer porosity. Other factors influencing the time to the onset of pseudosteady state are:[8]

1. Well location in reservoir
2. Shape of drainage area
3. Existence of commingled zones.

As noted previously, wellbore storage may affect the shape of the first semi-log straight line on a graph of p_{wD} versus log t_D. In a buildup test of a single-layer composite reservoir, effects of wellbore storage that may obscure the appearance of this line may be minimized by two-rate falloff testing.[34] The first semi-log straight line represents the total kh of the formation. Wellbore damage or improvement (skin factor) will also affect the appearance of the first semi-log straight line. By studying the effects of various

the appearance of the first semi-log straight line. By studying the effects of various parameters on many multilayer reservoir configurations, Earlougher *et al.*[9] showed that there is no general description for pressure buildup behaviour in layered reservoirs.

Kazemi [21] studied the effects of temperature on the thermodynamic properties of reservoir fluids by using a numerical simulator to generate falloff responses. He concluded that for a composite system, kh and front radius, R_D, of the swept zone can be estimated by proper analysis of the conventional pressure-falloff test data. If the burning front is not circular, the calculated value is between the minimum and maximum front radii.[21] During the early time of a buildup test, a graph of p_{wD} versus log t_D is linear for a composite system. The onset of non-linearity is related to the proximity of the reservoir boundaries[35] or mobility contrast.[22] The presence of zones of different temperature in non-isothermal reservoirs may resemble permeability boundaries during well testing.[36] A phase boundary at a constant radial distance from the well may be recognized also by a shift in the buildup semi-log straight line. A Cartesian graph of pressure versus buildup time may be used to estimate the distance to the phase boundary.[29,37] Not recognizing phase redistribution in the buildup test data, or the composite reservoir behaviour, may result in incorrect reservoir property estimates. Olarewaju and Lee[29] use an automatic history matching technique and the composite reservoir model to analyze buildup and falloff tests. During steam injection, heat loss to the surrounding formation causes steam condensation. An analytical study by Stanislav *et al.* [38] showed that results from falloff testing may underestimate the swept pore volume if steam condensation effects are not included.

Application of the composite reservoir model to analyze combustion falloff tests has been successfully carried out.[23,38,39] Da Prat *et al.* [23] verified the use of pseudosteady state

analysis to locate the burning front in the Miga Field, Eastern Venezuela. Onyekonwu *et al*.[39] provided falloff results obtained from combustion tests that showed good agreement between calculated and actual swept volume. However, the swept volume was found to include both the burned volume and also the high gas saturation zone ahead of the combustion front. Graphs were presented that can be used to make corrections that relate the swept volume to the burned volume.[39] A value of kh obtained from a combustion falloff test reflects the effective gas permeability-thickness at the average gas saturation behind the steam front.[40]

Severe reservoir heterogeneities can prevent establishment of pseudosteady state. Messner and Williams [41] observed this in falloff studies of multilayered reservoirs using a simulator in which certain blocks in each layer had the horizontal permeability, k_h, being much less than the vertical permeability, k_v. Automated type-curve matching can be used to estimate the swept-zone radius for a composite system, with low mobility contrast or with production-rate change.[42]

Satman [30] performed an analytical study of a three-layer composite system with different front radii in each layer (tilted front) and observed that a Cartesian straight line does not exist for low injection times. Earlougher *et al*.[9] also noticed that for low injection times, PSS does not occur for multilayered systems without crossflow. An insufficient stabilized flow period prior to a buildup test might result in well test data that appear like boundary effects on a pressure derivative curve, and cause misleading interpretation. Hence, it is necessary that the flow period prior to shut-in be much longer than buildup test duration for a reliable result in the composite model type-curve analysis.[28,43]

3. PROBLEM STATEMENT

The composite reservoir model has been applied successfully in well-test analyses of various reservoir configurations. A multi-layered composite reservoir model has also been used to simulate transient pressure response from reservoirs having different front shapes. However, a complete range of possible front shapes that may occur from EOR projects has not been studied. Thus, the objectives of this study are:

1. To develop an analytical solution for a multilayered composite reservoir without crossflow.
2. To analyze the effects of a tilted front, as may result due to gravity override in a steam-flood project, on dimensionless pressure derivative curves.
3. To investigate the effect of complex front shapes on Cartesian derivative responses of drawdown tests.

4. MATHEMATICAL MODEL FOR A MULTI-LAYERED COMPOSITE RESERVOIR

The mathematical model described in the following is similar to the one proposed by Satman[30]. The model includes wellbore storage and wellbore skin. The skin value may be different for different layers. The model describes a commingled, multi-layered composite system. The usual ideal conditions are assumed. These are:[30] (1) pressure gradients are small everywhere, so that the diffusivity equation in terms of pressure describes flow within each zone of layers, (2) gravity and capillary effects in each layer are negligible, and flow is radial and laminar, (3) the liquid has a small but constant compressibility, (4) there is no crossflow between the layers, (5) each layer is horizontal and of constant thickness, (6) the initial reservoir pressure is the same in each layer, (7) the well injects or produces at a constant rate, (8) mobility and storativity are constant within each zone of a layer but are different for the two regions (swept and unswept regions), (9) the front is considered stationary during the testing period. In the following, the subscripts j and m denote the layer number and region number, respectively. The model presented considers n layers and two regions. A significant difference between this analytical model and that of Satman[30] is that this study presents the pressure transient solution in a dimensionless form.

4.1 Mathematical Development

Fluid flow in Region 1 is described by the following partial differential equation:

$$\frac{k_{j1}}{\mu_{j1}}\left[\frac{\partial^2 p_{j1}}{\partial r^2}+\frac{1}{r}\frac{\partial p_{j1}}{\partial r}\right]=\left(\phi c_t\right)_{j1}\frac{\partial p_{j1}}{\partial t}$$

$$\text{for } j=1,\ldots \text{n and } r_w \le r \le R_j \tag{4.1}$$

The relevant partial differential equation for Region 2 is:

$$\frac{k_{j2}}{\mu_{j2}}\left[\frac{\partial^2 p_{j2}}{\partial r^2}+\frac{1}{r}\frac{\partial p_{j2}}{\partial r}\right]=\left(\phi c_t\right)_{j2}\frac{\partial p_{j2}}{\partial t}$$

$$\text{for } j=1,\ldots \text{n and } R_j \le r \le r_{ej} \ (or\ \infty) \tag{4.2}$$

In Eqs. 4.1 and 4.2, p_{jm} is the pressure in layer j and Region m. All other variables are defined in the nomenclature.

Appropriate initial and boundary conditions are:

Initial condition

$$p_{j1}(r,0)=p_{j2}(r,0)=p_i \text{ for } j=1,\ldots \text{n} \tag{4.3}$$

Inner boundary condition

$$p_{wf}(t) = p_{j1}(r_w, t) - s_j \left(r \frac{\partial p_{j1}}{\partial r} \right)\Bigg|_{r_w} \tag{4.4}$$

$$q = -C \frac{dp_{wf}}{dt} + 2\pi \sum_{j=1}^{n} \left(\frac{k}{\mu} \right)_{j1} h_j \left(r \frac{\partial p_{j1}}{\partial r} \right)\Bigg|_{r_w} \tag{4.5}$$

Outer boundary condition

$$\text{Infinite:} \quad p_{j2}(r \rightarrow \infty, t) = p_i \tag{4.6}$$

$$\text{Closed:} \quad \frac{\partial p_{j2}}{\partial r}\Bigg|_{r = r_{ej}} = 0 \tag{4.7}$$

$$\text{Constant-pressure:} \quad p_{j2}(r_{ej}, t) = p_i \tag{4.8}$$

Eqs. 4.4, and 4.6 through 4.8 apply for $j = 1, \ldots n$

Interface conditions

$$p_{j1}(R_j, t) = p_{j2}(R_j, t) \quad \text{for } j = 1, \ldots n \tag{4.9}$$

$$\left(\frac{k}{\mu} \right)_{j1} h_j \frac{\partial p_{j1}}{\partial r}\Bigg|_{r = R_j} = \left(\frac{k}{\mu} \right)_{j2} h_j \frac{\partial p_{j2}}{\partial r}\Bigg|_{r = R_j} \quad \text{for } j = 1, \ldots n \tag{4.10}$$

The problem may be presented in a dimensionless form using a set of dimensionless variables:

$$p_{Djm} = \frac{2\pi\left(\frac{k}{\mu}\right)_1 h\,(p_i - p_{jm})}{q}$$

for $j = 1, \ldots .n$ and $m = 1, 2$ (4.11)

$$t_D = \frac{\left(\frac{k}{\mu}\right)_1 t}{\left(\phi c_t\right)_1 r_w^2} \tag{4.12}$$

$$r_D = \frac{r}{r_w} \tag{4.13}$$

$$R_{Dj} = \frac{R_j}{r_w} \tag{4.14}$$

$$r_{eDj} = \frac{r_{ej}}{r_w} \tag{4.15}$$

$$p_{wD} = \frac{2\pi\left(\frac{k}{\mu}\right)_1 h\,(p_i - p_{wf})}{q} \tag{4.16}$$

$$s_j = \frac{2\pi\left(\frac{k}{\mu}\right)_1 h\left(\Delta p_{\text{skin}}\right)_j}{q} \tag{4.17}$$

$$C_D = \frac{C}{2\pi\left(\phi c_t\right)_1 h\, r_w^2} \tag{4.18}$$

$$\lambda_{j1} = \frac{\left(\frac{k}{\mu}\right)_{j1} h_j}{\left(\frac{k}{\mu}\right)_1 h} \tag{4.19}$$

$$\lambda_{j2} = \frac{\left(\frac{k}{\mu}\right)_{j2} h_j}{\left(\frac{k}{\mu}\right)_1 h} \tag{4.20}$$

$$\omega_{j1} = \frac{(\phi c_t)_{j1} h_j}{(\phi c_t)_1 h} \tag{4.21}$$

$$\omega_{j2} = \frac{(\phi c_t)_{j2} h_j}{(\phi c_t)_1 h} \tag{4.22}$$

where:

$$h = \sum_{j=1}^{n} h_j \tag{4.23}$$

$$\left(\frac{k}{\mu}\right)_1 = \frac{\sum_{j=1}^{n} \left(\frac{k}{\mu}\right)_{j1} h_j}{h} \tag{4.24}$$

$$(\phi c_t)_1 = \frac{\sum_{j=1}^{n} (\phi c_t)_{j1} h_j}{h} \tag{4.25}$$

Eqs. 4.1 through 4.10 are presented in a dimensionless form in the following:

$$\frac{\partial^2 p_{Dj1}}{\partial r_D^2} + \frac{1}{r_D} \frac{\partial p_{Dj1}}{\partial r_D} = \frac{\omega_{j1}}{\lambda_{j1}} \frac{\partial p_{Dj1}}{\partial t_D}$$

for $j = 1, \ldots n$, and $1 \leq r_D \leq R_{Dj}$ (4.26)

$$\frac{\partial^2 p_{Dj2}}{\partial r_D^2} + \frac{1}{r_D}\frac{\partial p_{Dj2}}{\partial r_D} = \frac{\omega_{j2}}{\lambda_{j2}}\frac{\partial p_{Dj2}}{\partial t_D}$$

$$\text{for } j = 1, \ldots n, \text{ and } R_{Dj} \le r_D \le r_{eDj} \ (or\ \infty) \tag{4.27}$$

Initial condition

$$p_{Dj1}(r_D, 0) = p_{Dj2}(r_D, 0) = 0 \tag{4.28}$$

Inner boundary condition

$$p_{wD}(t_D) = p_{Dj1}(1, t_D) - s_j\left(r_D\frac{\partial p_{Dj1}}{\partial r_D}\right)\Big|_{r_D=1} \tag{4.29}$$

$$C_D\frac{dp_{wD}}{dt_D} - \sum_{j=1}^{n}\lambda_{j1}\left(r_D\frac{\partial p_{Dj1}}{\partial r_D}\right)\Big|_{r_D=1} = 1 \tag{4.30}$$

Outer boundary condition

$$\text{infinite:}\quad p_{Dj2}(r_D \to \infty, t_D) = 0 \tag{4.31}$$

$$\text{closed:}\quad \frac{\partial p_{Dj2}}{\partial r_D}\Big|_{r_D=r_{eDj}} = 0 \tag{4.32}$$

$$\text{constant-pressure:}\quad p_{Dj2}(r_{eDj}, t_D) = 0 \tag{4.33}$$

Interface conditions:

$$p_{Dj1}(R_{Dj}, t_D) = p_{Dj2}(R_{Dj}, t_D) \tag{4.34}$$

$$\lambda_{j1} \left.\frac{\partial p_{Dj1}}{\partial r_D}\right|_{r_D = R_{Dj}} = \lambda_{j2} \left.\frac{\partial p_{Dj2}}{\partial r_D}\right|_{r_D = R_{Dj}} \tag{4.35}$$

Using the Laplace transformation technique, general solutions to Eqs. 4.26 and 4.27 are:

$$\bar{p}_{Dj1}(r_D, l) = A_j K_0\left(r_D \sqrt{\frac{\omega_{j1} l}{\lambda_{j1}}}\right) + B_j I_0\left(r_D \sqrt{\frac{\omega_{j1} l}{\lambda_{j1}}}\right)$$

$$for\ j = 1, \ldots n, and\ 1 \le r_D \le R_{Dj} \tag{4.36}$$

$$\bar{p}_{Dj2}(r_D, l) = C_j K_0\left(r_D \sqrt{\frac{\omega_{j2} l}{\lambda_{j2}}}\right) + D_j I_0\left(r_D \sqrt{\frac{\omega_{j2} l}{\lambda_{j2}}}\right)$$

$$\text{for } j = 1, \ldots n, \text{ and } R_{\beta j} \le r_D \le r_{eDj}(or\ \infty) \tag{4.37}$$

where l is the Laplace variable with respect to t_D.

Using Eq. 4.36, and Eq. 4.29 in Laplace space, an expression for $\bar{p}_{wD}$ is:

$$\bar{p}_{wD} = A_j \left[K_0\left(\sqrt{\frac{\omega_{j1} l}{\lambda_{j1}}}\right) + s_j \sqrt{\frac{\omega_{j1} l}{\lambda_{j1}}}\ K_1\left(\sqrt{\frac{\omega_{j1} l}{\lambda_{j1}}}\right)\right]$$

$$+ B_j \left[I_0\left(\sqrt{\frac{\omega_{j1} l}{\lambda_{j1}}}\right) - s_j \sqrt{\frac{\omega_{j1} l}{\lambda_{j1}}}\ I_1\left(\sqrt{\frac{\omega_{j1} l}{\lambda_{j1}}}\right)\right] \tag{4.38}$$

The coefficients A_j , B_j , C_j and D_j are obtained by using boundary conditions. Boundary conditions in Laplace space yield the following set of linear algebraic equations to solve for A_j through D_j :

From Eq. 4.30,

$$\alpha_{11j} A_j + \alpha_{12j} B_j + \sum_{j=1}^{n} \sqrt{\lambda_{j1}\, \omega_{j1}\, l}\; K_1\left(\sqrt{\frac{\omega_{j1}\, l}{\lambda_{j1}}}\right) A_j$$

$$- \sum_{j=1}^{n} \sqrt{\lambda_{j1}\, \omega_{j1}\, l}\; I_1\left(\sqrt{\frac{\omega_{j1}\, l}{\lambda_{j1}}}\right) B_j = \frac{1}{l} \qquad (4.39)$$

From Eq. 4.34,

$$\alpha_{21j} A_j + \alpha_{22j} B_j + \alpha_{23j} C_j + \alpha_{24j} D_j = 0 \qquad (4.40)$$

From Eq. 4.35,

$$\alpha_{31j} A_j + \alpha_{32j} B_j + \alpha_{33j} C_j + \alpha_{34j} D_j = 0 \qquad (4.41)$$

From Eq. 4.31 or 4.32 or 4.33,

$$\alpha_{43j} C_j + \alpha_{44j} D_j = 0 \qquad (4.42)$$

where:

$$\alpha_{11j} = C_D\, l \left[K_0\left(\sqrt{\frac{\omega_{j1}\, l}{\lambda_{j1}}}\right) + s_j \sqrt{\frac{\omega_{j1}\, l}{\lambda_{j1}}}\; K_1\left(\sqrt{\frac{\omega_{j1}\, l}{\lambda_{j1}}}\right)\right] \qquad (4.43)$$

$$\alpha_{12j} = C_D l \left[I_0\left(\sqrt{\frac{\omega_{j1} l}{\lambda_{j1}}}\right) - s_j \sqrt{\frac{\omega_{j1} l}{\lambda_{j1}}}\ I_1\left(\sqrt{\frac{\omega_{j1} l}{\lambda_{j1}}}\right)\right] \tag{4.44}$$

$$\alpha_{21j} = K_0\left(R_{Dj}\sqrt{\frac{\omega_{j1} l}{\lambda_{j1}}}\right) \tag{4.45}$$

$$\alpha_{22j} = I_0\left(R_{Dj}\sqrt{\frac{\omega_{j1} l}{\lambda_{j1}}}\right) \tag{4.46}$$

$$\alpha_{23j} = - K_0\left(R_{Dj}\sqrt{\frac{\omega_{j2} l}{\lambda_{j2}}}\right) \tag{4.47}$$

$$\alpha_{31j} = -\sqrt{\lambda_{j1}\,\omega_{j1}\,l}\ K_1\left(R_{Dj}\sqrt{\frac{\omega_{j1} l}{\lambda_{j1}}}\right) \tag{4.48}$$

$$\alpha_{32j} = \sqrt{\lambda_{j1}\,\omega_{j1}\,l}\ I_1\left(R_{Dj}\sqrt{\frac{\omega_{j1} l}{\lambda_{j1}}}\right) \tag{4.49}$$

$$\alpha_{33j} = \sqrt{\lambda_{j2}\,\omega_{j2}\,l}\ K_1\left(R_{Dj}\sqrt{\frac{\omega_{j2} l}{\lambda_{j2}}}\right) \tag{4.50}$$

For an infinite reservoir, $D_j = 0$, and thus,

$$\alpha_{24j} = \alpha_{34j} = \alpha_{43j} = \alpha_{44j} = 0 \tag{4.51}$$

For a closed outer boundary,

$$\alpha_{24j} = - I_0\left(R_{Dj}\sqrt{\frac{\omega_{j2} l}{\lambda_{j2}}}\right) \tag{4.52}$$

$$\alpha_{34j} = -\sqrt{\lambda_{j2}\,\omega_{j2}}\,l\,I_1\left(R_{Dj}\sqrt{\frac{\omega_{j2}\,l}{\lambda_{j2}}}\right) \tag{4.53}$$

$$\alpha_{43j} = -\,K_1\left(r_{eDj}\sqrt{\frac{\omega_{j2}\,l}{\lambda_{j2}}}\right) \tag{4.54}$$

$$\alpha_{44j} = I_1\left(r_{eDj}\sqrt{\frac{\omega_{j2}\,l}{\lambda_{j2}}}\right) \tag{4.55}$$

For a constant-pressure outer boundary,

$$\alpha_{24j} = -\,I_0\left(R_{Dj}\sqrt{\frac{\omega_{j2}\,l}{\lambda_{j2}}}\right) \tag{4.56}$$

$$\alpha_{34j} = -\sqrt{\lambda_{j2}\,\omega_{j2}}\,l\,I_1\left(R_{Dj}\sqrt{\frac{\omega_{j2}\,l}{\lambda_{j2}}}\right) \tag{4.57}$$

$$\alpha_{43j} = K_0\left(r_{eDj}\sqrt{\frac{\omega_{j2}\,l}{\lambda_{j2}}}\right) \tag{4.58}$$

$$\alpha_{44j} = I_0\left(r_{eDj}\sqrt{\frac{\omega_{j2}\,l}{\lambda_{j2}}}\right) \tag{4.59}$$

For a finite reservoir case, algebraic manipulations of Eqs. 4.38 through 4.42 would yield expressions for A_j, B_j, C_j, D_j, and p_{wD}:

From Eq. 4.42:

$$D_j = -\,\frac{\alpha_{43j}}{\alpha_{44j}}\,C_j \tag{4.60}$$

Using Eq. 4.60 in Eq. 4.40 yields:

$$C_j = -\frac{(\alpha_{21j}\, A_j + \alpha_{22j}\, B_j)\,\alpha_{44j}}{(\alpha_{23j}\, \alpha_{44j} - \alpha_{24j}\, \alpha_{43j})} \tag{4.61}$$

Using Eqs. 4.60 and 4.61 in Eq. 4.41 yields:

$$B_j = -\delta_j A_j \tag{4.62}$$

where:

$$\delta_j = \frac{\alpha_{31j}\,(\alpha_{23j}\, \alpha_{44j} - \alpha_{24j}\, \alpha_{43j}) - \alpha_{21j}\,(\alpha_{33j}\, \alpha_{44j} - \alpha_{34j}\, \alpha_{43j})}{\alpha_{32j}\,(\alpha_{23j}\, \alpha_{44j} - \alpha_{24j}\, \alpha_{43j}) - \alpha_{22j}\,(\alpha_{33j}\, \alpha_{44j} - \alpha_{34j}\, \alpha_{43j})} \tag{4.63}$$

Substituting Eq. 4.62 into Eq. 4.38 yields:

$$A_j = \frac{\bar{p}_{wD}}{\gamma_j} \tag{4.64}$$

where:

$$\gamma_j = K_0\left(\sqrt{\frac{\omega_{j1}\, l}{\lambda_{j1}}}\right) + s_j \sqrt{\frac{\omega_{j1}\, l}{\lambda_{j1}}}\; K_1\left(\sqrt{\frac{\omega_{j1}\, l}{\lambda_{j1}}}\right)$$

$$- \delta_j \left[I_0\left(\sqrt{\frac{\omega_{j1}\, l}{\lambda_{j1}}}\right) - s_j \sqrt{\frac{\omega_{j1}\, l}{\lambda_{j1}}}\; I_1\left(\sqrt{\frac{\omega_{j1}\, l}{\lambda_{j1}}}\right)\right] \tag{4.65}$$

Finally, substituting Eqs. 4.62 and 4.64 into Eq. 4.39 yields:

$$\bar{p}_{wD} = \frac{1}{l\left[\frac{\alpha_{11j}}{\gamma_j} - \frac{\alpha_{12j}\,\delta_j}{\gamma_j} + \sum_{j=1}^{n} \frac{\sqrt{\lambda_{j1}\,\omega_{j1}}\,l}{\gamma_j}\left\{K_1\left(\sqrt{\frac{\omega_{j1}}{\lambda_{j1}}}\,l\right) + \delta_j I_1\left(\sqrt{\frac{\omega_{j1}}{\lambda_{j1}}}\,l\right)\right\}\right]} \tag{4.66}$$

Eq. 4.66 can be inverted numerically using the Stehfest[17] inversion algorithm to obtain p_{wD}.

For an infinite reservoir case, $D_j = 0$, and algebraic manipulations, similar to the case for finite reservoir, of Eqs. 4.38 through 4.41 yield:

$$C_j = -\frac{\alpha_{21j}\,A_j + \alpha_{22j}\,B_j}{\alpha_{23j}} \tag{4.67}$$

Again, Eqs. 4.62, 4.64, 4.65, and 4.66 express B_j, A_j, γ_j, and $\bar{p}_{wD}$, respectively, with:

$$\delta_j = \frac{\alpha_{31j}\,\alpha_{23j} - \alpha_{33j}\,\alpha_{21j}}{\alpha_{32j}\,\alpha_{23j} - \alpha_{33j}\,\alpha_{22j}} \tag{4.68}$$

This completes the analytical solution of the transient pressure problem for a radial, two region, multilayer composite system.

4.2 Model Validation

A computer program has been developed to generate pressure transient responses for a multilayered, composite reservoir. Pressure and pressure derivative responses for different cases were generated by using a numerical inversion algorithm developed by Stehfest.[17] The computer program is included as Program #1 in App. A. Table 4.1

Table 4.1: Sample input data for the computer program in App. A

$C_D = 0.0$	
Number of layers = 3	
$\lambda_{j1} = 0.3333$ j = 1, 2, 3	$\lambda_{j2} = 0.03333$ j = 1, 2, 3
$\omega_{j1} = 0.3333$ j = 1, 2, 3	$\omega_{j2} = 0.003333$ j = 1, 2, 3
$S_1 = 0.0$	$R_{Dmax} = 220$
$S_2 = 0.0$	$R_{D2} = 210$
$S_3 = 0.0$	$R_{Dmin} = 200$ (front angle = 45°)
Number of cycles of data required = 9	
$t_{D1} = 100$	
Number of terms to be used in the Stehfest[17] algorithm (NTERM) = 8	

$h_j = 10$

M = 10

F = 100

Tables B1 and B2 present other sample input data for reservoirs with different M and number of layers.

presents sample input data for a three-layer composite resevoir with M = 10, F = 100, C_D = s = 0.0 and a 45° front angle. In the following, model validation efforts are described.

Various tests were run using this analytical model and compared to results obtained in the literature on the pressure transient testing of homogeneous, composite, and layered reservoirs. In all the validation cases, conventional drawdown tests were run for a single well located in either an infinite or a bounded reservoir. Figure 4.1 shows the dimensionless pressure versus dimensionless time graph for a single-layer homogeneous reservoir with s = 5, and C_D values of 0, 1000, and 10^4. The computed values match those of Agarwal *et al* .[44] Figure 4.2 shows dimensionless pressure behaviour for a three-layer homogeneous reservoir (with equivalent properties in each layer). For this case, λ and ω are 0.3333 for all the three layers. Values of C_D = 100 and s = 10 are used for this case. Values used in plotting Fig. 4.2 match those of Agarwal *et al.* [44]

Figure 4.3 is a graph of drawdown pressure response for a two-layered reservoir, with different permeabilities in the top layer (layer 1) and the bottom layer (layer 2). The ratio of h_1/h_2 = 1.0, $(\phi c_t)_1 / (\phi c_t)_2$ = 1.0 and $(k/\mu)_1 / (k/\mu)_2$ = 10. Also, $s_1 = s_2$ = 0 and C_D = 0. The values obtained match those in Table 4 of Tariq and Ramey[16]. To compare the results of Fig. 4.3 with those of Tariq and Ramey[16], note that Fig. 4.3 is the result of data obtained for an infinite reservoir, while Tariq and Ramey[16] use a dimensionless outer radius r_{eD} = 10,000. The late time dimensionless pressure values are therefore different. Figure 4.4 applies to the case of a well in a single-layer composite reservoir with C_D = s = 0. A log-log graph of semi-log pressure derivative versus dimensionless time is shown for M = 10 and 100. The variable M is the ratio of the mobility of the inner region (Region 1) to that of the outer region (Region 2). The minimum front

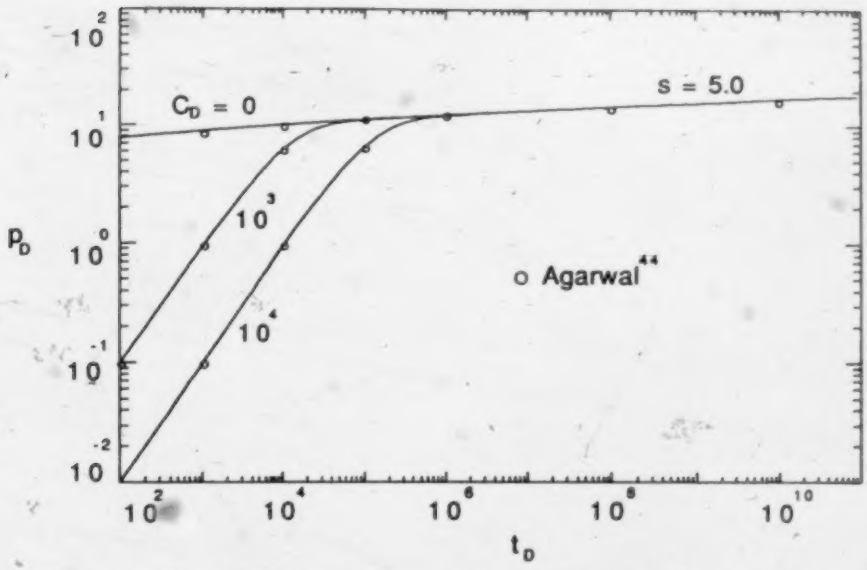

Fig. 4.1- Dimensionless pressure response for a 1-layer homogeneous reservoir

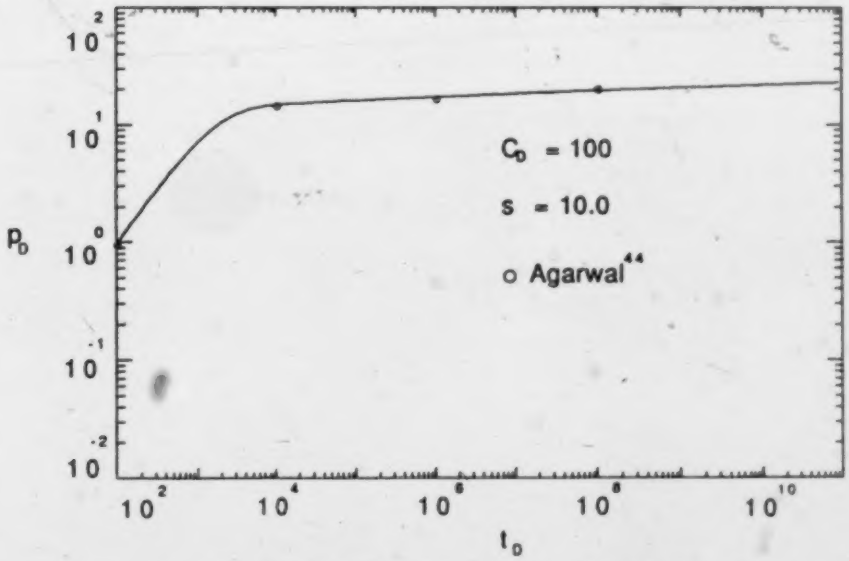

Fig. 4.2- Dimensionless pressure response for a 3-layer homogeneous reservoir

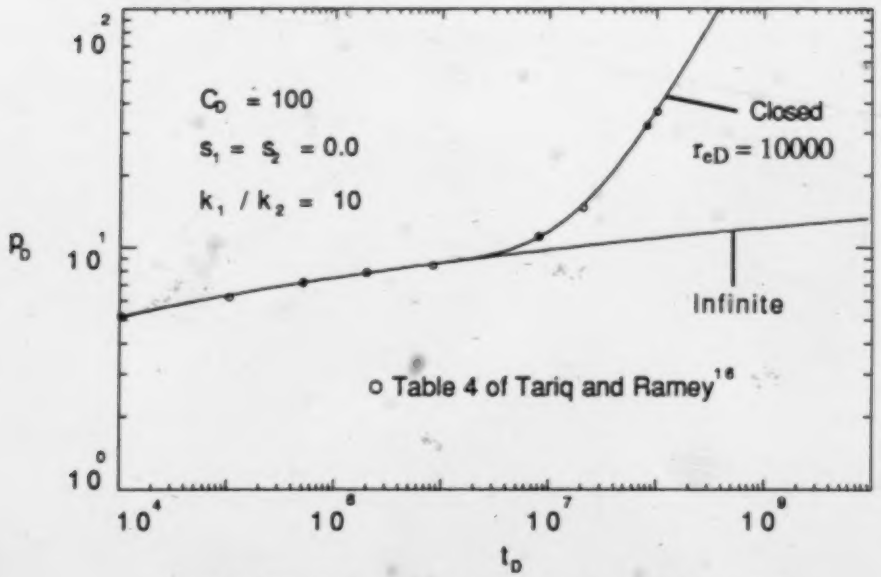

Fig. 4.3- Dimensionless pressure response for a 2-layer heterogeneous reservoir

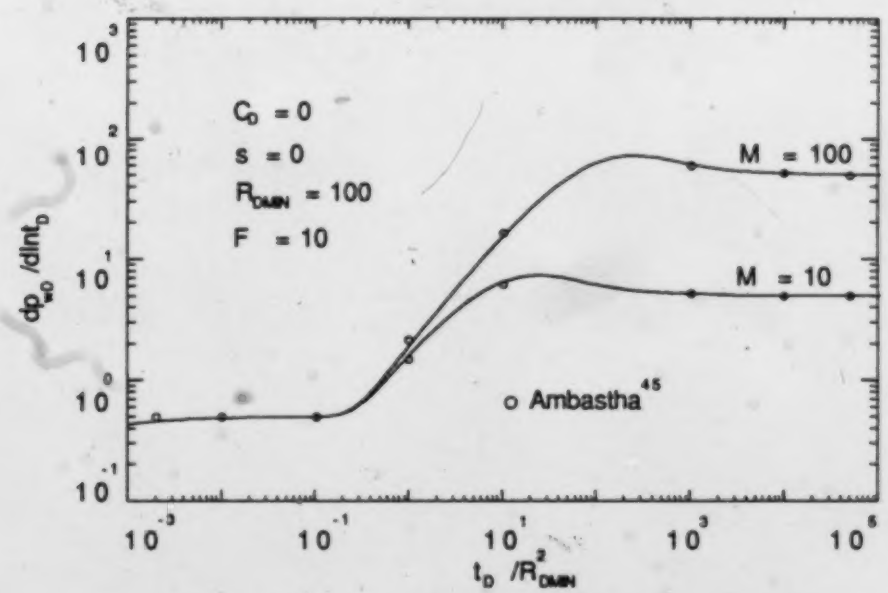

Fig. 4.4 - Pressure derivative response for a single-layer composite reservoir

radius, R_{Dmin}, is 100, and the storativity ratio $F = ((\phi c_t)_1 / (\phi c_t)_2) = 10$. The values obtained for this simulation match those reported by Ambastha[45].

Figure 4.5 shows the pressure transient response for a two-layered composite reservoir with $C_D = 31.64$, $s_1 = s_2 = 0$, $R_{D1} = 670.3$, and $R_{D2} = 439.6$. The parameters used to generate Fig. 4.5 are obtained from Table 1 of Satman.[30] Mobility and storativity ratios for regions 1 and 2 are $\lambda_{j1} = 0.5$, $\lambda_{j2} = 0.00235$, $\omega_{j1} = 0.5$, and $\omega_{j2} = 0.02845$, respectively for j = 1 and 2. Satman[30] presents a graph of pressure difference versus real time (hours) for the same parameters. From the definition of p_{wD} and t_D, real data may be converted to the dimensionless form using the following equations:

$$\Delta p = p_{wD} / 0.15883 \text{ (kPa)} \tag{4.69}$$

$$t = t_D / 6.984 \times 10^5 \text{ (hrs.)} \tag{4.70}$$

As per Fig. 4.5, the results from this study match Satman's[30] results quite well. Figure 4.6 presents a drawdown pressure derivative type-curve for a bounded homogeneous reservoir with skin and wellbore storage. The parameters used in generating the curves in Fig. 4.6 are presented in Table 4.2. Both closed and constant-pressure outer boundary cases are shown. The values obtained match those of Fig. 5.2 in Ref. 45.

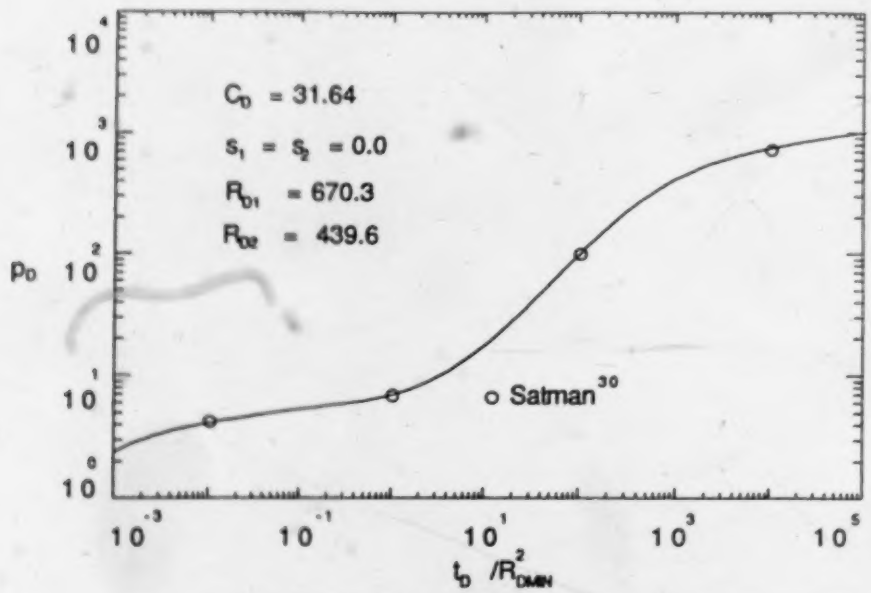

Figure 4.5 - Pressure transient response for a two-layer composite reservoir

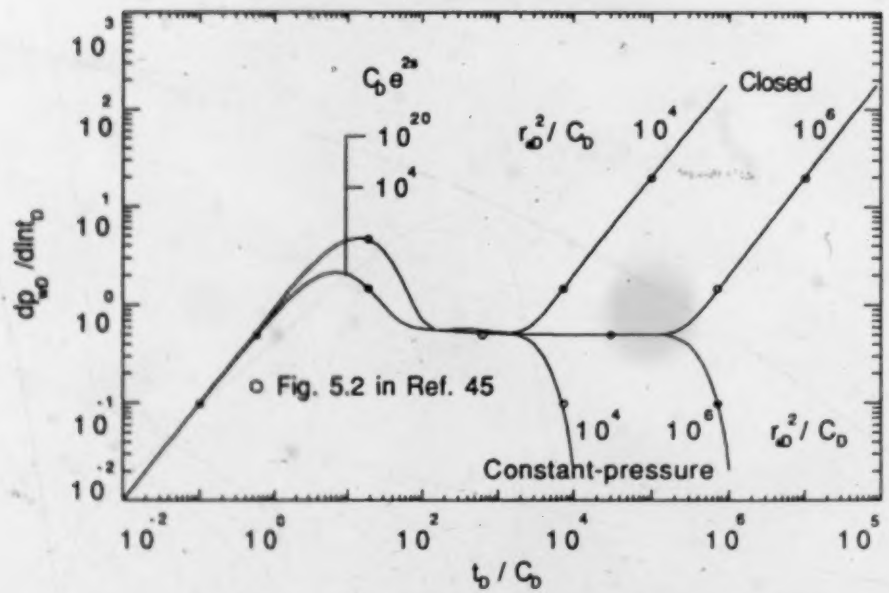

Fig. 4.6 - Drawdown pressure derivative type-curve

Table 4.2: Parameters used to generate Fig. 4.6

C_D	s	r_{eD}	$C_D e^{2s}$	r_{eD}^2/C_D
10^5	5.76	31623	10^{10}	10^4
10^3	1.15	31623	10^4	10^6

5. RESULTS AND DISCUSSION

A reservoir undergoing a thermal recovery process develops a swept region closest to the well. The presence of steam, in the case of a steam flood, and air or any oxidizing gas, in the case of a forward in-situ combustion process, characterizes such a region. The circular zone surrounding the well will have rock and/or fluid properties that are different from properties in the unaltered reservoir outside the circular altered zone. As discussed in Section 2, a composite reservoir is an idealized model typically employed in studying the behaviour of wells undergoing secondary or tertiary oil recovery processes. Figure 5.1 shows a schematic diagram of a two-region, radial multilayered composite reservoir. Region 1 represents the area swept by the injected fluid. The radial extent of the fluid (front radius) may be different for each layer of the reservoir, as represented by the vertical solid lines R_1, R_2, and R_3, on Fig. 5.1. The effect of different front shapes on pressure responses can, therefore, be studied using this model. One of the important parameters sought from well tests in composite reservoirs is an estimate of the swept volume, or front (discontinuity) radius. However, fronts in many composite reservoir configurations, such as thermal recovery and CO_2 flooding, are usually not cylindrical due to gravity and fingering effects. In the case of a steam flood, effects of gravity override would result in a configuration represented by the dotted line that is qualitatively shown on Fig. 5.2. This configuration is referred to as a reservoir with a tilted front.

In this study, a tilted front is simulated in the mathematical model as a multilayered composite reservoir with no interlayer crossflow, where the dimensionless distance to the front R_D, can take different appropriate values for different layers, as shown on Fig. 5.2. The upper layer is assigned the largest radial discontinuity radius, R_{Dmax}, while the bottom layer has the minimum, R_{Dmin}.

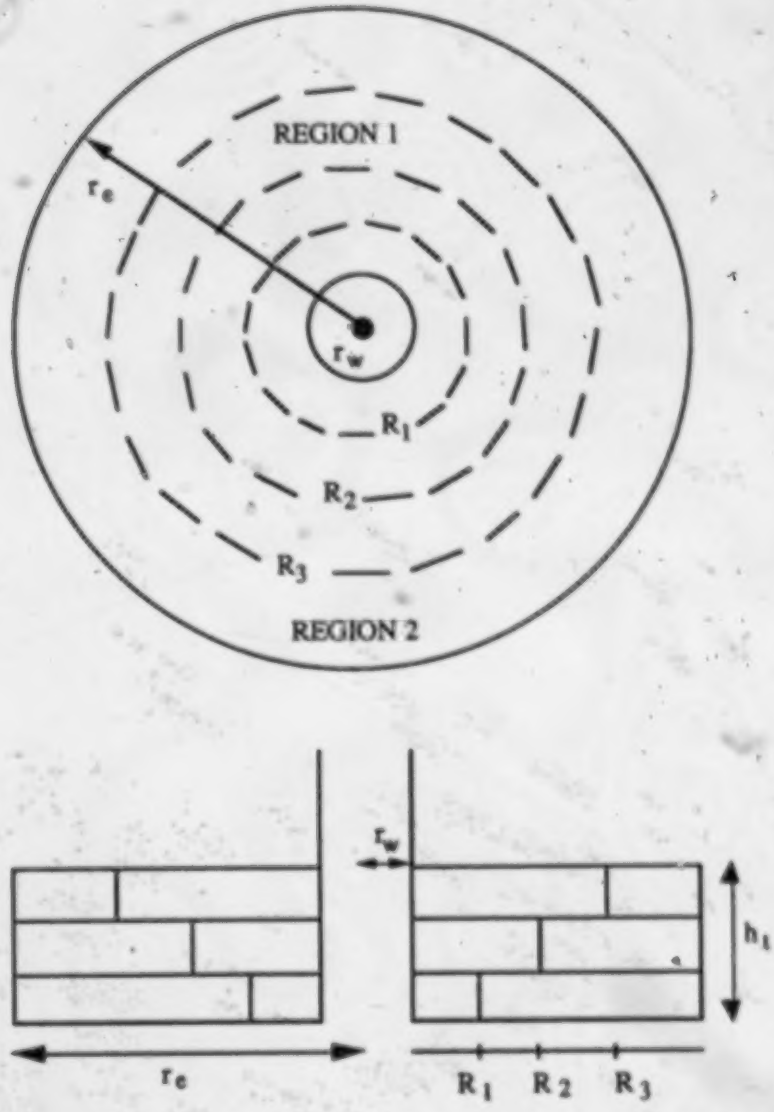

Figure 5.1 ; Schematic diagram of a two-region multilayer composite reservoir.

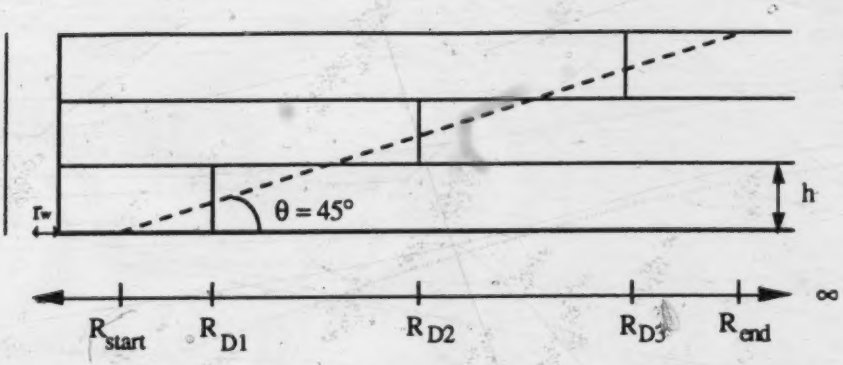

Fig. 5.2: Schematic diagram of a reservoir with a tilted front

The difference in radial extent between R_{Dmax} and R_{Dmin}, together with the thickness, h_t, of the whole reservoir, is used to determine the front angle, θ. Calculation of front radii for a given number of layers and front angles follows.

5.1 Calculation of Front Radii

The inner region of a multilayered composite reservoir is visualized as cylinders of varying radii stacked one on top of another. The cylinder having the smallest radius is at the bottom of the stack. Figure 5.3 shows a schematic of the front-view section of such a reservoir model. By drawing a line R'R", such that a given half-cylinder $ABCR_1$, has a volume equal to the volume of the resulting cone frustum ABR"R', a tilted front with a specified angle θ, may be drawn by proportionally adjusting radius R_1 (length $\overline{AR_1}$). The dotted line R'R" represents the tilted front while line CR_1 is a step approximation to the tilted front.

Consider the half-cones OBR" and OAR' with heights $(h+h_1)$, and h_1, respectively.

Then, $$\tan\theta = \frac{h}{R'' - R'} = \frac{h + h_1}{R''} = \frac{h_1}{R'} \qquad (5.1)$$

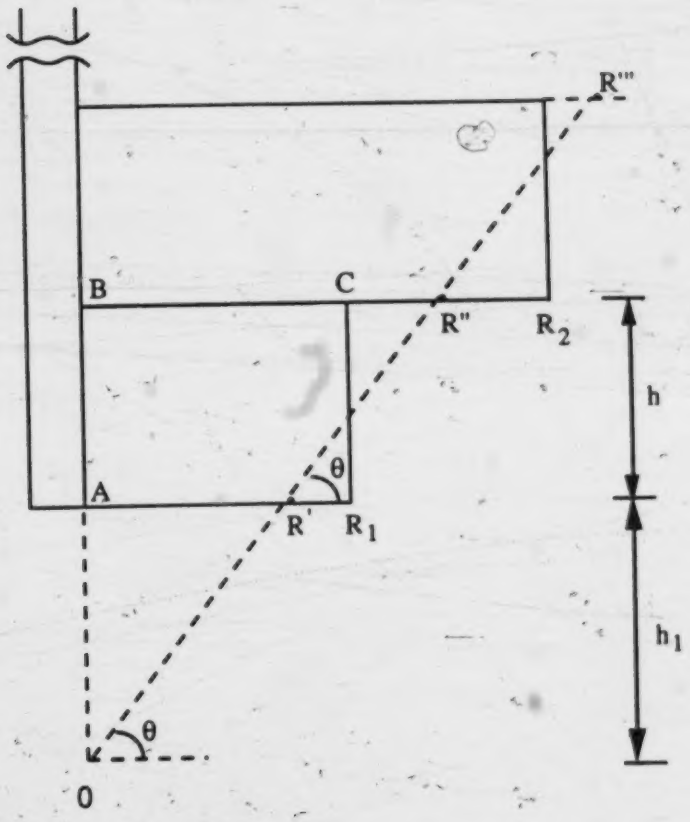

Fig. 5.3 : A Schematic of a front-view section of a reservoir with a tilted front.

Rearranging Eq. 5.1 yields:

$$h_1 = R' \tan\theta \qquad (5.2)$$

$$R'' = R' + h \cot\theta \qquad (5.3)$$

$$R'' = (h + h_1) \cot\theta \qquad (5.4)$$

The volume of the half cone frustum ABR"R' is:

$$V_{cf} = \frac{\pi}{3}\left[R''^2 (h + h_1) - R'^2 h_1 \right](0.5) \tag{5.5}$$

Substituting Eq. 5.1 into Eq. 5.5 yields:

$$V_{cf} = \frac{\pi}{3} \tan\theta \left[R''^3 - R'^3 \right](0.5) \tag{5.6}$$

Equating the volume of the cylinder $ABCR_1$ to that of the cone frustum ABR"R', and substituting Eq. 5.3 into the resulting expression yields the following quadratic equation:

$$R'^2 + (h \cot\theta) R' + \left[\frac{h^2 \cot^2\theta}{3} - R_1^2 \right] = 0 \tag{5.7}$$

For a specified minimum front radius R_1 (R_{Dmin}), a front angle θ, and layer thickness h, the starting point of the tilted front R' (R_{start} in Fig. 5.2), may be calculated from:

$$R' = \frac{-(h \cot\theta) + \sqrt{(h \cot\theta)^2 + 4\left(R_1^2 - h^2 \cot^2(\theta)/3\right)}}{2} \tag{5.8}$$

The value of R" can be calculated using Eq. 5.3. For all subsequent layers, R" obtained for the previous layer becomes R' for the next layer. Replacing R_1 in Eq. 5.7 by a general R_j, we obtain:

$$R_j = \sqrt{\frac{1}{3h} \tan\theta \left[R''^3 - R'^3 \right]} \tag{5.9}$$

The variable R_j can be presented similarly in dimensionless form by affixing the appropriate symbol. A computer program to calculate the values of front radii for any given angle, θ, minimum front radius R_1 (or R_{Dmin}), layer thickness, h, and number of

layers, n, is presented in App. A. Table 5.1 presents values of dimensionless radii R_D for each layer of a five-layer model for selected values of front angles. Tables B3 through B6 in App. B present R_D values for models with 2, 3, 6, and 10 layers. All layers are of equal thickness and the reservoir is considered to be of infinite extent in the radial direction, i.e., an infinitely-large layered composite reservoir.

Table 5.1: Front radii for a five-layer composite reservoir (h_{tD} = 30)

Front Angle (Degrees)	Dimensionless Front Radius R_D						
	R_{start}	R_{Dmin}	R_{D2}	R_{D3}	R_{D4}	R_{Dmax}	R_{end}
10	183	200	234	268	302	336	353
20	192	200	217	233	249	266	274
30	195	200	210	221	231	242	247
45	197	200	206	212	218	224	227
60	198	200	203	207	210	214	216
90	200	200	200	200	200	200	200

5.2 Drawdown Response

The parameters considered for drawdown pressure derivative responses are mobility ratio, M, storativity ratio, F, front angle, θ, and dimensionless front radius, R_D. The definitions of the preceding ratios are given in Section 4. The effects of wellbore skin (s) and wellbore storage (C_D) are also considered briefly.

5.2.1 Effect of Number of Layers

Various investigators[16,18,19,20] have shown that multilayer reservoir models exhibit characteristics that are similar to a single-layer reservoir as long as dimensionless properties are defined in terms of average reservoir properties of k, h, ϕ and μ. Satman[30] used a two-layered system to analyze the pressure transient behaviour in a stratified system with fluid banks (composite system). The fluid and rock properties in Region 1 were equal for both layers. Similarly, those of Region 2 were equal for both layers. However, Region 1 properties were different from Region 2 properties. In his model, the two front radii represented a front angle of approximately 23° , although the angle was not stated explicitly. Satman and Oskay[33] also presented a similar study using a 5-layer model. Five cases with different front radii values for four of the five layers were considered. The middle layer (layer 3) was assigned the same front radii in all cases. Using the two extreme front radii for each case and total formation thickness, we calculate front angles ranging in slope from approximately 2° to 9°. Reference 33 does not provide a basis for the values assigned to the front radii. They also did not state explicitly the front angle. The transient pressure responses of these five cases were compared to that of a composite reservoir having a sharp front. Other studies[31,32] have presented analytical solutions for multilayered composite reservoirs and shown that the behaviour of a two-layer system is representative of one with any number of layers greater than two. Figures 5.4 through 5.8 present the effect of number of layers on the pressure derivative. For any given M, F, C_D, s, and R_D, any number of layers (2 or more) can represent the transient pressure derivative for angles $\geq 30°$. When the front angle is less than 30°, pressure response during the transition flow period is mildly dependent on the number of layers, as shown on Fig. 5.4. The response of a five-layer reservoir matches that of a ten-layer reservoir even at these low angles (less than 30°).

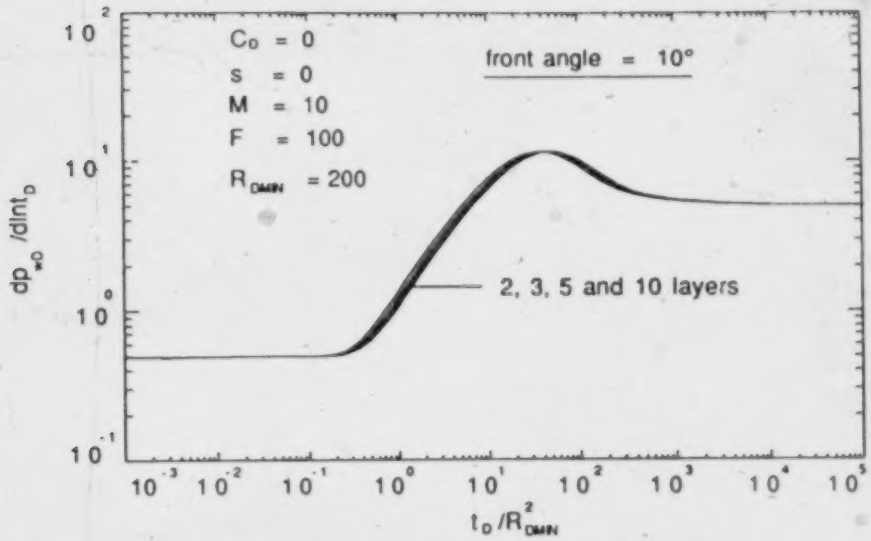

Fig. 5.4 -Effect of number of layers on pressure derivative (front angle = 10°)

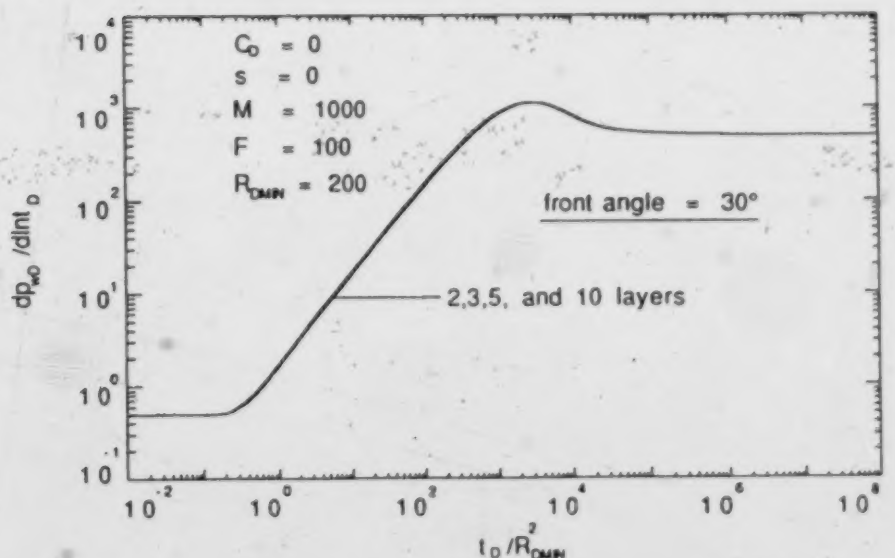

Fig. 5.5-Effect of number of layers on pressure derivative (front angle = 30°)

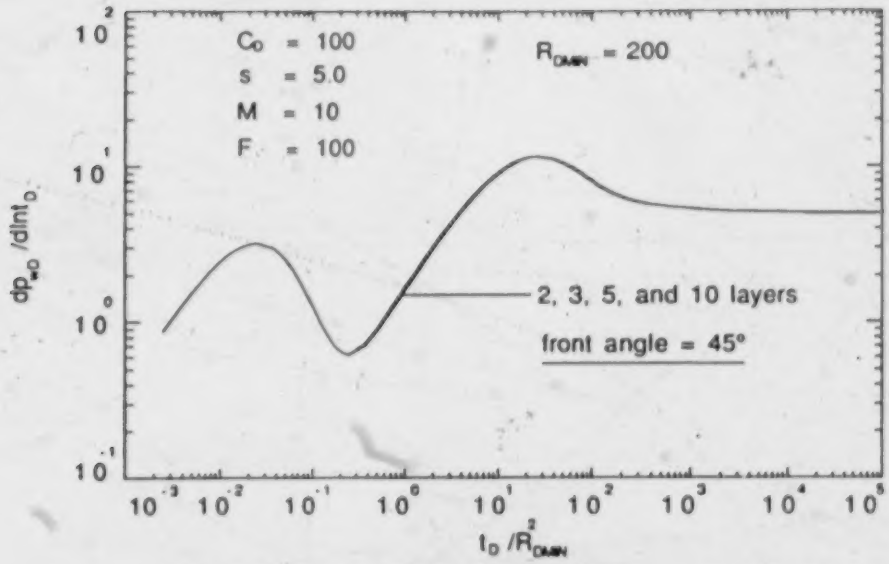

Fig. 5.6-Effect of number of layers on pressure derivative (front angle = 45°)

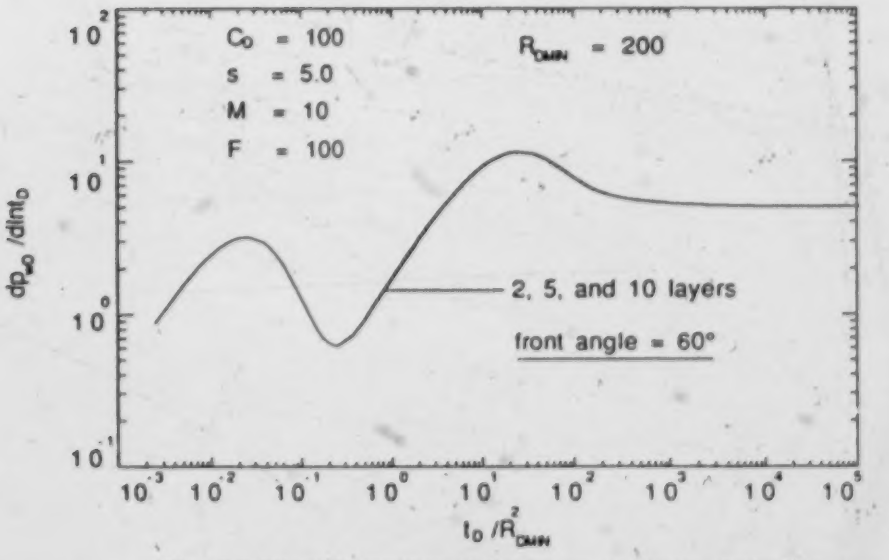

Fig. 5.7-Effect of number of layers on pressure derivative (front angle = 60°)

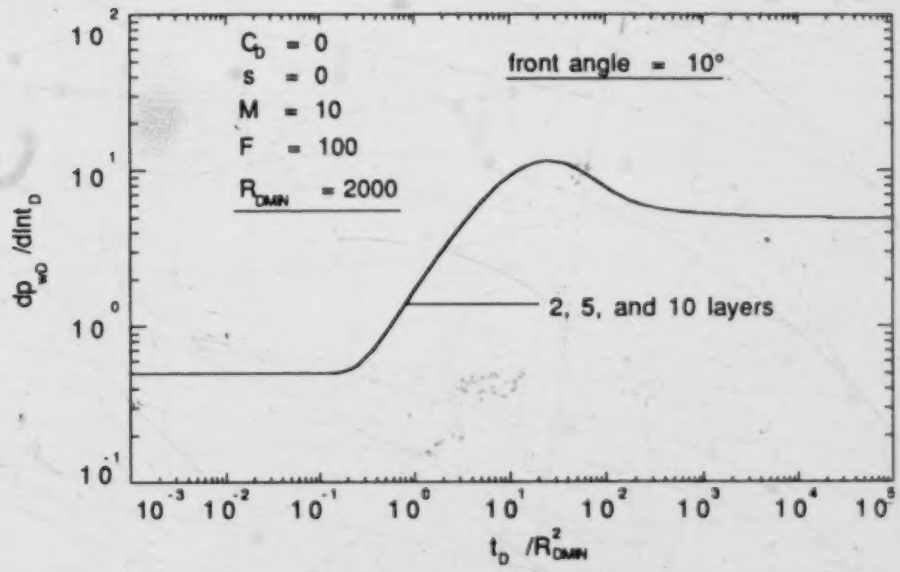

Fig. 5.8-Effect of number of layers on pressure derivative (R_{DMIN} = 2000)

However, presence of noise in well test data may make it difficult to distinguish between the response of a two-layer and that of a ten-layer reservoir. Figure 5.8 shows the effect of number of layers on the pressure derivative for a composite reservoir with R_{Dmin} = 2000. Other reservoir properties are similar to those of Fig. 5.4. For R_{Dmin} = 2000, any number of layers greater than one may be used to represent a commingled reservoir system having a front angle ≥ 10°.

5.2.2 Correlating Parameter

Satman *et al.*[24] and Tang[25] correlated pressure responses neglecting skin or wellbore storage. They graphed p_{wD} - ln (R_D/500) versus t_{De} to correlate pressure responses for all front radii with the response for R_D = 500 for a single-layer composite reservoir. Ambastha and Ramey[46] also showed that the use of t_D/R_D^2 as a correlation parameter was valid for practical purposes in a single-layer composite reservoir. They used R_D values of 50, 100 and 1000 which appeared to form a single curve for all times. This observation was based on an analysis of a single-layer composite reservoir model in which the front is necessarily vertical (or sharp).

Figures 5.9 through 5.13 present the effect of minimum front radius on pressure derivative. For minimum front radius values of 100 and 200, t_{De}, defined as

$$t_{De} = \frac{t_D}{R_{Dmin}^2} \tag{5.10}$$

is not valid as a correlation parameter for front angles of 10°, 30° and 45°. However, a minimum front radius ≥ 1000 and θ ≥ 10° produces a pressure response similar to that of a composite reservoir having a sharp front. This is shown on Fig. 5.9. Figures 5.12 and 5.13 show similar plots for front angles of 60°, and 90° (sharp front), respectively.

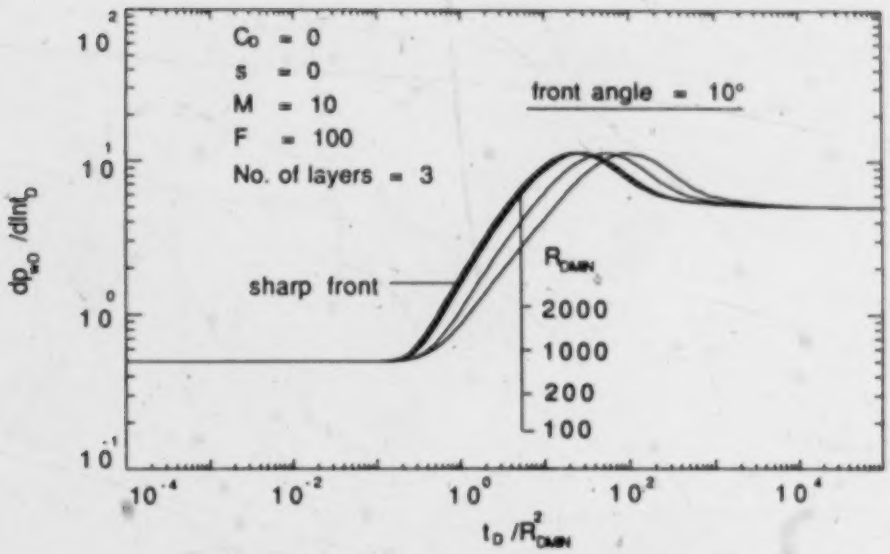

Fig. 5.9-Effect of minimum front radius on pressure derivative (front angle = 10°)

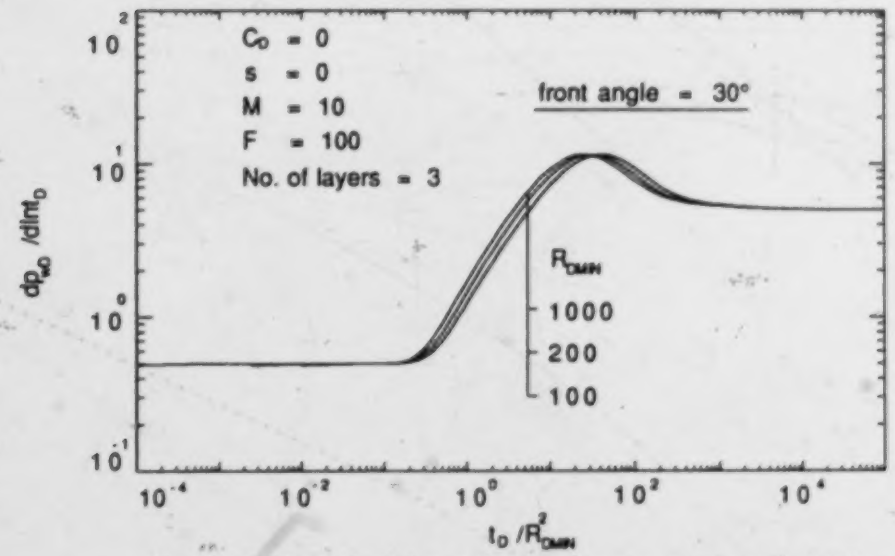

Fig. 5.10-Effect of minimum front radius on pressure derivative (front angle = 30°)

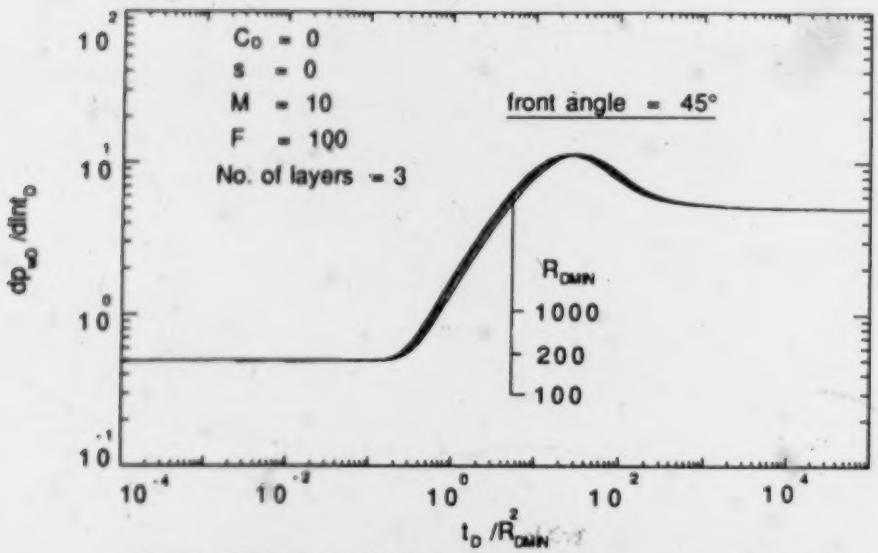

Fig. 5.11-Effect of minimum front radius on pressure derivative (front angle = 45°)

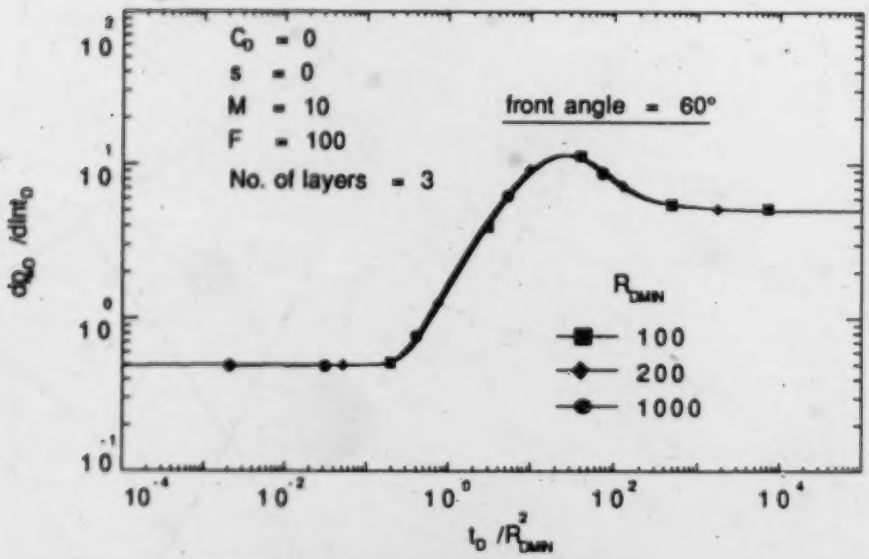

Fig. 5.12-Effect of minimum front radius on pressure derivative (front angle = 60°)

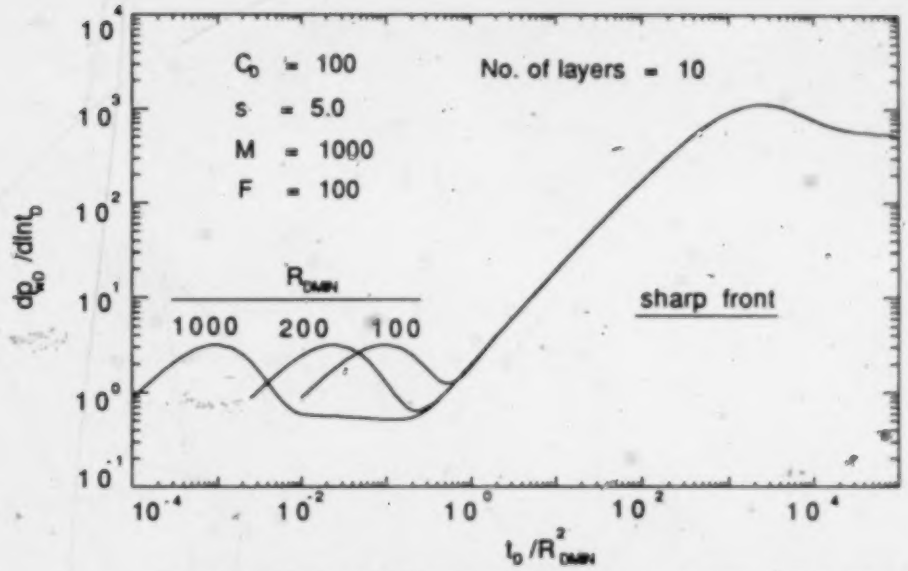

Fig. 5.13-Effect of minimum front radius on pressure derivative (front angle = 90°)

Type-curve matching methods are, therefore, recommended for estimating R_{Dmin} for multilayered composite reservoirs having values of $R_{Dmin} < 1000$.

5.2.3 Effect of Front Angle

Figures 5.14 through 5.16 present the effect of front angle on the pressure derivative for $R_{Dmin} = 200$. These figures show that for all practical purposes, data for front angle values of $\theta \geq 30°$ can be analyzed using the type-curves for a sharp front.[46] Also, for $\theta \geq 30°$, times for specific flow events at the early and late times closely match those for a sharp front. Some differences exist during the transition flow regime. Thus, during the early transition period, a Cartesian graph of pressure versus time may show the existence of pseudosteady state behaviour for a range of front angle values. This is discussed in Section 5.2.7 of this study. The time to the end of the first semi-log straight line, $(t_{De})_{end}$, is dependent on the front angle. The time to the start of the second semi-log straight line, $(t_{De})_{II}$, is independent of the front angle. Ambastha and Ramey[46] reported the following design equations for these times (accurate to within 2% in the pressure derivative):

$$(t_{De})_{end} = 0.18 \qquad (5.11)$$

and

$$(t_{De})_{II} = 90(1 + \log F)\, M \qquad (5.12)$$

The time to the maximum derivative was investigated for different values of front angle. Figures 5.17 through 5.19 show the combined effects of the number of layers and the front angle on the pressure derivative. For front angle values of $\theta \geq 30°$, the time to the maximum derivative is independent of θ. The design equations developed by Ambastha and Ramey[46] (for a sharp front) can thus be extended to apply for the following angle ranges:

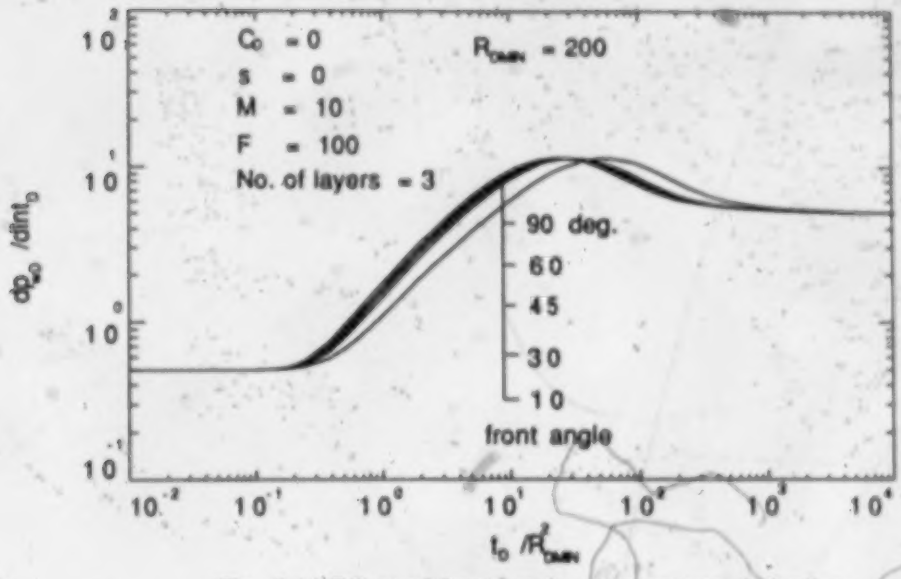

Fig. 5.14-Effect of front angle on pressure derivative
(M = 10, F = 100)

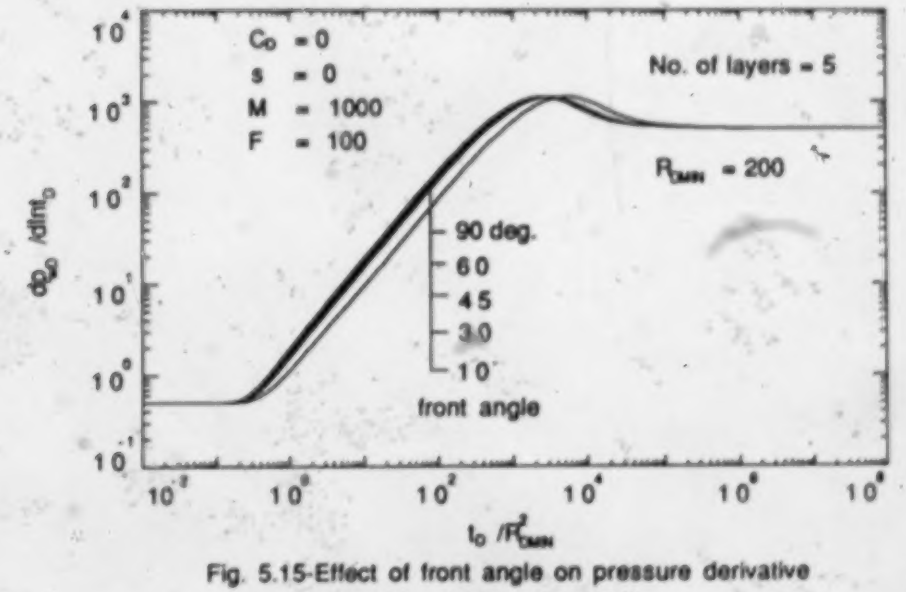

Fig. 5.15-Effect of front angle on pressure derivative
(M = 1000, F = 100)

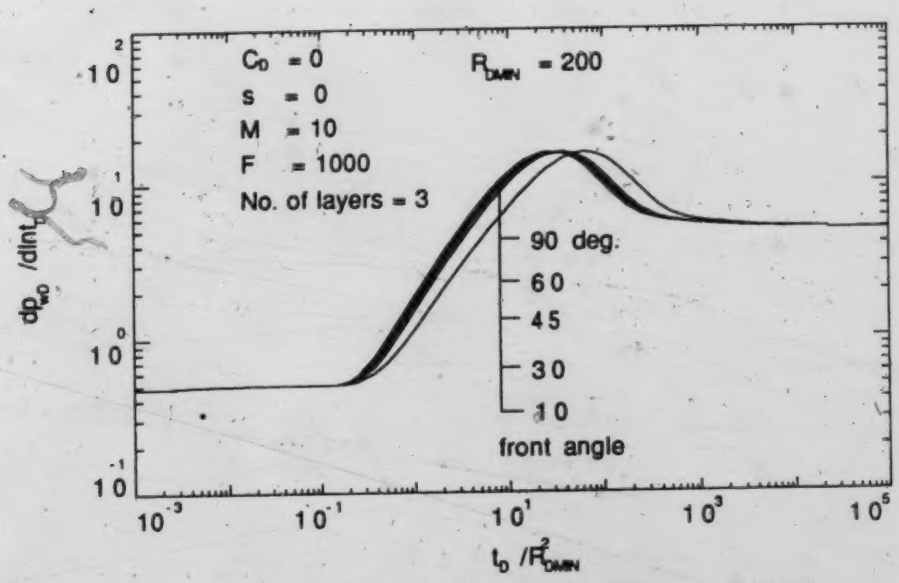

Fig. 5.16-Effect of front angle on pressure derivative
(M = 10, F = 1000)

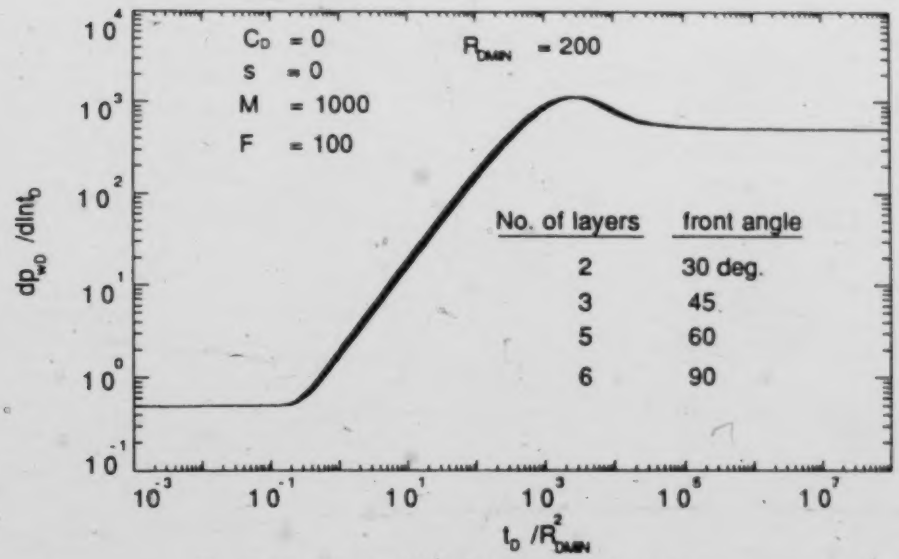

Fig. 5.17- Effect of layering and front angle on pressure derivative (M = 1000)

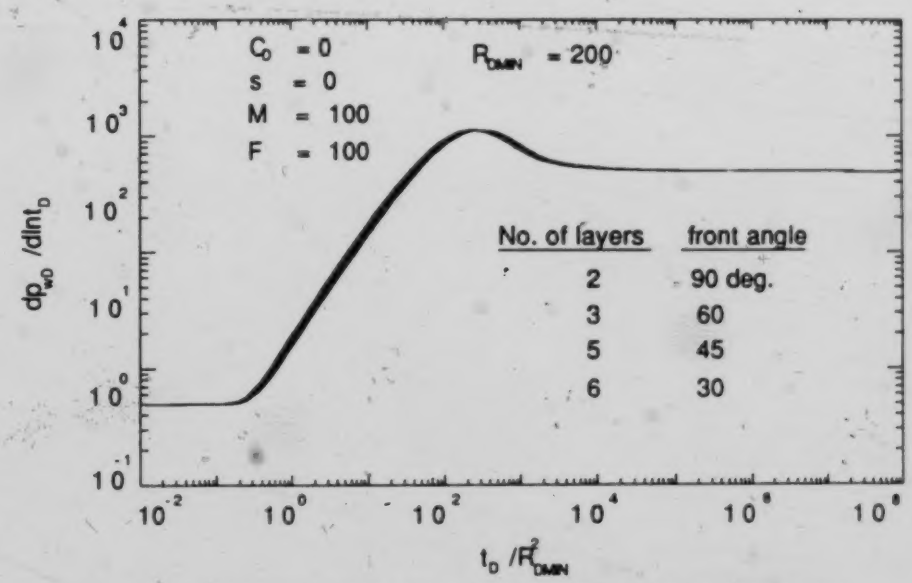

Fig. 5.18- Effect of layering and front angle on pressure derivative (M = 100)

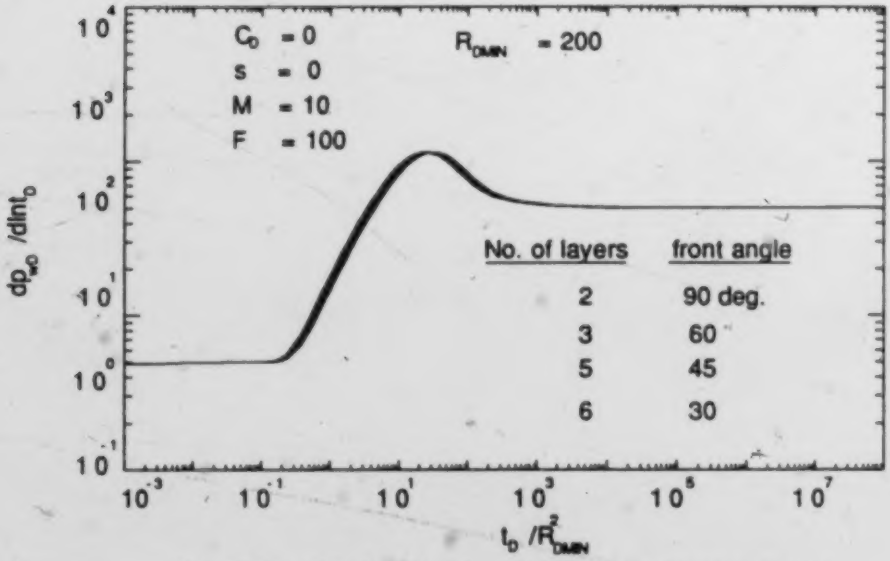

Fig. 5.19- Effect of layering and front angle on pressure derivative (M = 10)

$$(t_{De})_{end} = 0.18 \qquad 30° \le \theta \le 90° \qquad (5.13)$$

$$(t_{De})_{max} = (1.8 + 0.4 \log F)\, M \qquad 30° \le \theta \le 90° \qquad (5.14)$$

$$(t_{De})_{II} = 90(1 + \log F)\, M \qquad 10° \le \theta \le 90° \qquad (5.15)$$

5.2.4 Effect of Mobility and Storativity Ratios

Figures 5.20 through 5.22 present the effect of mobility ratio on semi-log pressure derivative behaviour for a storativity ratio of 100 and front angles of 10°, 30°, 45°, 60° and 90°. The first semi-log straight line has a slope of 0.5 and is characteristic of the mobility of the swept region. The second semi-log straight line corresponds to the outer region mobility and has a slope of M/2.[46] The pressure derivative curve attains a maximum value during the transition period (between the two semi-log straight lines) and rises above M/2, for $M \ge 1$. Mobility ratio does not affect the time to the end of first semi-log straight line for all front angles. The time to the maximum derivative and the magnitude of the maximum derivative are affected by mobility ratio.[46] The transition period is longer for higher mobility ratios. Figure 5.22 shows that the pressure response curve for front angles $\ge 45°$ is the same as that of a composite reservoir with a sharp front.

Figures 5.23 through 5.25 present the effect of storativity ratio on the semi-log pressure derivative behaviour for different front angles. A minimum front radius of 200 and a mobility ratio of 100 is used. For all front angles and a storativity ratio greater than unity, the pressure derivative curve rises to a value greater than M/2 during the transition period, and passes through a maximum slope. Storativity ratio does not affect the time to the end of the first semi-log line.[26,46] The time to the maximum derivative in the

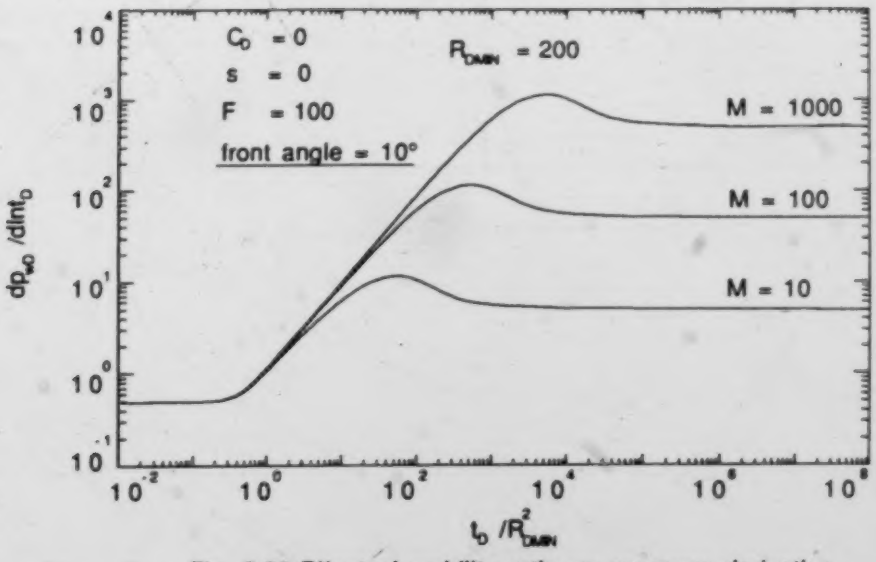

Fig. 5.20-Effect of mobility ratio on pressure derivative (front angle = 10°)

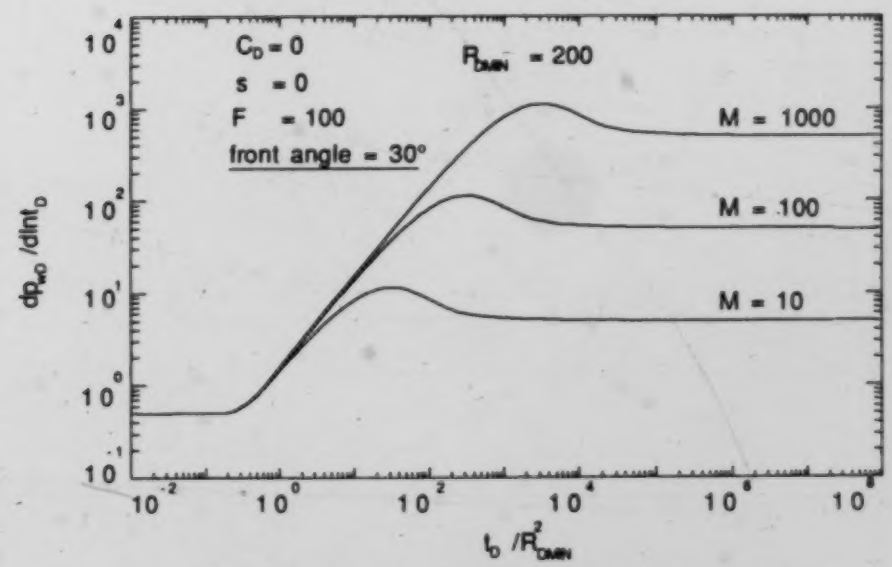

Fig. 5.21-Effect of mobility ratio on pressure derivative (front angle = 30°)

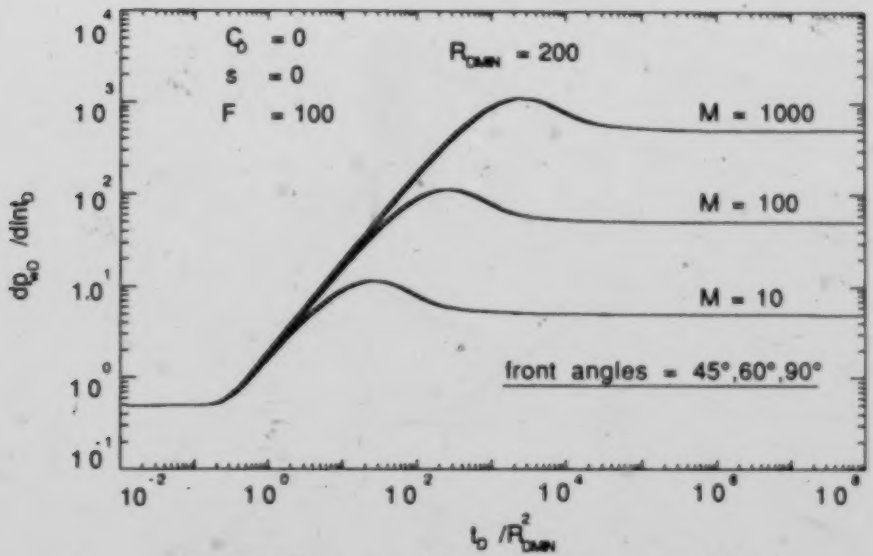

Fig. 5.22-Effect of mobility ratio on pressure derivative (front angles = 45°, 60°, and 90°)

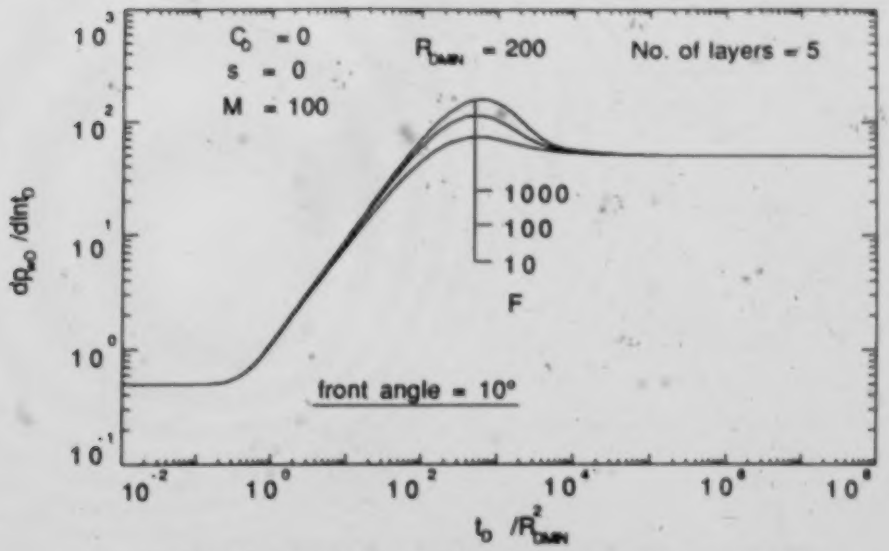

Fig. 5.23-Effect of storativity ratio on pressure derivative (front angle = 10°)

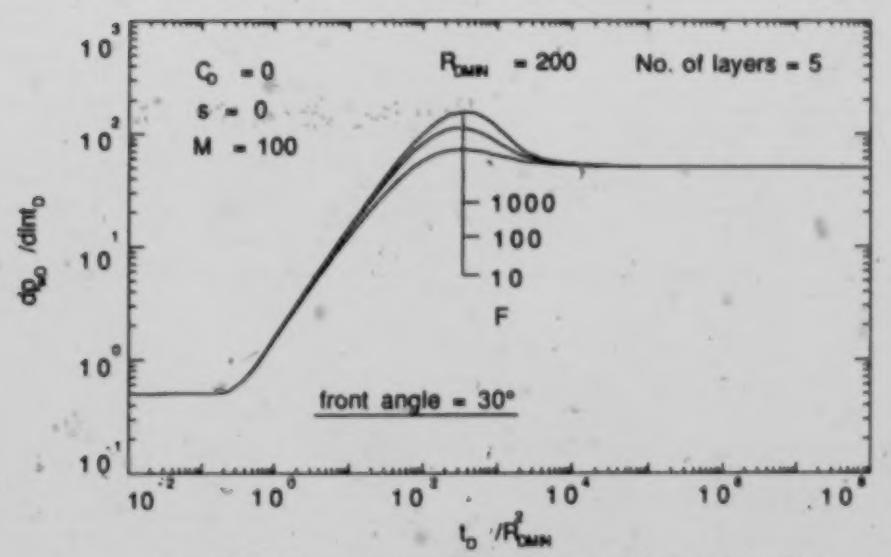

Fig. 5.24-Effect of storativity ratio on pressure derivative (front angle = 30°)

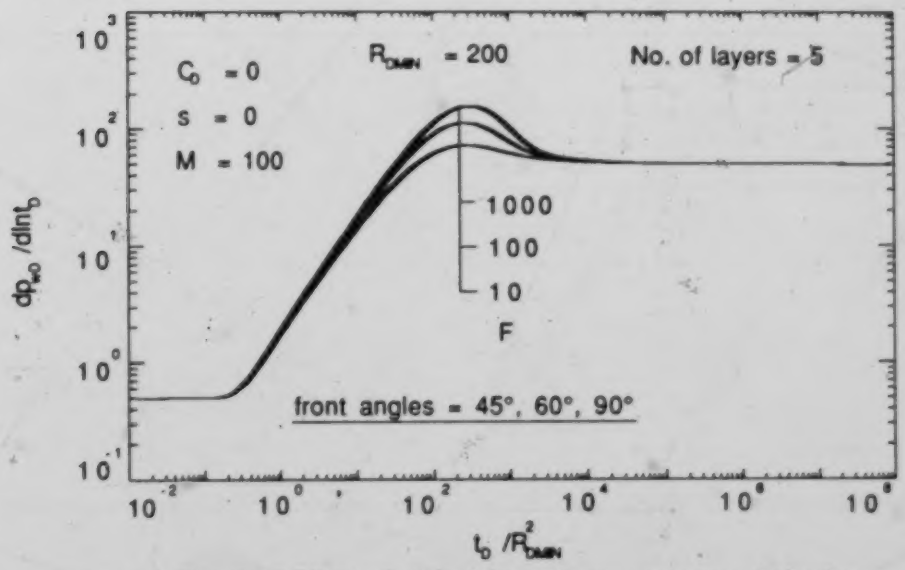

Fig. 5.25-Effect of storativity ratio on pressure derivative (front angles = 45°, 60° and 90°)

transition is mildly affected by storativity ratio, and so is the magnitude of the maximum slope. Late time transients are not affected by the storativity ratio.[26,46] These observations apply for front angles from 10° to 90°.

5.2.5 Determination of Front Radius

Pressure-time data may be used to estimate a front radius by the following methods:[46]

1. Deviation Time Method
2. Intersection Time Method
3. Type-Curve Matching Method
4. Pseudosteady State Method

The deviation time method is based on a relation between the real time to the end of the first semi-log straight line and a theoretically derived dimensionless deviation time. Various investigators have proposed different values for the dimensionless time, ranging from 0.054 to 1.39.[45] For this method, the equation used to calculate the front radius, in SI units, is:

$$R = \sqrt{\frac{(k/\mu)_1}{(\phi c_t)_1} \cdot \frac{t_{end}}{(t_{De})_{end}}} \qquad (5.16)$$

where t_{end} is the time to the end of the first semi-log line on a pressure versus log (time) graph, in seconds, and $(t_{De})_{end}$ is the dimensionless deviation time based on front radius. Depending on the value of $(t_{De})_{end}$ used, a significant difference in answers obtained for front radius will result from the use of Eq. 5.16. The intersection time between the two semi-log straight lines on a p_{wf} versus log(time) graph has also been used to estimate front radius.[47] This is the intersection time method. Reference 47 also

proposed a type-curve matching method. Automated type curve matching methods can be used to analyze thermal recovery well tests.[42] Reference 45 shows that both the Deviation Time and the Intersection Time methods are not suitable for analyzing composite reservoirs because they are sensitive to the value of dimensionless time that is applied. Also, wellbore storage may mask the first semi-log line and the well-test will not be run long enough to observe the second semi-log line.[45] A derivative type-curve matching method may be applied provided that sufficient test data are available and that appropriate conditions, as described in Ref. 45, are established.

The pseudosteady state method is based on the observation by Eggenschwiler *et al.*[22] that the swept region of a composite reservoir could behave like a closed system for a short duration after the end of the semi-log line corresponding to the inner region mobility. During pseudosteady state, a Cartesian straight line may develop whose slope is related to the front radius (or swept volume). Satman and Oskay[33] found that for reservoirs with a tilted front, as would occur due to gravity override in the case of steam-flood processes, there is not a unique straight line on the pressure-time plot following the first semi-log straight line. This non-uniqueness means that the result of these well test analyses depends on the slope of the Cartesian straight line chosen for the pseudosteady state period. In SI units, the swept volume is calculated using the following expression:

$$V_s = \frac{qB}{m_c c_t} \tag{5.17}$$

For a sharp front,

$$V_s = \pi R^2 h \phi, \tag{5.18}$$

where R is the radius of the sharp front. The error involved in the estimation of R is dependent on mobility ratio, storativity ratio and the time at which the Cartesian straight

line is drawn on the pressure-time plot.[25] Satman and Oskay[33] studied multi-layered composite reservoirs with front angles ranging from approximately 2° to 9° and compared the transient pressure responses to that of a composite reservoir with a sharp front. They found that the time to reach pseudosteady state in a composite reservoir with a tilted front can be much longer than it is for a composite reservoir with a sharp front. Those layers that have the nearest distance to the front may experience pseudosteady state while others may still be in the transient states. This behaviour was noted by Lefkovits *et al.*[3] and by Tariq and Ramey.[16] The geometry of the swept region is, therefore, a critical factor in the application of the pseudosteady state method for calculating the swept volume. The pseudosteady state method may, therefore, be used to identify the existence of a straight Cartesian line and hence avoid the non-uniqueness problem. Correlations have been developed for specific time events on a pressure derivative graph. These correlations are useful in chosing a correct PSS Cartesian straight line.[45]

5.2.6 Validity of Using an Average Radius

The swept volume of a multilayer reservoir with a tilted front can be represented by a single-layer composite reservoir having an equivalent swept volume. Consider a multilayer reservoir having n layers each with a front radius R_{Dj} and a swept volume storativity $(\phi c_t)_j$, where j represents the layer number. Let the single-layer composite reservoir have an effective storativity defined as $(\phi c_t)_{eff}$. Equating the storativity values gives:

$$\sum_{j=1}^{n} (\phi\, c_t\, h)_j = (\phi c_t)_{eff} \sum_{j=1}^{n} h_j \qquad (5.19)$$

where h_j is the thickness of each layer.

Rearranging Eq. 5.19 yields:

$$(\phi c_t)_{eff} = \frac{\sum_{j=1}^{n} (\phi c_t h)_j}{\sum_{j=1}^{n} h_j} \tag{5.20}$$

To relate the volumes of the two systems, the sum of the product of swept pore volume and compressibility of all the layers of the multilayer reservoir must be equal to the product of effective storativity and swept volume of the single-layer reservoir. If the front radius of the single-layer composite reservoir is R_{avg}, then:

$$\sum_{j=1}^{n} (\phi c_t \pi R_D^2 h)_j = [(\phi c_t)_{eff} \pi R_{avg}^2 h_t] \tag{5.21}$$

$$\text{where} \quad h_t = \sum_{j=1}^{n} h_j \tag{5.22}$$

Solving for R_{avg} gives:

$$R_{avg}^2 = \frac{\sum_{j=1}^{n} (\phi c_t R_D^2 h)_j}{(\phi c_t)_{eff} h_t} \tag{5.23}$$

Substituting for $(\phi c_t)_{eff}$ from Eq. 5.20 into Eq. 5.23 yields:

$$R_{avg} = \sqrt{\frac{\sum_{j=1}^{n} (\phi c_t R_D^2 h)_j}{\sum_{j=1}^{n} (\phi c_t h)_j}} \tag{5.24}$$

The pressure response of a multilayered composite reservoir with a tilted front can then be compared to that of a single-layer composite reservoir having equivalent properties. If the responses are found to be the same, then a single-layer composite reservoir model can be used to obtain the swept volume for a reservoir with a tilted front. Figures 5.26 through 5.28 present such a comparison for R_{Dmin} = 200 and front angles of 10°, 30°, and 60°. The validity of using R_{Davg} to represent a tilted front applies to all front angles greater than or equal to 10°, for all practical purposes. Figure 5.29 shows that the preceding observation also applies for R_{Dmin} = 2000. When analyzing the transient pressure data to obtain an estimate for the swept volume, a Cartesian straight line corresponding to the PSS behaviour for the swept volume is sought. Thus, the effect of a tilted front on Cartesian pressure derivative is considered next.

5.2.7 Pseudosteady state Analysis

The dimensionless pressure for a well in a homogeneous reservoir is given by:[48]

$$p_{wD} = 2\pi t_{DA} + \frac{1}{2}\ln\left[\frac{A}{r_w^2}\right] + \frac{1}{2}\ln\left[\frac{2.2458}{C_A}\right] \qquad (5.20)$$

where t_{DA} is the dimensionless time based on area. For a multilayered composite system, t_{DA} should be based on the swept area, where $A = \pi R_{avg}^2$. A Cartesian pressure derivative would be 2π during the pseudosteady state period. This is shown in Fig. 5.30 for mobility and storativity ratios of 1000, and a front angle of 60° represented by 3, 5, 6 and 10 layers having a minimum front radius of 200. A slope of -1 appears during the infinite-acting radial flow regimes of the inner and outer regions on the same log-log scale. Figure 5.30 shows that any number of layers greater than 2 used to represent a tilted front is satisfactory.

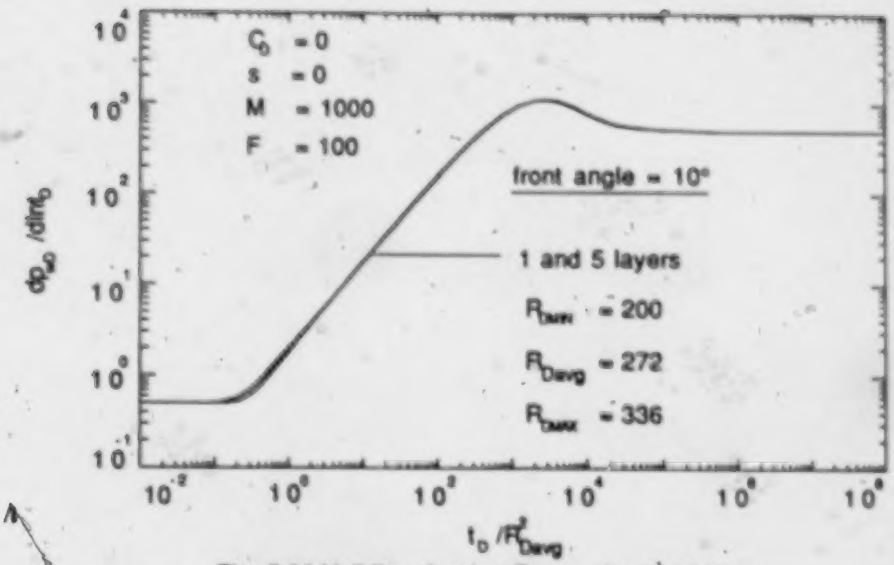

Fig. 5.26-Validity of using R_{Davg} for tilted front (front angle = 10°)

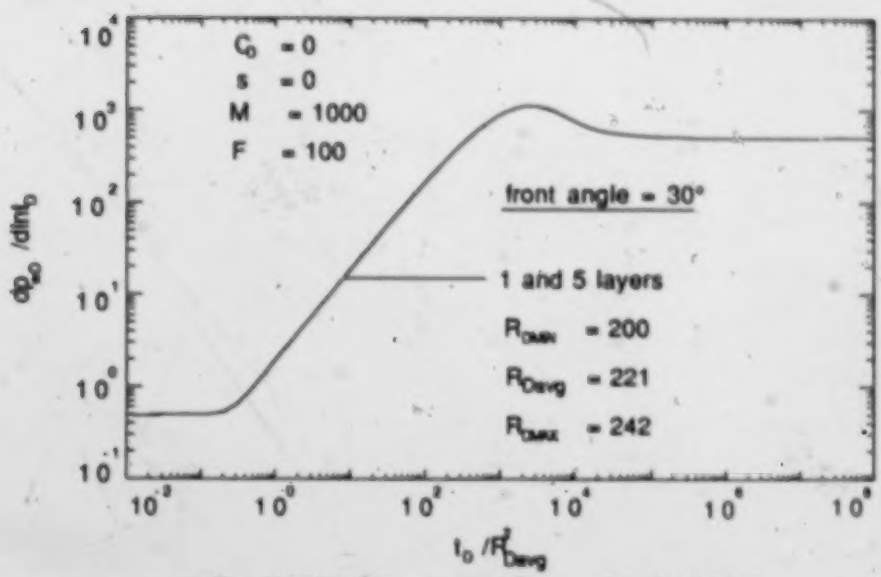

Fig. 5.27-Validity of using R_{Davg} for tilted front (front angle = 30°)

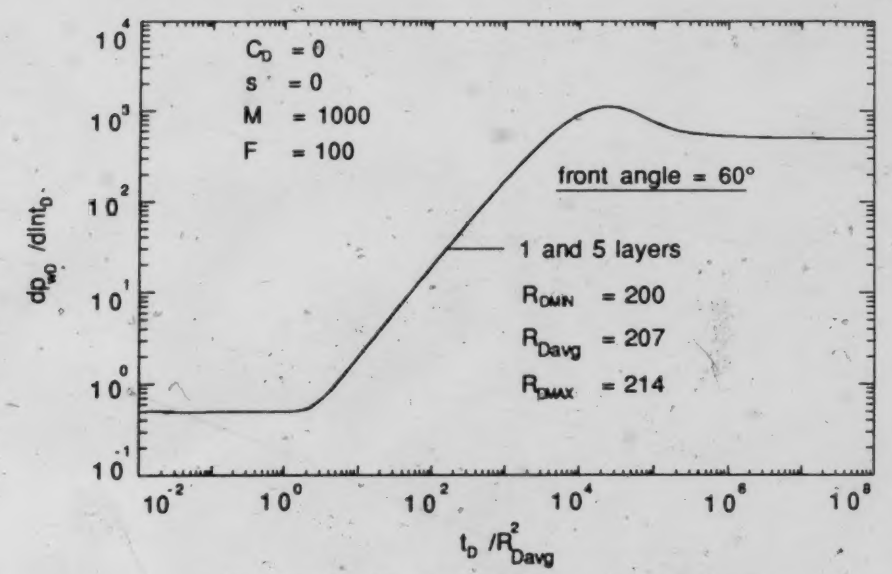

Fig. 5.28-Validity of using R_{Davg} for tilted front
(front angle = 60°)

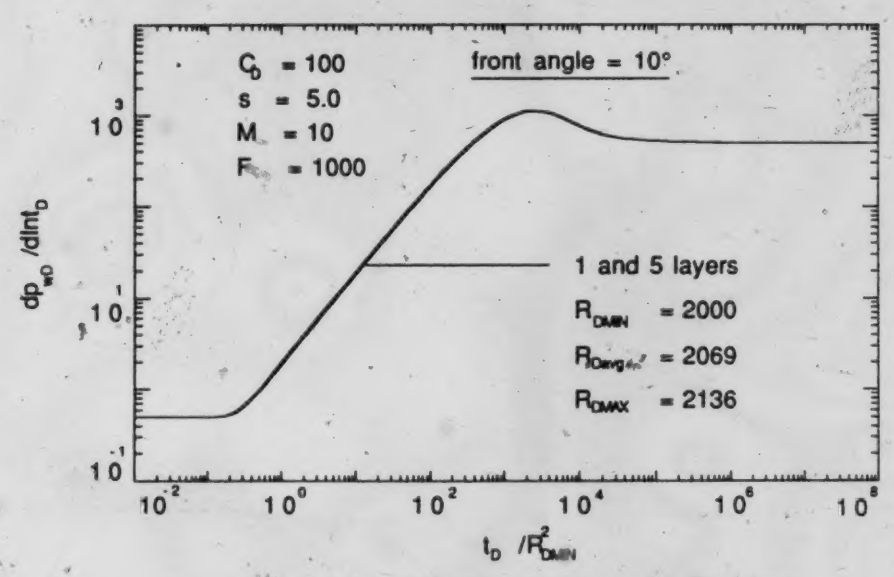

Fig. 5.29 - Validity of using R_{Davg} for tilted front
(R_{DMIN} = 2000, front angle = 10°)

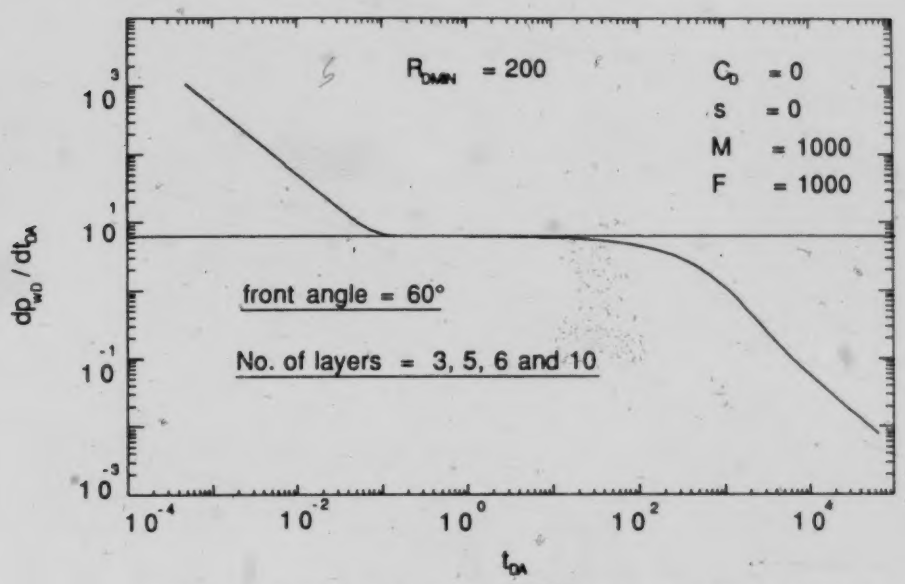

Fig. 5.30-Effect of number of layers on cartesian derivative (front angle = 60°)

Figures 5.31 through 5.35 present the effect of minimum front radius on the Cartesian derivative. Minimum dimensionless front radii of 100, 200 and 1000 are used for a five-layer reservoir with a mobility ratio of 1000, a storativity ratio equal to 100, C_D and skin of zero, for angles of 10°, 20°, 30°, 45° and 60°, respectively. Figures 5.31 and 5.32 show that for front angles of 10° and 20°, the dimensionless minimum front radius affects the time to the beginning of pseudosteady state and the duration thereof. A type-curve matching procedure is recommended to analyze the combined effects of minimum front radius and front angle on well test data. However, given noise in real data, it may be difficult to distinguish between data for a minimum dimensionless front radius of 100 and 1000. For front angles in the $30° \leq \theta \leq 90°$ range, dimensionless minimum front radius has no effect on the Cartesian derivative graph. This is shown by the existence of a single curve in Figures 5.33 through 5.35.

Figure 5.36 presents the effect of mobility ratio on the Cartesian derivative for a storativity ratio of 100, a front angle of 45° represented by 5 layers and a minimum front radius of 200. As shown before, early and late time pressure derivative data show a slope of -1 on a Cartesian log-log graph. At the beginning of pseudosteady state, a constant slope of 2π results. The duration of this constant slope increases with increasing mobility ratio. Figure 5.37 presents the effect of storativity ratio on the Cartesian pressure derivative for a 5-layer composite reservoir with a front angle of 45° having a mobility ratio of 100. Early and late time slopes are -1 and the duration of pseudosteady state increases with increasing storativity ratio. Storativity ratio affects the intermediate pressure derivative values in the transition period. However, storativity ratio has no effect on the late time behaviour of the Cartesian derivative. Correlations for the time to the end of pseudosteady state behaviour for a single-layer composite system

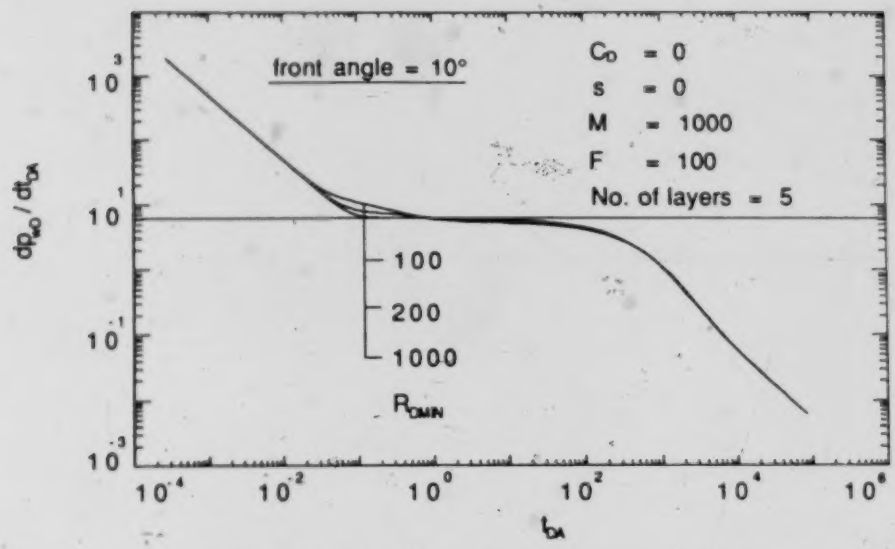

Fig. 5.31-Effect of minimum front radius on cartesian derivative (front angle = 10°)

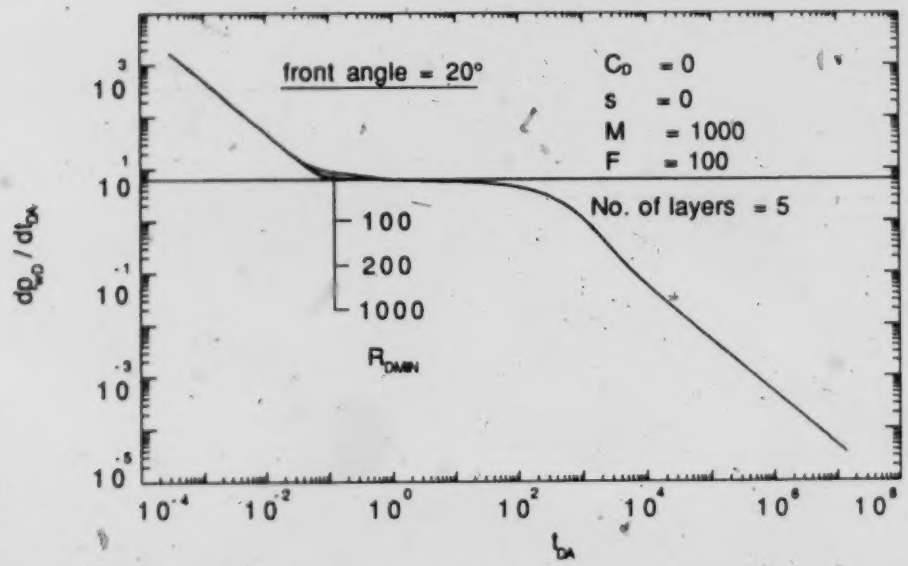

Fig. 5.32-Effect of minimum front radius on cartesian derivative (front angle = 20°)

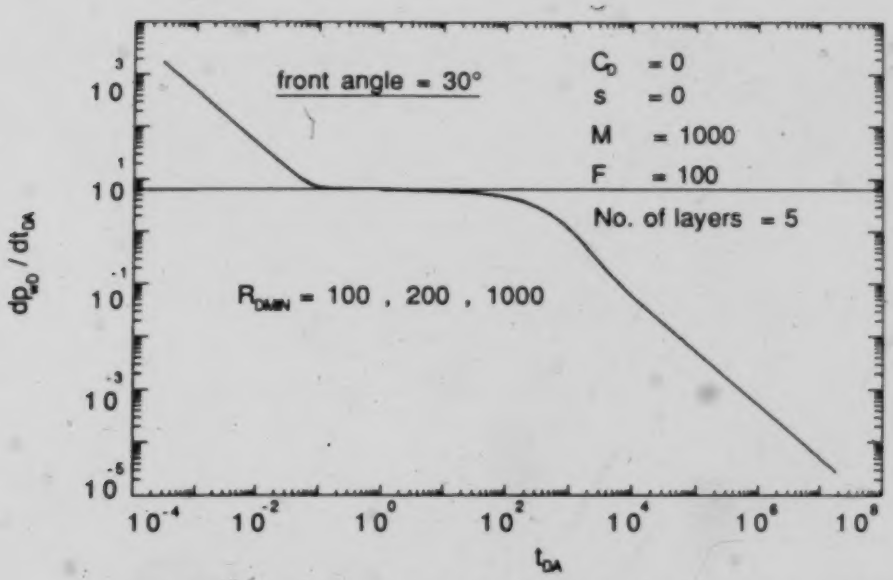

Fig. 5.33-Effect of minimum front radius on cartesian derivative (front angle = 30°)

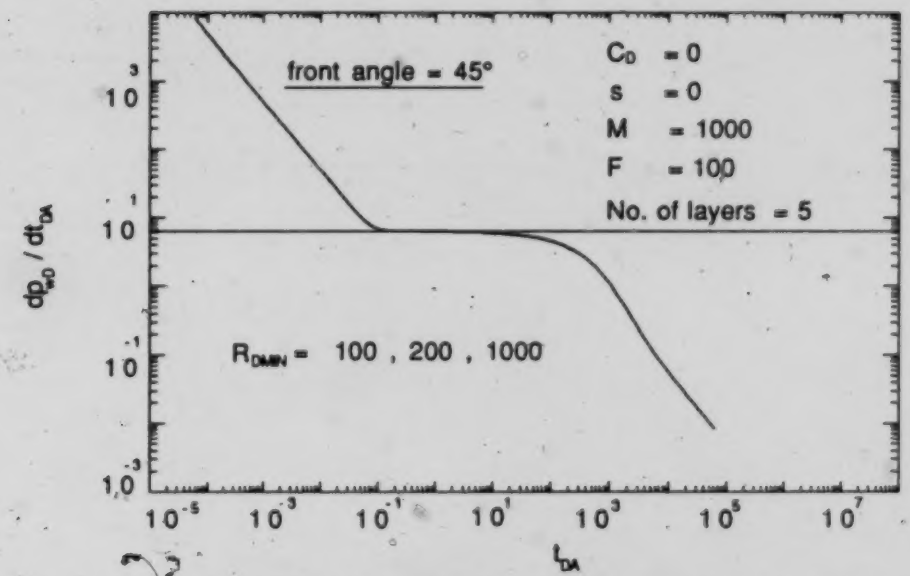

Fig. 5.34-Effect of minimum front radius on cartesian derivative (front angle = 45°)

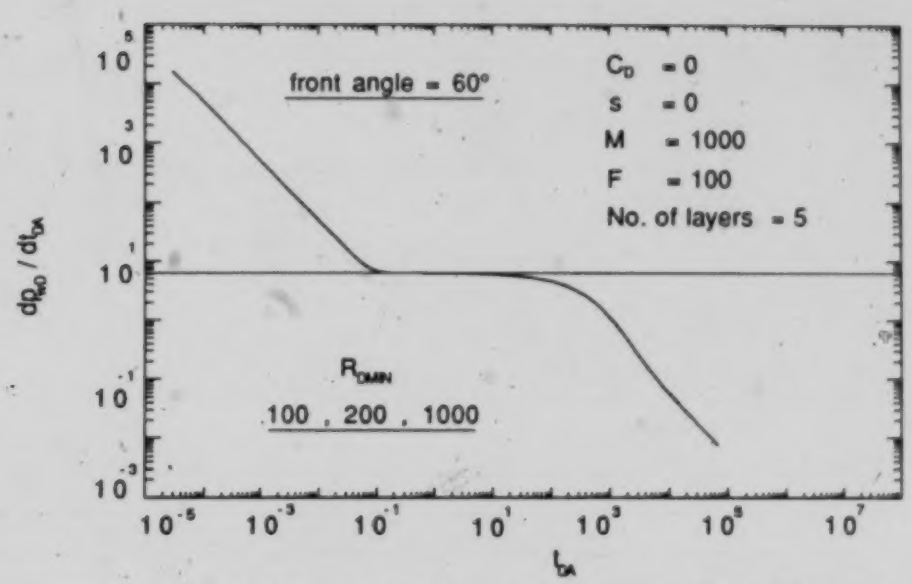

Fig. 5.35-Effect of minimum front radius on Cartesian derivative (front angle = 60°)

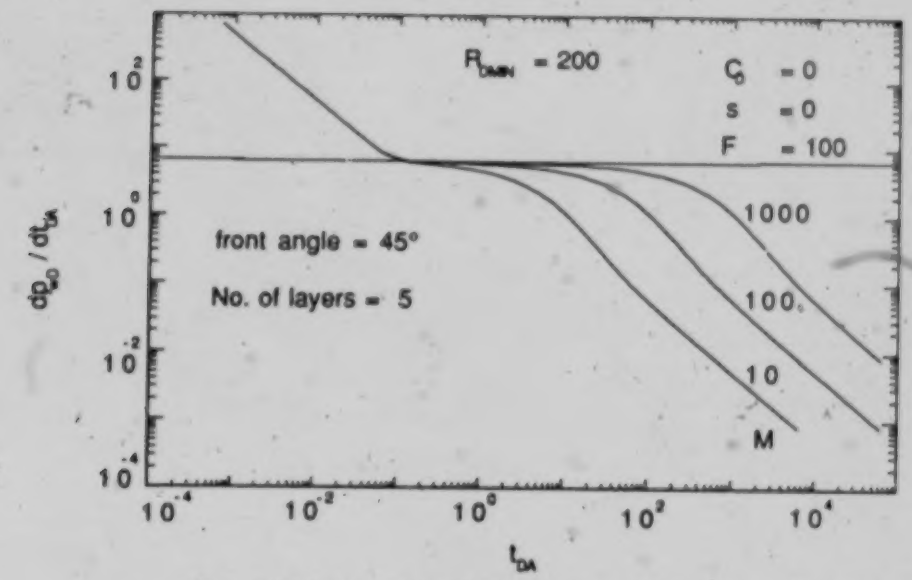

Fig. 5.36-Effect of mobility ratio on Cartesian derivative

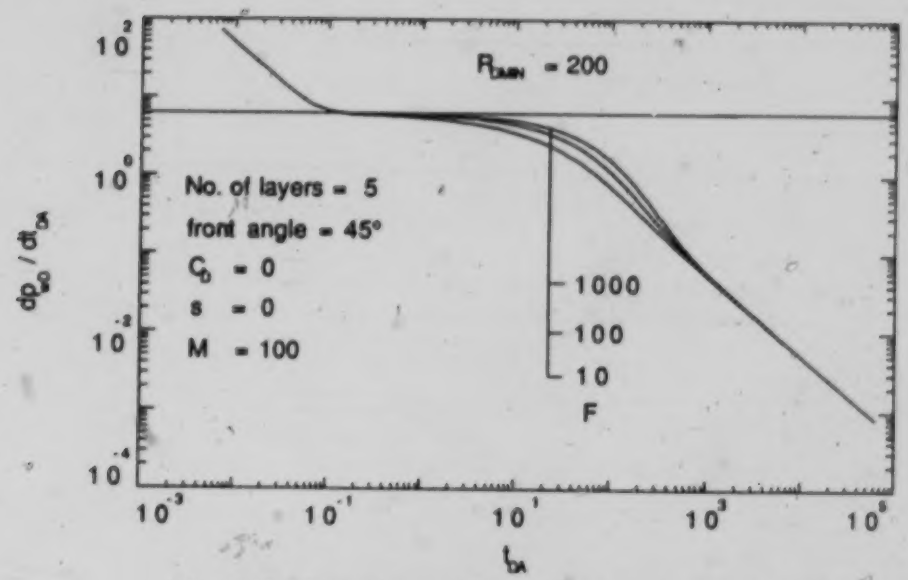

Fig. 5.37-Effect of storativity ratio on Cartesian derivative

as developed by Ambastha[45] will also apply for all front angles studied in this work, i.e., $10° \leq \theta \leq 90°$.

Figures 5.38 through 5.40 present the effect of front angle on the Cartesian derivative for a 5-layer system with M = 1000, F = 100, R_{Dmin} = 200 and front angles of 10°, 20°, and 30° and 90°, respectively. Figure 5.36 shows that a constant slope of 2π does not appear at all for a front angle of 10°. Similar observations were made by Satman and Oskay[33] when they studied a five-layer system with front angles ranging from approximately 2° to 9°. They concluded that only the swept volume up to the nearest distance to the front may be calculated based on the slope of the apparent Cartesian straight line. Figure 5.38 indicates that for a 10° front angle, a constant Cartesian pressure derivative would not develop on well-test data to indicate the existence of pseudosteady state behaviour, for the mobility and storativity ratios studied here. Figure 5.37 presents a similar plot for a front angle of 20°. A slope of 2π is evident although it takes longer to develop compared to the case when the front is sharp. This was noted also by Satman and Oskay.[33] For a sharp front, a slope of 2π appears at t_{DA} = 0.1. While Ref. 33 suggested that the time to reach pseudosteady state in a composite system with a tilted front can be much longer than it is for a composite reservoir with a sharp front, this study shows that this applies only for the case when $\theta < 20°$, if pseudosteady state occurs at all. For $30° < \theta < 90°$, as shown in Fig. 5.40, pseudosteady state occurs shortly after the end of the first semi-log straight line. The pressure transient responses for a multi-layered reservoir with tilted front angles greater than or equal to 30° are the same as that of a composite reservoir with a sharp front.

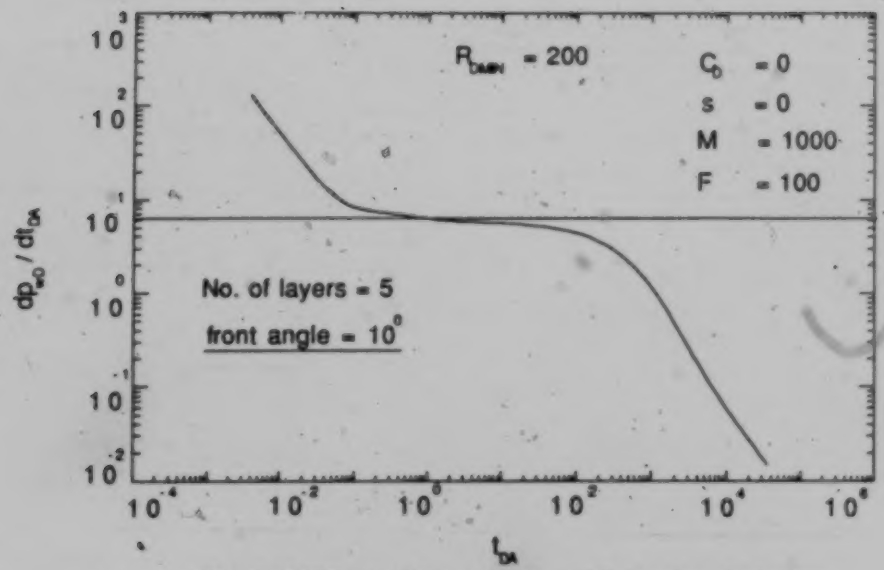

Fig. 5.38-Effect of front angle on Cartesian derivative (front angle = 10°)

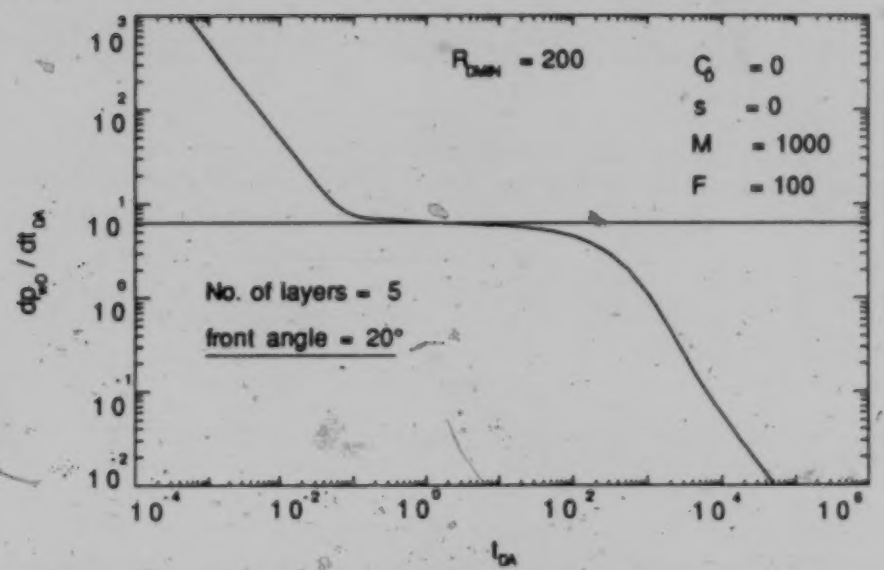

Fig. 5.39-Effect of front angle on Cartesian derivative (front angle = 20°)

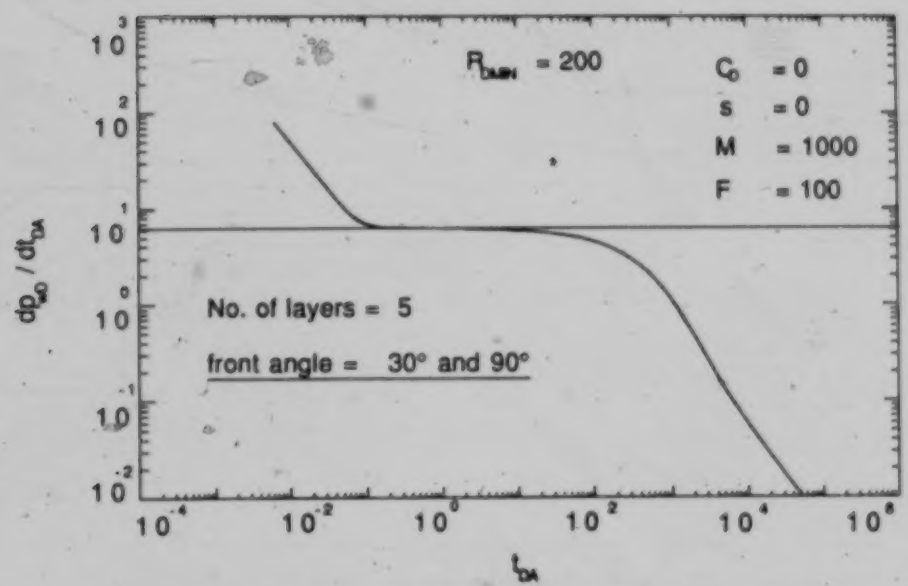

Fig. 5.40-Effect of front angle on Cartesian derivative
(front angle = 30°and 90°)

5.2.8 Sensitivity Studies

Preliminary drawdown sensitivity studies have been performed to investigate further the effects of front angle and layer properties. These studies intend to explore other areas of research that require detailed analysis depending on how certain parameters may influence the pressure derivative curve. This section is necessarily limited due to the many possible combinations of composite reservoir parameters that may occur.

Using five layers, the effect of individual layer mobilities on the pressure derivative was investigated for front angles of 10° and 60°. A minimum front radius of 200, a mobility ratio of 10, and a storativity ratio of 1000 were used in the analysis. The magnitude of mobility is different for each layer, but mobility ratio is the same for every layer. Relative storativities are the same for each layer, in a given region. Effects of skin and wellbore storage are not considered. Table 5.2 presents data used in the analysis, for the case of mobility increasing from "top to bottom". Relative mobility values for each layer and each region are shown. Table 5.3 presents data for the case of mobility increasing from "bottom to top". Table 5.4 presents data for the case of a "random pattern" mobility among the five layers. Figures 5.41 and 5.42 present the effect of the different patterns of layer mobilities on pressure derivative. The three patterns considered here are for the cases shown in Tables 5.2 through 5.4. The magnitude of front angle has an effect on the time to the end of the first semi-log straight line. The time to the maximum derivative and the magnitude of the maximum derivative are dependent on the slope of the tilted front. The average permeability is constant for all the three cases represented by Tables 5.2 through 5.4. Kucuk *et al.*[19] studied layered reservoirs without crossflow and concluded that individual layer properties cannot be estimated uniquely from the

Table 5.2 : Mobility increasing from 'top to bottom'.

layer number	REGION 1		REGION 2	
	mobility (k/μ)	relative mobility	mobility (k/μ)	relative mobility
1	1000	0.602	100	0.0602
2	500	0.301	50	0.0301
3	100	0.0602	10	0.00602
4	50	0.0301	5	0.00301
5	10	0.00602	1	0.000602

Table 5.3 : Mobility increasing from 'bottom to top'.

layer number	REGION 1		REGION 2	
	mobility (k/μ)	relative mobility	mobility (k/μ)	relative mobility
1	10	0.00602	1	0.000602
2	50	0.0301	5	0.00301
3	100	0.0602	10	0.00602
4	500	0.301	50	0.0301
5	1000	0.602	100	0.0602

Table 5.4 : 'Random mobility' pattern

layer number	REGION 1		REGION 2	
	mobility (k/μ)	relative mobility	mobility (k/μ)	relative mobility
1	10	0.00602	1	0.000602
2	1000	0.602	100	0.0602
3	100	0.0602	10	0.00602
4	50	0.0301	5	0.00301
5	500	0.301	50	0.0301

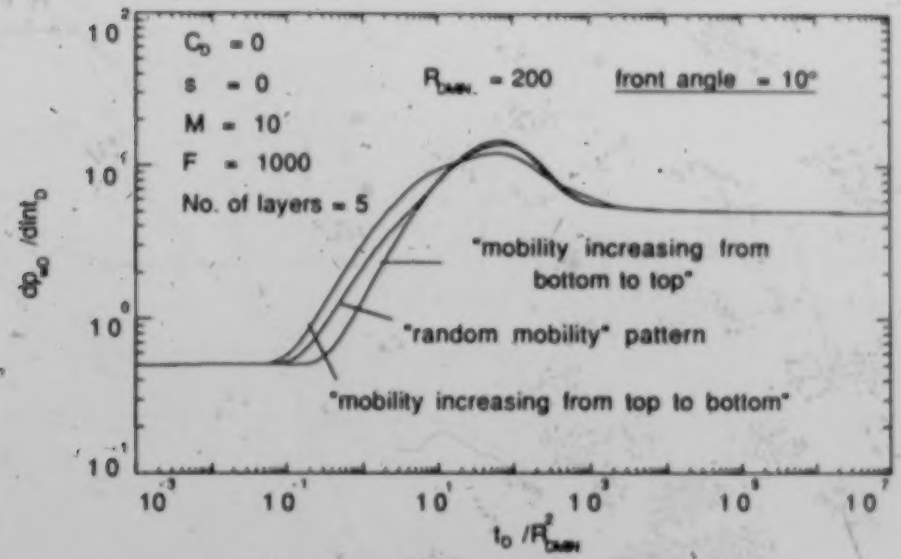

Fig. 5.41-Effect of different patterns of layer mobilities on pressure derivative (front angle = 10°)

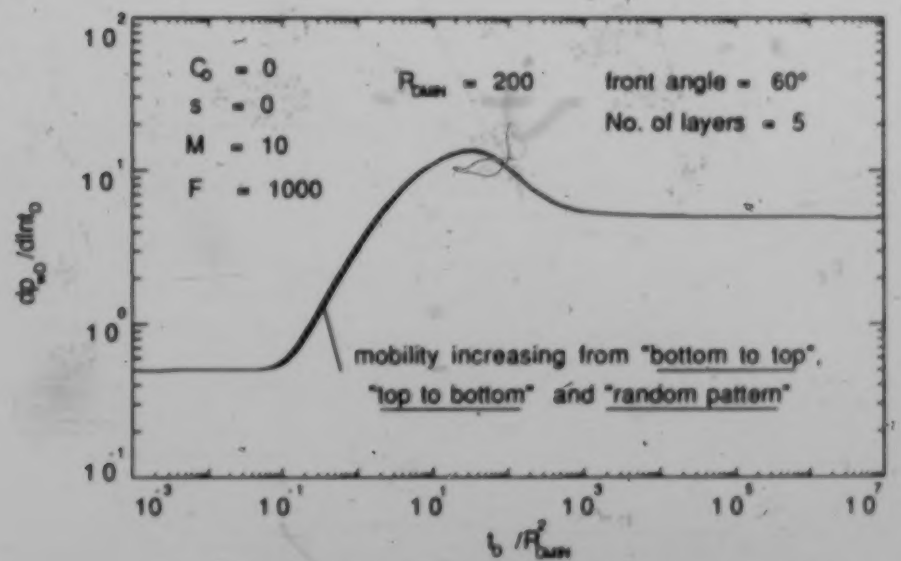

Fig. 5.42-Effect of different patterns of layer mobilities on pressure derivative (front angle = 60°)

conventional drawdown or buildup tests using only wellbore pressure data. Only average properties can be calculated. Layer parameters can be estimated uniquely from measured wellbore and sandface rates which are acquired from each layer simultaneously.[10,19,20] These investigators[10,19,20] performed their studies on layered reservoirs, with or without crossflow. The study of a similar approach should be conducted for the analysis of layered composite reservoirs with a tilted front.

Larsen[18] studied the effects of wellbore skin factors of individual layers for an infinitely-large reservoir without interlayer crossflow. By using only wellbore pressures, he proposed some general methods to determine both skin factors and flow capacities for each layer. Skin factors were found to affect the appearance of the conventional semi-log straight line.[18] If a reservoir exhibits single-layer behaviour, an effective skin for multilayered reservoirs can be determined.[18] Figure 5.43 presents the effect of skin on pressure derivative for the cases of (1) equal skin in every layer and (2) different values of skin for every layer. Figure 5.43 shows that having variable skin factors among the layers has an effect on the slope of the first semi-log straight line and also the intermediate time response to some extent. Late time response is not affected by the skin factors. The parameters used in Fig. 5.43 are: $M = 10$, $F = 1000$, $R_{Dmin} = 200$, and a front angle of 10° represented by five layers. The effect of variable skin factors among layers on pressure and Cartesian derivatives can be studied for various front angles to determine any correlations that may exist. The effects of wellbore storage are considered next.

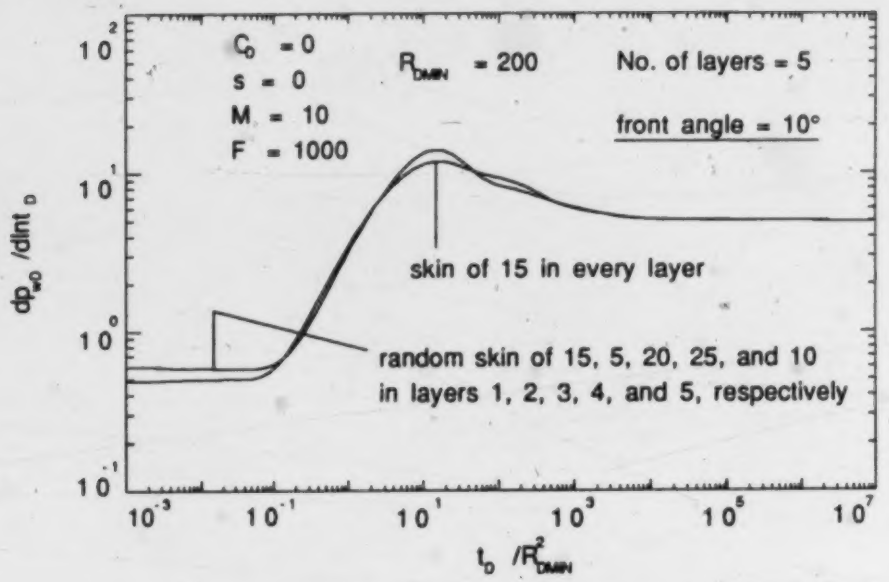

Fig. 5.43- Effect of skin on pressure derivative

5.2.9 Wellbore Storage Effects

Wellbore storage, C_D, can mask the appearance of the first semi-log straight line and the transition region in a pressure derivative curve, depending on the magnitude of C_D. During the storage-dominated region, a log-log graph of semi-log pressure derivative exhibits a unit slope. Agarwal *et al.*[44] used C_D and s as parameters to present the pressure drawdown behaviour of a well with skin and wellbore storage producing at a constant rate. References 49 and 50 used C_De^{2s} as a correlation parameter to present the pressure drawdown behaviour of a well producing at a constant rate from a homogeneous reservoir. For a composite reservoir with a sharp front, Ambastha[45] validated the use of C_De^{2s} and R_D^2/C_D as correlation parameters. Figure 5.44 presents the effect of C_De^{2s} on the pressure derivative. A single line appears in the early time data for all front angles considered. A three-layer reservoir with a skin factor of 5.0 in every layer and a wellbore storage of 4.54 is used in Fig. 5.44. The mobility ratio is 10, F = 1000, and R_{Dmin}= 200. Figures 5.45 and 5.46 show the effects of different values of C_De^{2s} on the pressure derivative for layered composite reservoirs. A mobility ratio of 10 and a storativity ratio of 1000 are used. Figure 5.45 shows the pressure derivative response for a reservoir with a front angle of 60°, represented by 3 and 5 layers, with C_De^{2s} as a correlating parameter. Increasing the value of C_De^{2s} increases the time for which pressure transients are dominated by wellbore storage effects. Figure 5.46 shows the pressure derivative response for a layered composite reservoir with a front angle of 45°, for different values of C_De^{2s}. By varying any or all of the parameters used to develop Fig. 5.46, suitable type-curves may be prepared from the computer program in App. A.

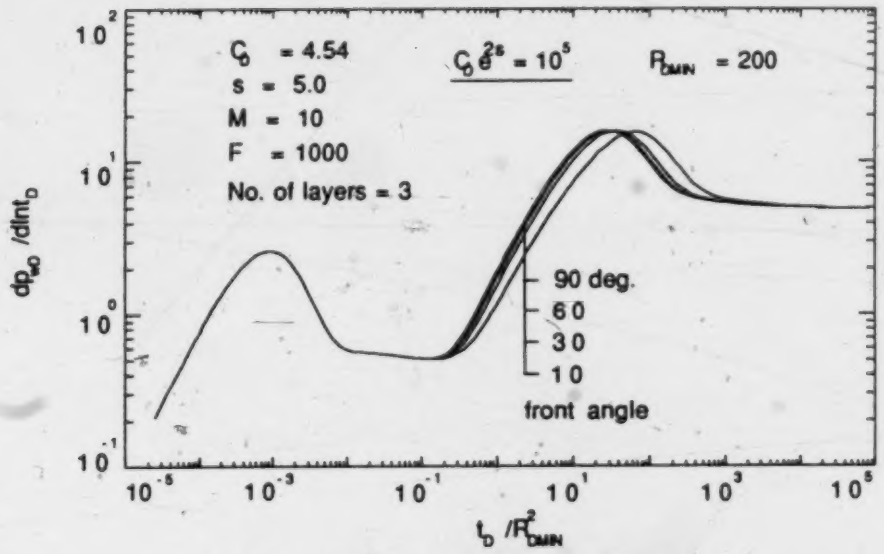

Fig. 5.44 - $C_D e^{2s}$ as a correlation parameter.

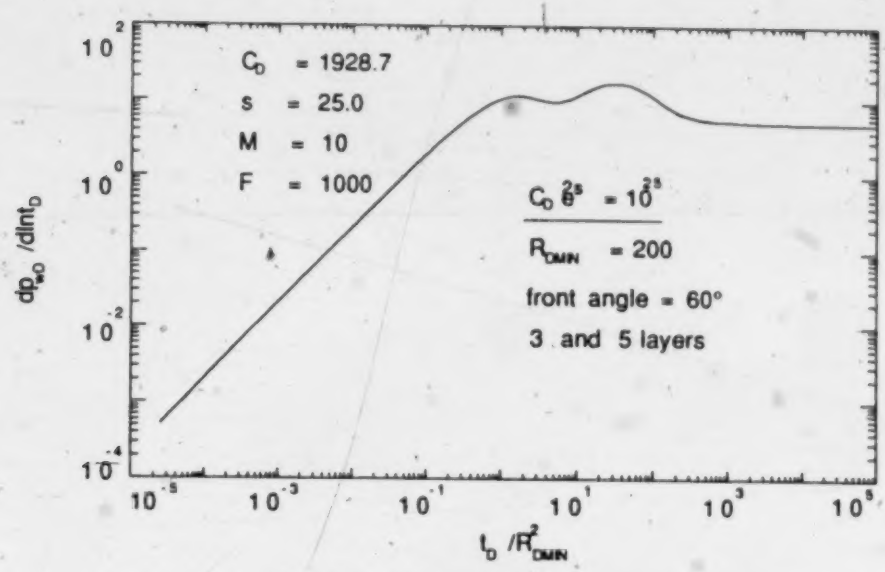

Fig. 5.45- Effect of $C_D e^{2s}$ on pressure derivative
(front angle = 60°)

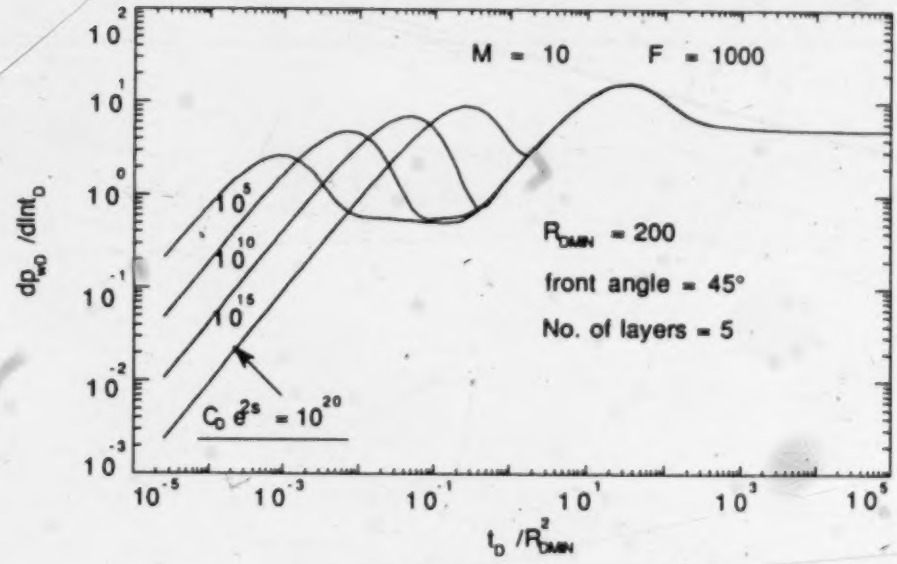

Fig. 5.46- Effect of $C_D e^{2s}$ on pressure derivative
(front angle = 45°)

5.2.10 Effects of Complex Front Shapes

Vogel[51] proposed a steam injection model in which steam override due to gravity would occur almost instantaneously within the region closest to the injection well. The steam front would, therefore, be very steep close to injection point and then level-off almost horizontally along the top section of the payzone. Figures 5.47 through 5.50 show four possible model configurations (Cases A, B, C, D) of the steam front. The model consists of a 10-layer composite reservoir with a minimum front radius R_{Dmin} = 200. The bottom six layers have different front radii in each layer representing a front angle of 60°. For case A, the remaining four layers have a 20° slope across layers 7 and 8, followed by a 10° slope across layers 9 and 10. This is shown schematically in Fig. 5.47. In case B, a 20° front angle runs across layers 7 through 10, as shown in Fig. 5.48. Figure 5.49 shows a schematic diagram for case C, where the top four layers have front radii representing a 10° slope. Figure 5.50 shows a schematic for case D in which a 60° front angle is represented by all 10 layers of the model. Table 5.5 presents the values of front radii for each layer for the four different cases. Figure 5.51 presents the effect of the shape of the front, for the four different cases, on the drawdown pressure derivative curve. All the four cases described above produce derivative curves that are indistinguishable from each other. The common parameters used in the four models are shown in Fig. 5.51. A Cartesian derivative plot is shown in Fig. 5.51. A short duration constant slope of 2π appears for all cases, but there are no differences among the curves, for all practical purposes. The value of average front radius, R_{Davg}, used in the x-axis of the Cartesian derivative graph of Fig. 5.52 is calculated using Eq. 5.19. Based on the model used in this study, transient pressure response is not sensitive to the presence of a steam chest in the top portions of the reservoir.

CASE A

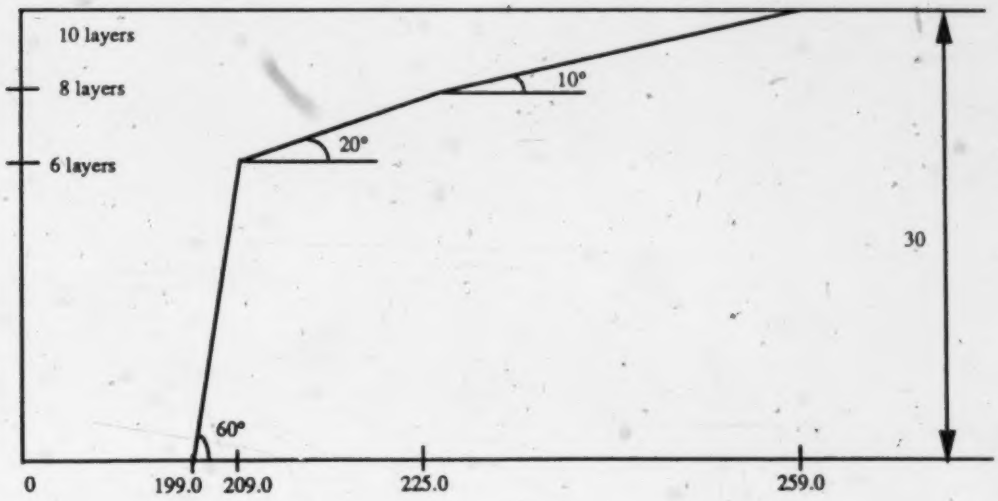

Fig. 5.47 : A schematic diagram for case A of Table 5.5

CASE B

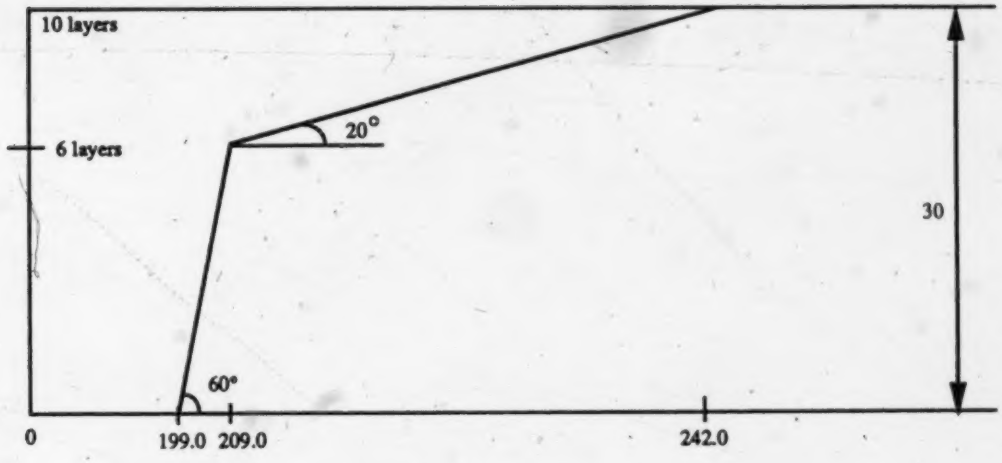

Fig. 5.48: A schematic diagram for case B of Table 5.5

CASE C

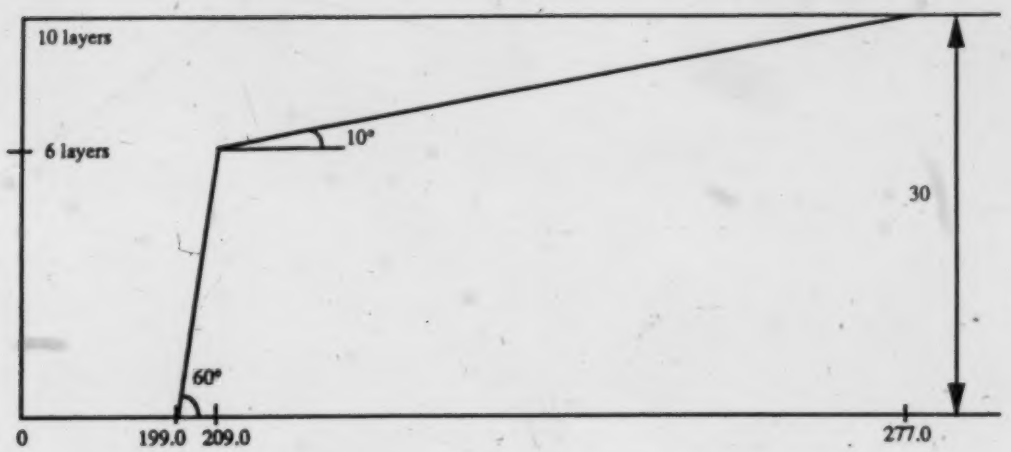

Fig. 5.49 : A schematic diagram for case C of Table 5.5

CASE D

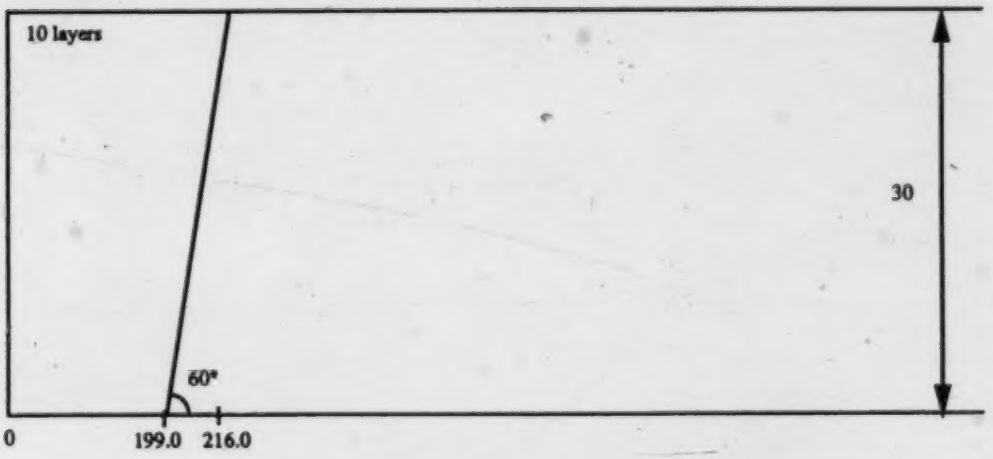

Fig. 5.50 : A schematic diagram for case D of Table 5.5

Table 5.5 : Front radii for Cases A, B, C, and D

layer No. (top to Bottom)	CASE A	CASE B	CASE C	CASE D
1	259.0	242.0	277.0	216.0
2	244.0	235.0	261.0	214.0
3	225.0	225.0	244.0	212.0
4	218.0	218.0	227.0	210.0
5	209.0	209.0	209.0	209.0
6	207.0	207.0	207.0	207.0
7	205.0	205.0	205.0	205.0
8	203.0	203.0	203.0	203.0
9	202.0	202.0	202.0	202.0
10	200.0	200.0	200.0	200.0
R_{avg}	219.0	216.0	226.0	209.0

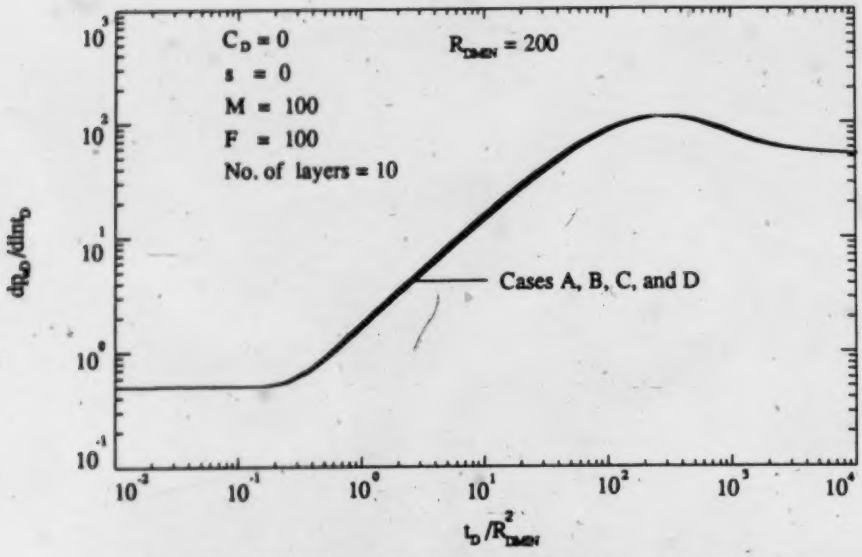

Fig. 5.51-Effect of a steam chest on pressure derivative.

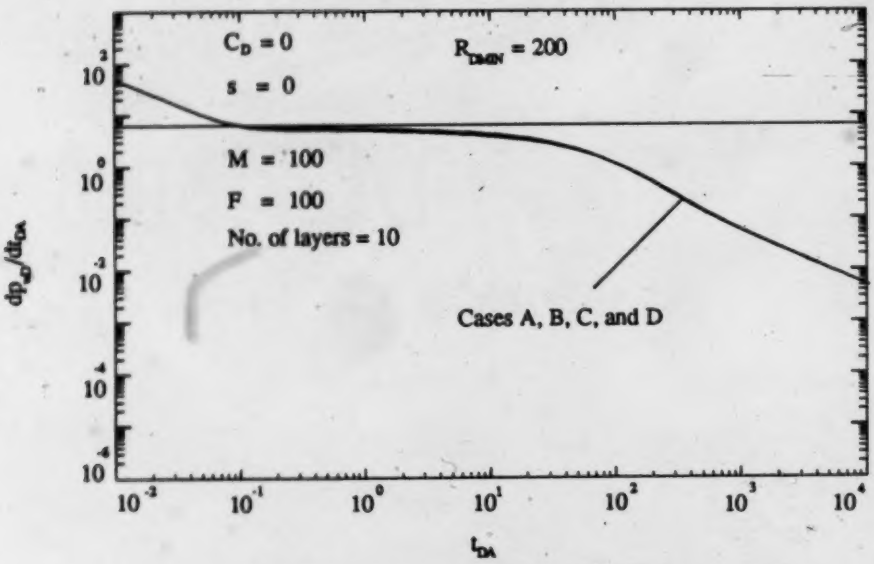

Fig. 5.52-Effect of a steam chest on Cartesian derivative.

Figure 5.53 presents a schematic diagram for two front shapes E and F. The shapes are represented by a five-layer reservoir with M = 1000, F = 100 and C_D = s = 0.0. Front radii values representing the front shape for Case E are depicted at the bottom scale of Fig. 5.53. For Case F, the bottom two layers have front radii of 808 and 500. Case E has R_{Dmin} = 100 while Case F has R_{Dmin} = 500. The swept volumes of the two cases are equal. Figure 5.54 presents a schematic for Case G which also has R_{Dmin} = 100. The swept volume of Case G is equal to that of cases E and F. Also, the properties of the respective regions are the same for the three cases. Figure 5.55 presents the Cartesian pressure derivative response for cases E, F and G. Pseudosteady state does not occur for any of these three cases. The responses from cases E and G are the same, and are different from that of Case F. Figure 5.55 shows that the shape of the Cartesian derivative curve is influenced by the minimum front radius. Figure 5.56 presents the pressure derivative response for a five-layer composite reservoir with front angles of 10° and 170°. A 10° slope has the minimum radius assigned to the bottom layer and the maximum radius at the top-most layer. A front angle of 170° is obtained by reversing the order of front radius values among the layers such that R_{Dmin} is at the top-most layer and R_{Dmax} at the bottom layer. The swept volumes represented by the two angles are equal. The pressure derivative response is essentially the same for these two angles implying that for equal values of R_{Dmin} and swept volume, the pressure transient responses will also be the same. Figure 5.57 presents the effect of storativity variation for a layered composite reservoir on the Cartesian pressure derivative. Both curves A and B in Fig. 5.57 are for a 5-layer reservoir with a front angle of 10° and M = 1000. For curve B, different values of steam compressibilities in each of the five layers are used to simulate a steam-flood project where extreme gravity override has occurred. Storativity values

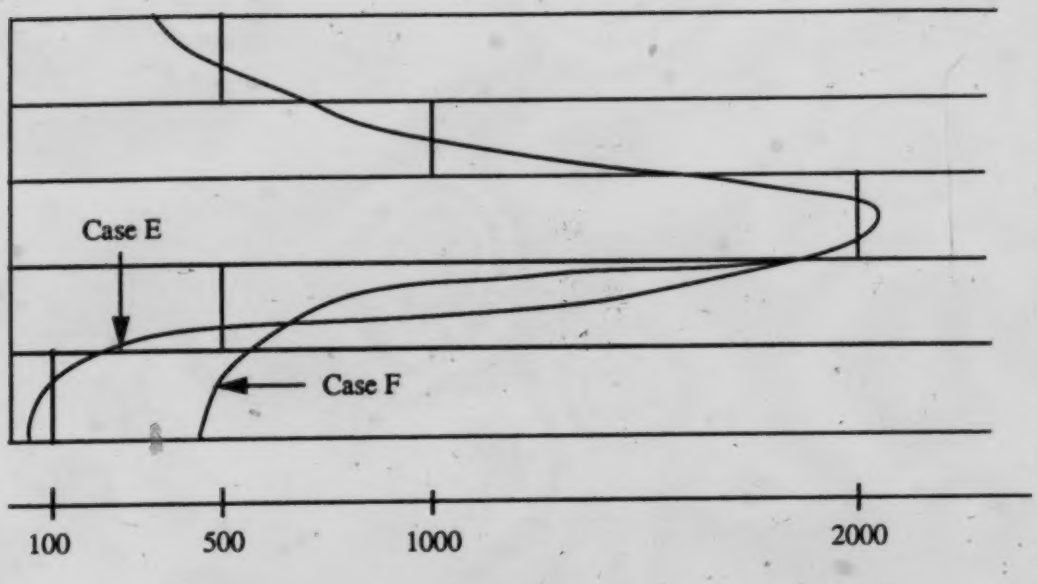

Fig. 5.53 : A schematic diagram for cases E and F

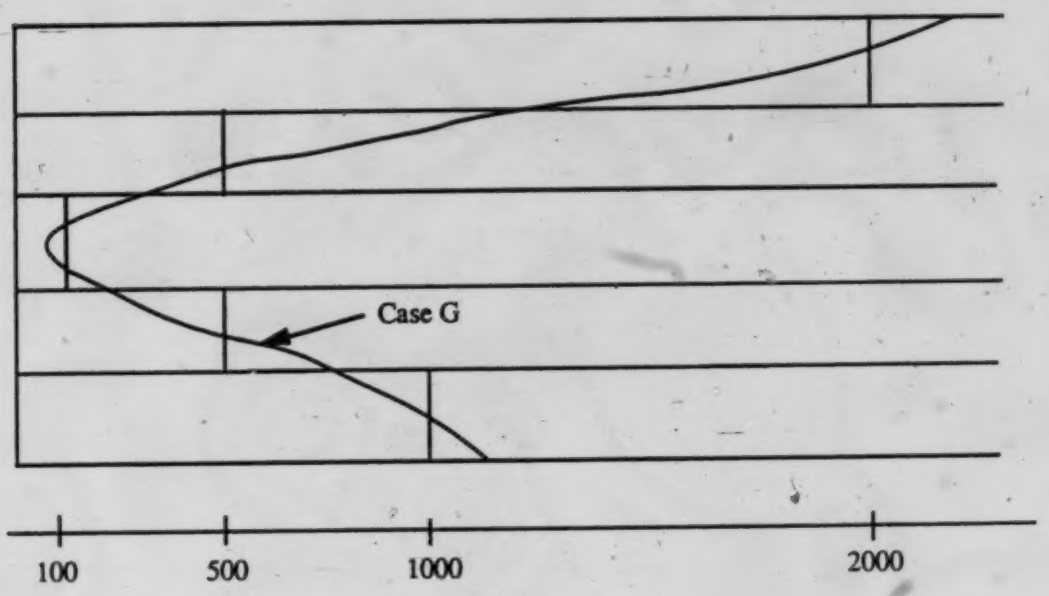

Fig. 5.54 : A schematic diagram for case G

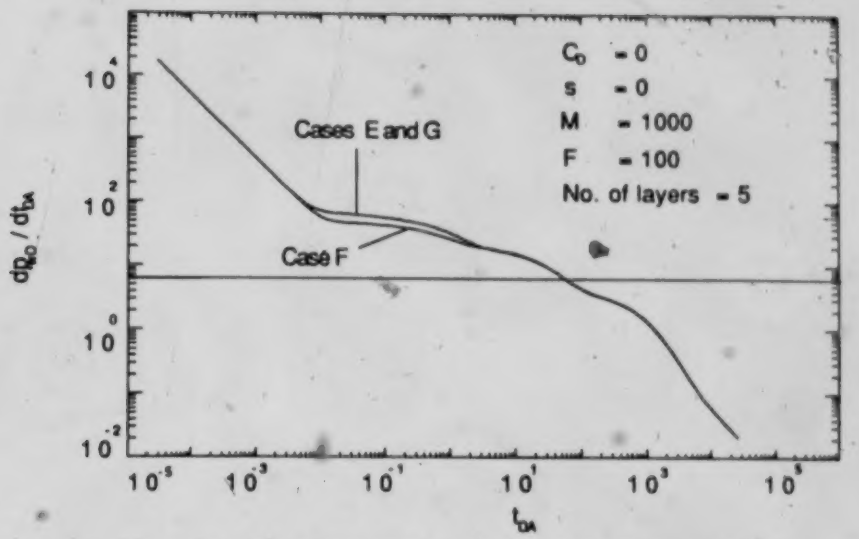

Fig. 5.55- Effect of front shapes on Cartesian derivative

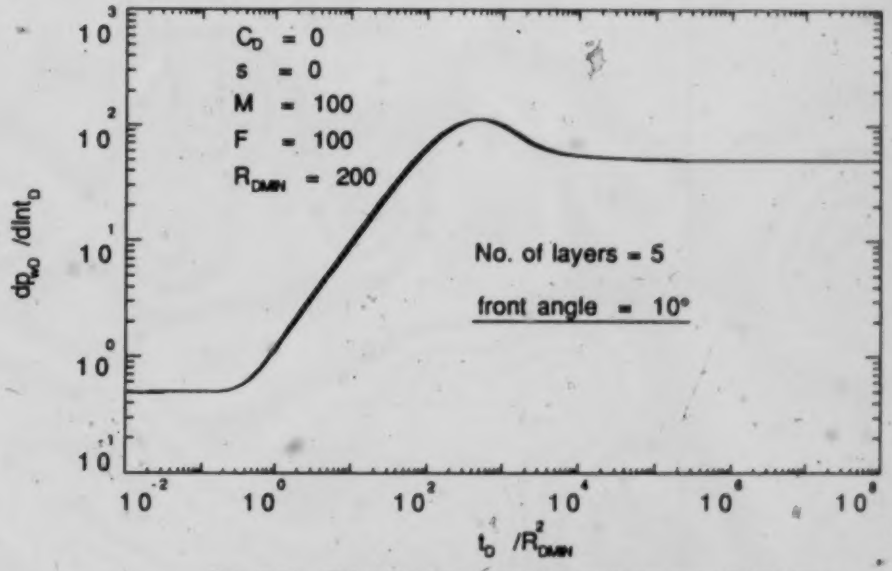

Fig. 5.56- Effect of front angle on pressure derivative.
(front angles = 10° and 170°)

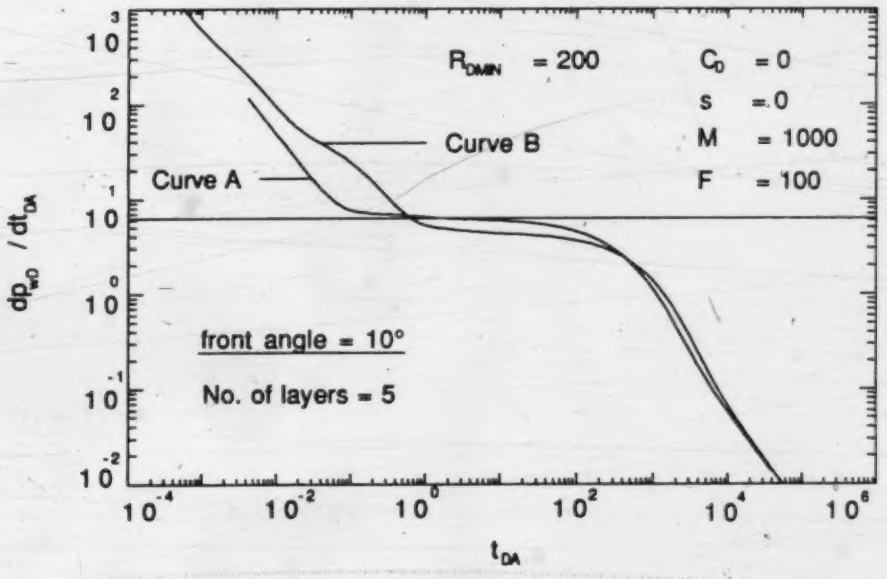

Fig. 5.57-Effect of storativity variation on Cartesian derivative

would thus be high at the topmost layer and low at the bottom layer. For this simulation, the bottom layer (layer 5) has a steam compressibility value of 1.0 E-06 psi^{-1}, while layers 4, 3, 2, and 1 have steam compressibility values of 10.0 E-06, 20.0 E-06, 200 E-06, and 400 E-06 psi^{-1}, respectively. Curve A represents the pressure response for the case of equal storativity values for all layers, in a given region. Pseudosteady state does not occur for the case of varying storativity values, but a short duration PSS appears for curve A. Further investigation is required to analyze the effect of varying storativity patterns among layers of a layered composite reservoir.

5.3 Buildup Response

For any pressure-buildup test, bottom-hole well pressure may be expressed by using the principle of superposition. The dimensionless pressure is:

$$p_{wDs}(\Delta t_D) = \frac{2\pi kh(p_{ws} - p_{wf})}{qB\mu} = p_{wD}(t_{pD}) + p_{wD}(\Delta t_D) - p_{wD}(t_{pD} + \Delta t_D) \quad (5.26)$$

To analyze buildup (or falloff) data, a Miller-Dyes-Hutchinson[13] graph or a Horner[14] graph may be used. The slopes of these graphs are defined as:[43]

$$\text{Horner Slope} = -\left(\frac{t_{pD}+\Delta t_D}{t_{pD}}\right)\Delta t_D \cdot \frac{dp_{wDs}(\Delta t_D)}{d(\Delta t_D)} \quad (5.27)$$

$$\text{MDH Slope} = \frac{dp_{wDs}}{d\ln(\Delta t_D)} = \frac{\Delta t_D\, dp_{wDs}(\Delta t_D)}{d(\Delta t_D)} \quad (5.28)$$

Buildup responses from infinitely large homogeneous or fractured reservoirs could be correlated with the corresponding drawdown response using the Agarwal[52] graph.

Ref. 43 shows that:

$$\text{Agarwal Slope} = \left(\frac{t_{pD}+\Delta t_D}{t_{pD}}\right)\Delta t_D \cdot \frac{dp_{wDs}(\Delta t_D)}{d(\Delta t_D)} = -\text{ Horner Slope.}$$

Therefore, either an Agarwal or Horner slope may be used to analyze producing (injection) time effects on buildup (falloff) responses from layered composite reservoirs.

The MDH and Agarwal (or negative Horner) slopes are graphed against a dimensionless shut-in time based on the minimum discontinuity radius defined as:

$$\Delta t_{De} = \frac{(k/\mu)_1 \, \Delta t}{(\phi c_t)_1 \, R^2_{min}} = \frac{\Delta t_D}{R^2_{Dmin}} \tag{5.29}$$

Figure 5.58 shows that the number of layers used to represent a tilted front has no effect on the Agarwal slope.

Figures 5.59 and 5.60 show the effect of minimum front radius on the MDH and the Agarwal slopes, respectively. Figures 5.59 and 5.60 are for $t_{pD} / R^2_{Dmin} = 1.0$, $C_D = 0$, $s = 0$, $M = 1000$, $F = 100$ and a 10° front angle. A semi-log straight line corresponding to the inner region mobility develops on both the MDH and Agarwal slopes. The minimum front radius affects the shape of the curve in the transition zone. Producing time prior to shut-in will significantly affect the shape of the Agarwal slope for the same minimum front radii. A second semi-log straight line corresponding to the outer region mobility develops on the Agarwal (or Horner) graph, but not on the MDH graph. This observation is consistent with the results presented in Ref. 43. In Figures 5.59 and 5.60, two troughs appear along the same curve in the transition zone for front radii of 100 and 200. As the magnitude of front radius increases, the earlier trough obtains even smaller values while the later trough straightens. Thus, for minimum front radii of 500 and 1000, only one trough appears. Prior to the appearance of the second semi-log straight line in the Agarwal slope of Fig. 5.60, the curve attains a maximum value which is greater than M/2. The buildup time required to reach this maximum value is dependent on both the values of minimum front radius and front angle, for a given

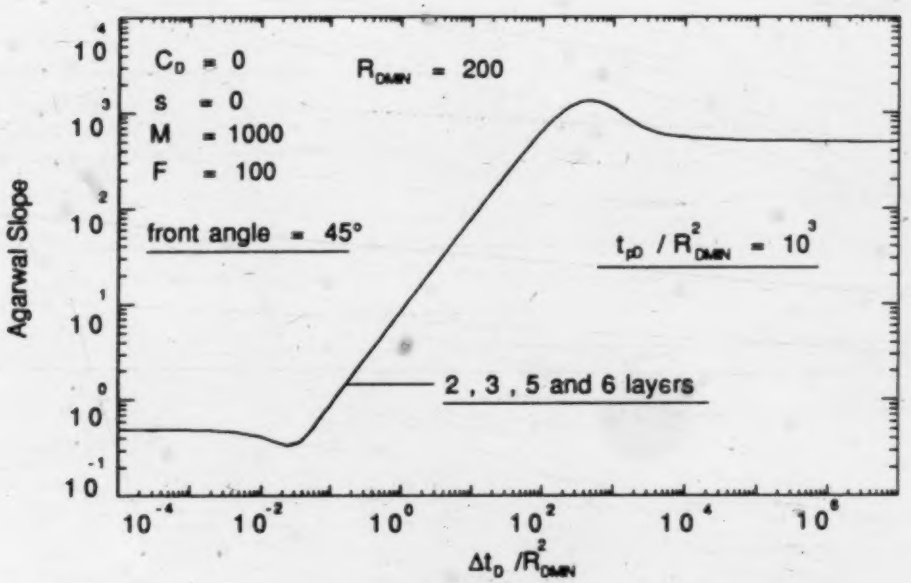

Fig. 5.58- Effect of number of layers on Agarwal slope.

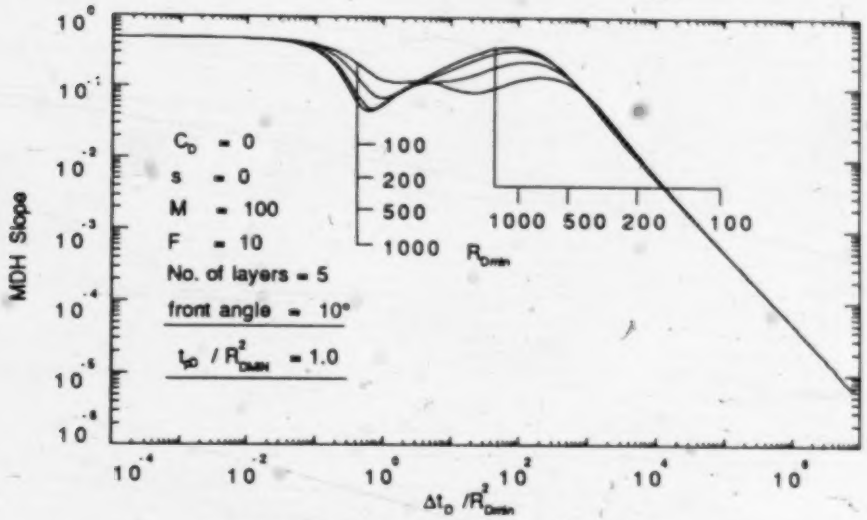

Fig. 5.59- Effect of minimum front radius on MDH slope.

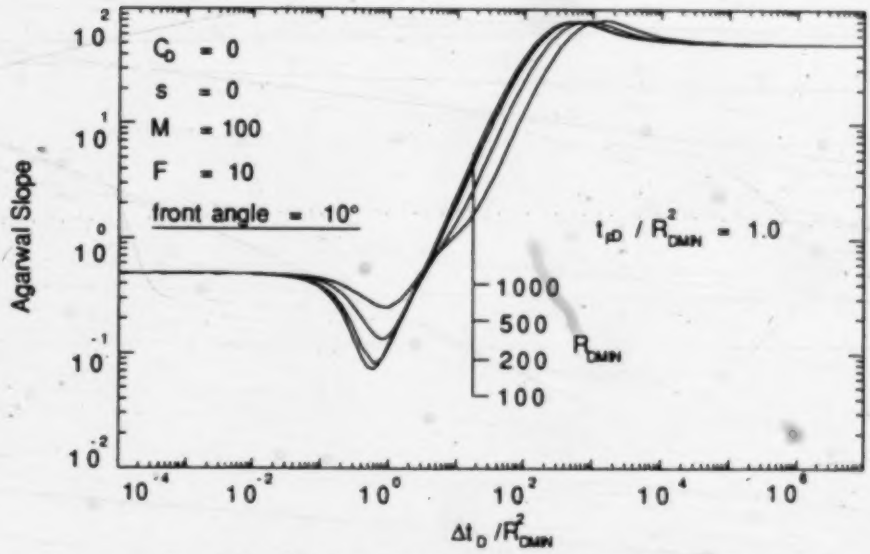

Fig. 5.60- Effect of minimum front radius on Agarwal slope (front angle = 10°)

producing time. However, the MDH slope does not show even a maximum slope of one-half after the end of the first semi-log line. (see Fig. 5.59)

As the front angle increases, the appearance of the curve changes, with the second trough eventually straightening. This is shown on Figures 5.61 through 5.63. Figure 5.62 shows that for a front angle of 60°, a second trough does not appear for any value of R_{Dmin} shown. The value of the minimum slope also decreases as the front angle increases, but it cannot be quantified due to possible instability in the Stehfest[17] algorithm during the intermediate time region corresponding to the development of troughs and a minimum slope. The algorithm is more unstable for higher values of mobility ratio. Figures 5.62 and 5.63 show that the value of minimum front radius does not affect the time to the maximum derivative when the front angle is equal or greater than 60° with the parameters shown on Figs. 5.62 and 5.63. t_{pD} / R^2_{Dmin} is a correlating parameter for buildup pressure response for a well in a layered composite reservoirs with a sharp front [43] as shown on Fig. 5.63.

Figures 5.64 through 5.66 show the effect of front angle on the Agarwal slope for a five-layer composite reservoir with $C_D = s = 0$, $M = 1000$, $F = 100$, and $R_{Dmin} = 200$. The magnitude of the front angle affects the appearance of the curve during the transition period only. For a given minimum front radius and producing (or injection) time, early transition can be characterized by the value of the front angle. The time to the maximum derivative is different only for the 10° front angle. Figure 5.66 shows that for front angles over the range $45° \le \theta \le 90°$, the analysis developed for composite reservoirs with a sharp front may be applied without great loss in accuracy. The foregoing conclusions will also apply when producing (or injection) times are increased, as shown on Fig. 5.67 for $t_{pD} / R^2_{Dmin} = 10^4$.

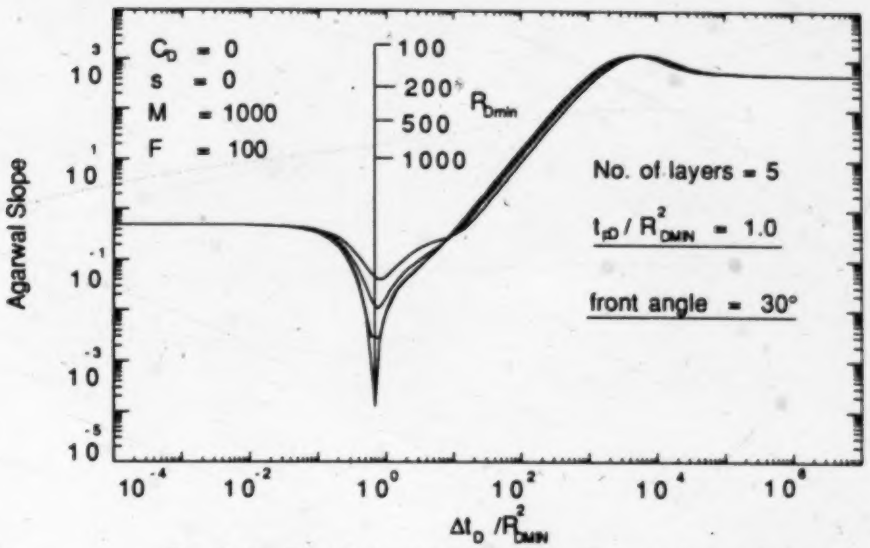

Fig. 5.61- Effect of minimum front radius on Agarwal slope (front radius = 30°)

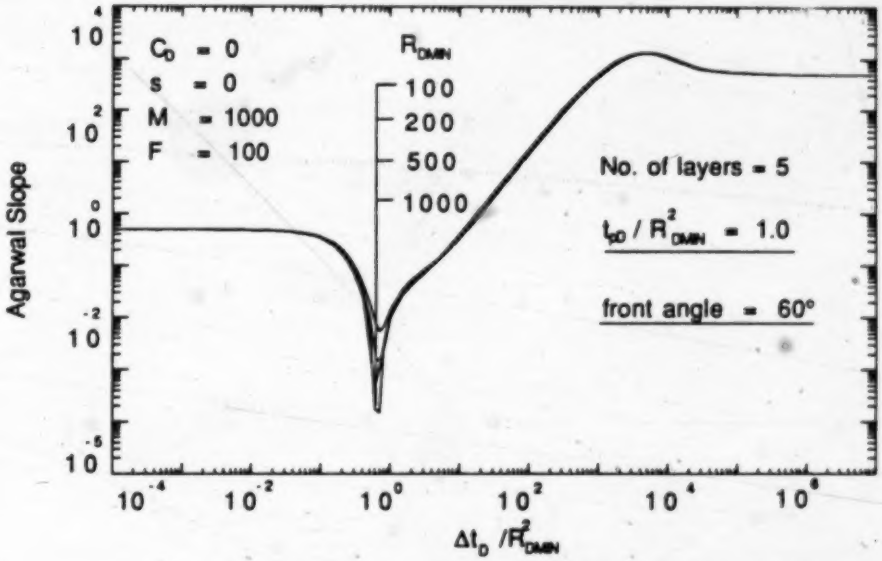

Fig. 5.62- Effect of minimum front radius on Agarwal slope (front radius = 60°)

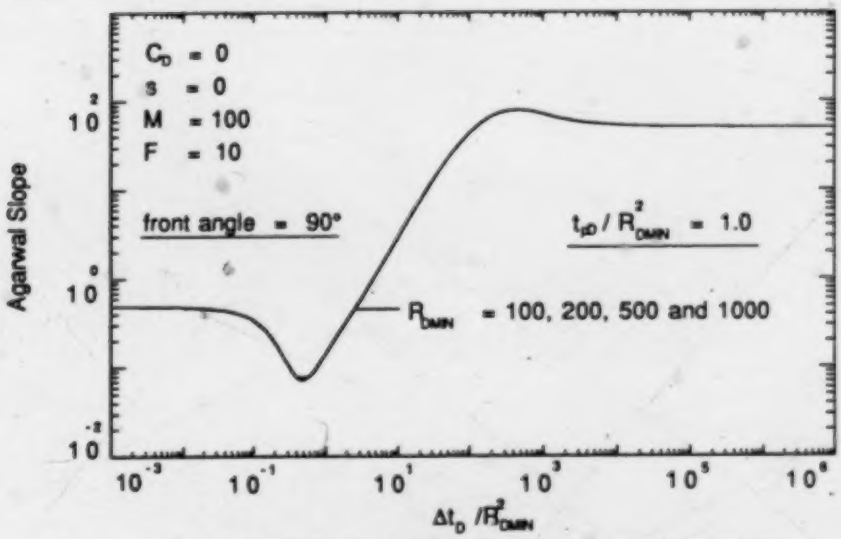

Fig. 5.63- Effect of minimum front radius on Agarwal slope (front radius = 90°)

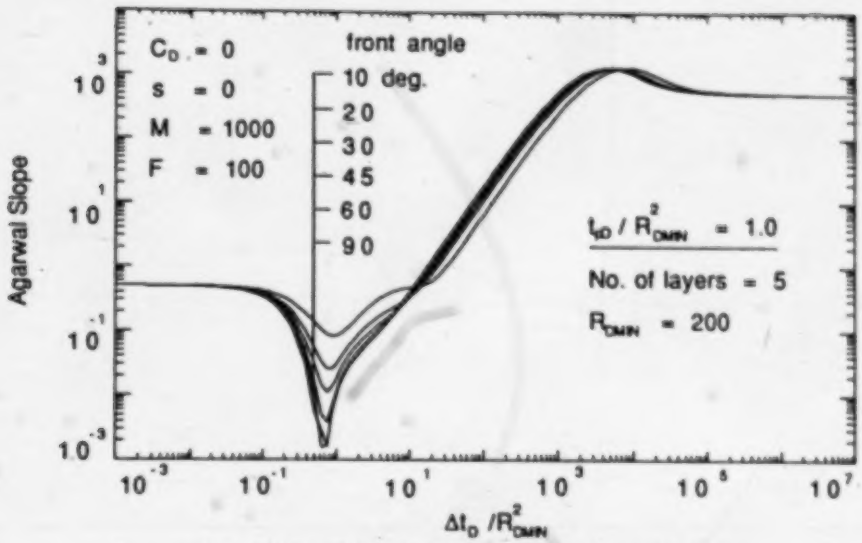

Fig. 5.64 - Effect of front angle on Agarwal slope
(10°, 20°, 30°, 45°, 60° and 90°)

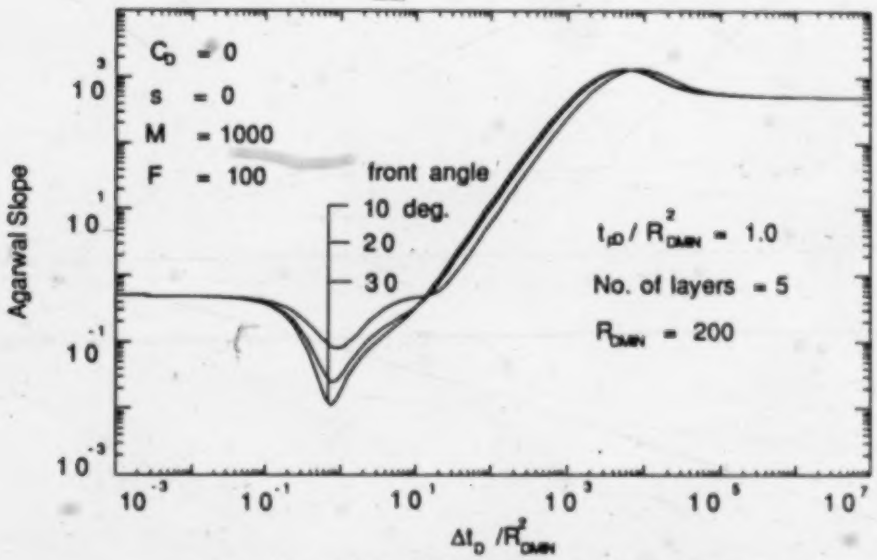

Fig. 5.65 - Effect of front angle on Agarwal slope
(10°, 20° and 30°)

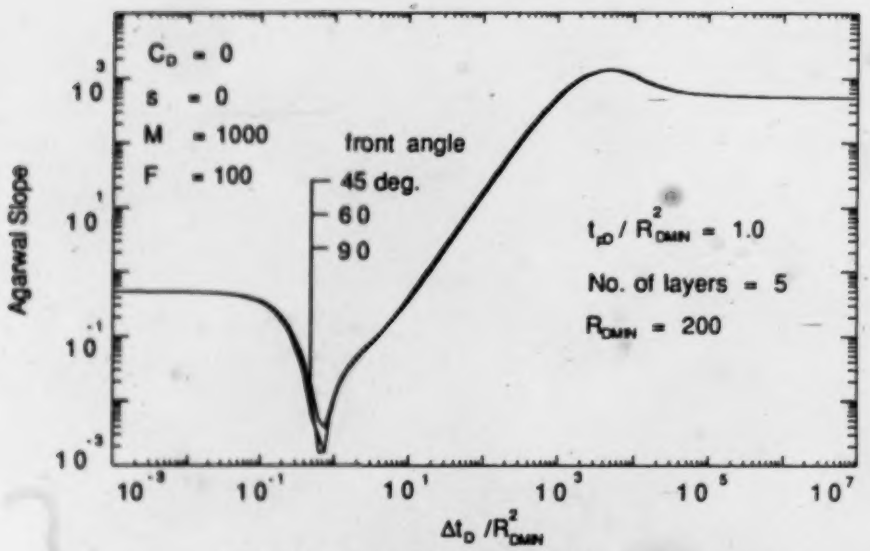

Fig. 5.66 - Effect of front angle on Agarwal slope (45°, 60° and 90°)

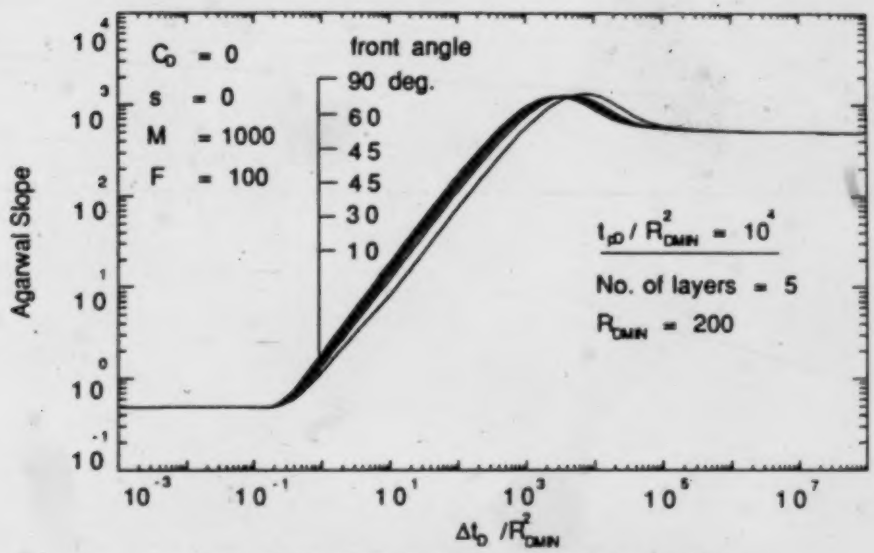

Fig. 5.67 - Effect of front angle on Agarwal slope
($t_{pD} / R^2_{Dmin} = 10^4$)

Figure 5.68 shows the effect of producing (or injection) time, t_{pD}/R^2_{Dmin}, on the Agarwal slope for a five-layer composite system with M = 1000, F = 100, $C_D = 0 = s$, front angle, $\theta = 45°$, and $R_{Dmin} = 200$. Figure 5.68 also shows the drawdown response for the same 5-layer system. Deviation time is dependent on producing time. For t_{pD}/R^2_{Dmin} values less than 10^4, the deviation is characterized by a decrease in magnitude from the 0.5 value of the semi-log straight line. For $1.0 \le t_{pD}/R^2_{Dmin} \le 10^4$, deviation from the semi-log line occurs earlier than $(t_{De})_{end} = 0.18$. The value of t_{pD}/R^2_{Dmin} affects significantly the magnitude of the minimum Agarwal slope, but affects mildly the time to a minimum or maximum slope, or the magnitude of the maximum slope. Thus, the deviation time method may produce an inaccurate estimate of the front volume (or radius) for short production (or injection) times for reservoirs with a tilted front. This observation is consistent with the results of Ref. 43 for a sharp front case. Ambastha and Ramey[43] describe other reservoir parameters or configurations that may produce well-test data that resemble a buildup (or falloff) test after a short producing (or injection) time.

Figures 5.69 through 5.71 show the effect of mobility ratio on the Agarwal slope for a five-layer system with $C_D = s = 0$, F = 100, $R_{Dmin} = 200$ and front angle, $\theta = 20°$. Figure 5.69 shows that for $t_{pD}/R^2_{Dmin} = 0.1$, mobility ratio does not affect the deviation time and that the slopes of the curves for mobility ratios of 10, 100 and 1000 decrease after deviation from the first semi-log line. The magnitude of the minimum slope is affected significantly by the mobility ratio. A higher mobility ratio results in a lower minimum value. Mobility ratio mildly affects the time to the minimum slope. Figure 5.70 shows that mobility ratio affects the deviation time from the first semi-log straight line for $t_{pD}/R^2_{Dmin} = 100$. Mobility ratios of 100 and 1000 show a decrease in the magnitude of the Agarwal slope after deviation from the semi-log slope value of 0.5.

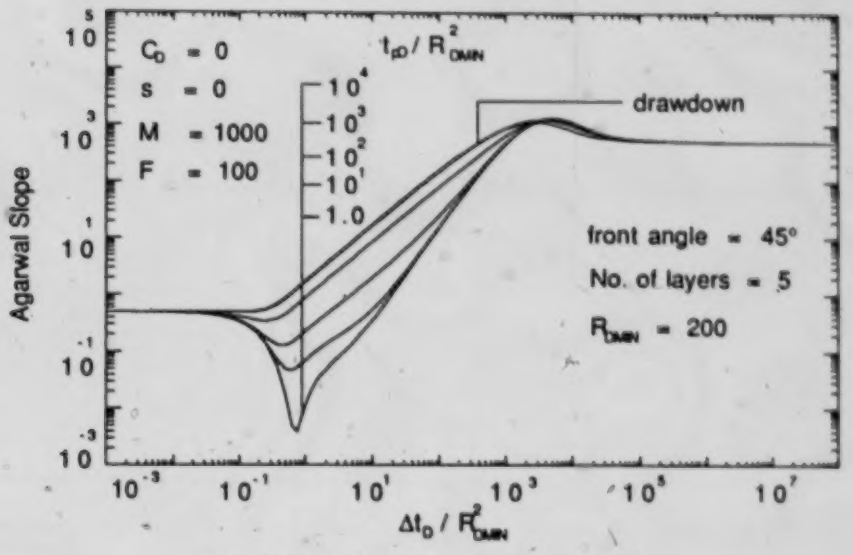

Fig. 5.68-Effect of t_{pD} on Agarwal slope

($t_{pD} / R^2_{Dmin} \geq 1.0$)

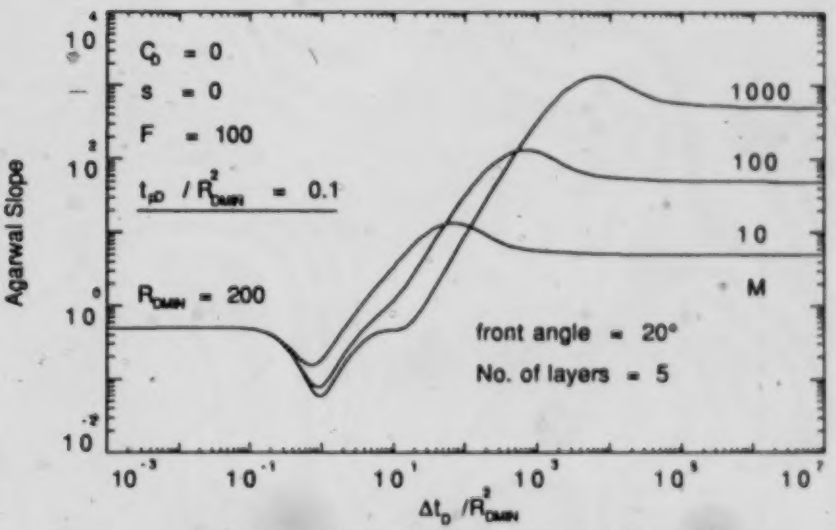

Fig. 5.69 - Effect of mobility ratio on Agarwal slope

($t_{pD} / R^2_{Dmin} = 0.1$)

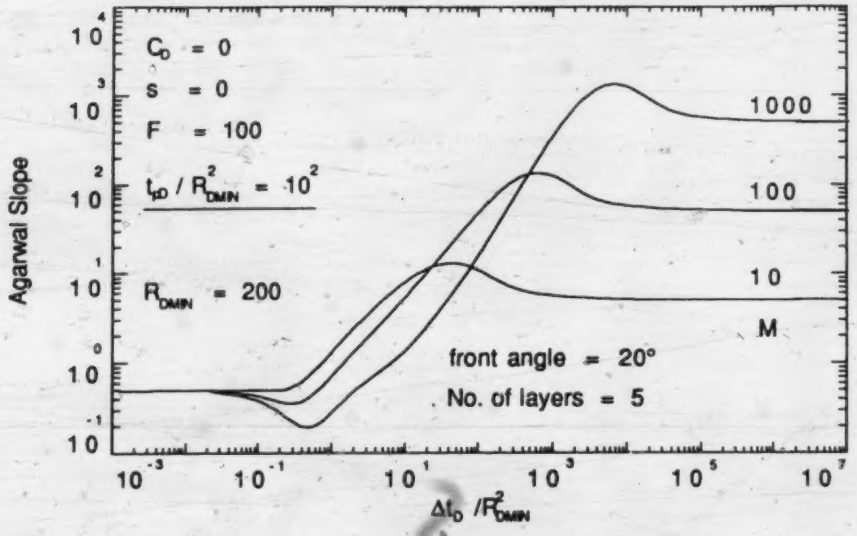

Fig. 5.70 - Effect of mobility ratio on Agarwal slope
(t_{pD} / R^2_{Dmin} = 100)

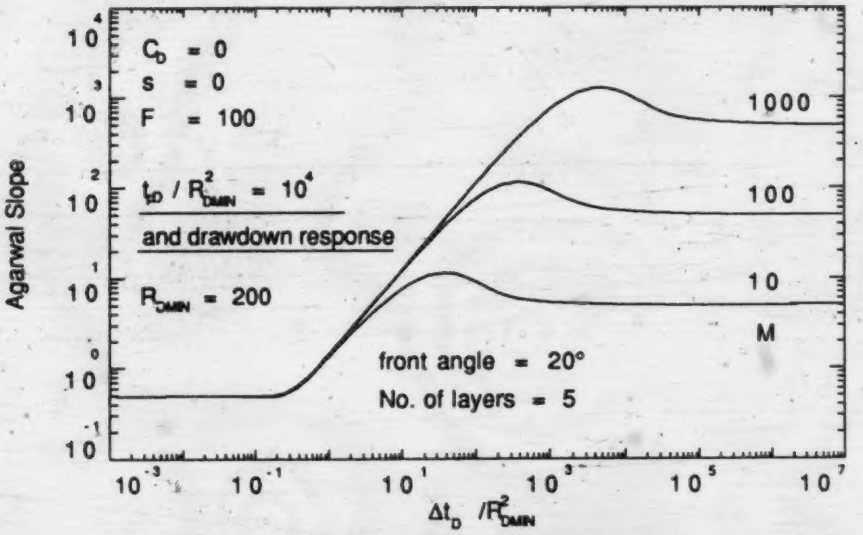

Fig. 5.71- Effect of mobility ratio on Agarwal slope
($t_{pD} / R^2_{Dmin} = 10^4$ and drawdown response)

Curves for mobility ratios of 100 and 1000 have deviation times less than that for the curve with a mobility ratio of 10. For $t_{pD} / R^2_{Dmin} \geq 10^4$, the curves are similar to those of a drawdown response for a system with equivalent properties. This is shown in Fig. 5.71. Both the times to the maximum slope and the magnitudes of the maximum slope are significantly affected by the mobility ratios.

Figures 5.72 through 5.74 show the effect of storativity ratio, F, on the Agarwal slope for a five-layer system with $C_D = s = 0$, $M = 1000$, $R_{Dmin} = 200$ and front angle $\theta = 20°$. Curves are shown for storativity ratios of 10, 100, and 1000. For $t_{pD} / R^2_{Dmin} =$ 0.1 and 100, the higher the storativity ratio the lower the magnitude of the minimum slope and the higher the magnitude of the maximum slope. For $t_{pD} / R^2_{Dmin} \geq 10^4$, a minimum slope of magnitude less than 0.5 does not appear. For all the three cases considered above, storativity has no effect on the dimensionless deviation time.

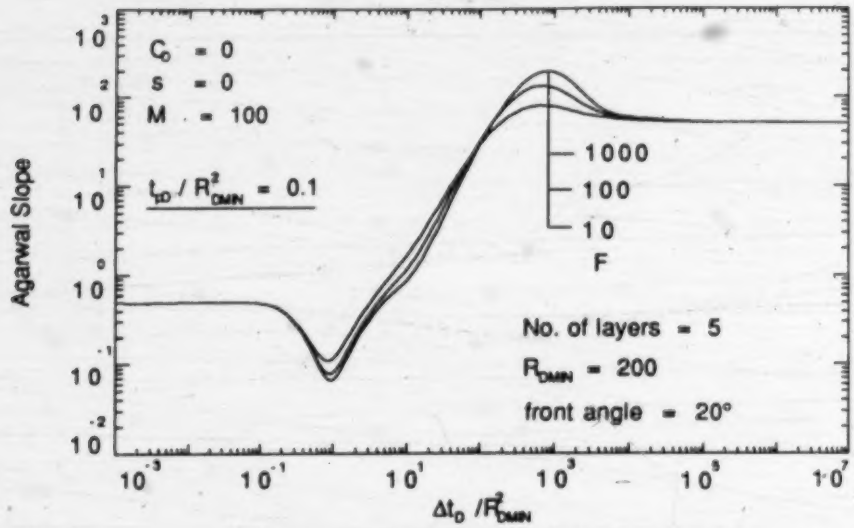

Fig. 5.72 - Effect of storativity ratio on Agarwal slope
(t_{pD} / R^2_{Dmin} = 0.1)

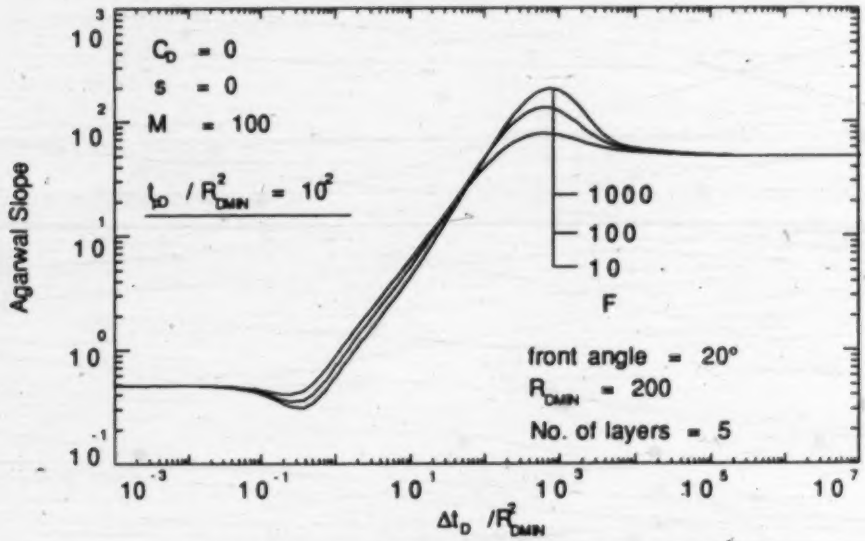

Fig. 5.73 - Effect of storativity ratio on Agarwal slope
(t_{pD} / R^2_{Dmin} = 100)

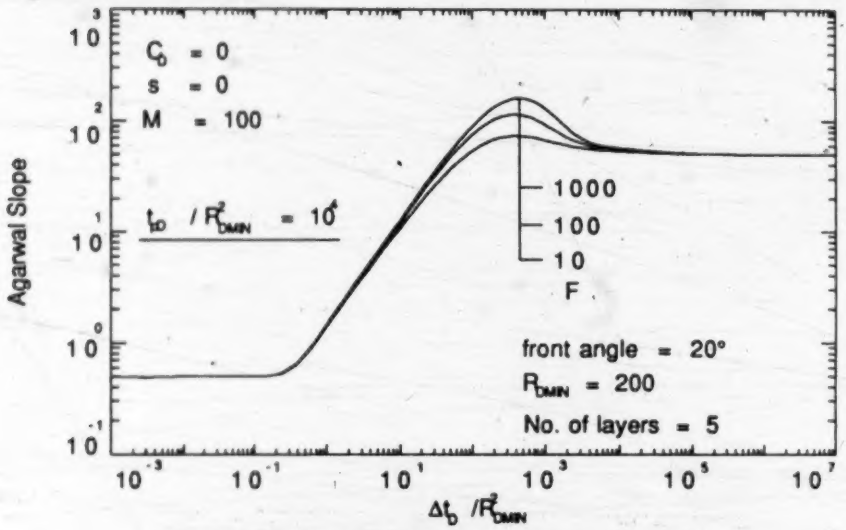

Fig. 5.74- Effect of storativity ratio on Agarwal slope
(t_{pD} / R^2_{Dmin} = 10^4)

6. CONCLUSIONS AND RECOMMENDATIONS

6.1 Conclusions

The following are the conclusions resulting from this study:

1. For a multilayered composite reservoir, both the number of layers used to represent a tilted front and the minimum front radius of such a front affect the pressure derivative response.

2. The magnitude of the front angle affects the shape of the pressure derivative curves, for a range of values of minimum front radii.

3. The use of an average radius (sharp front) to represent a tilted front is valid for all front angle values considered in this study, as long as the swept volume of the tilted front is equal to that of the sharp front model.

4. Reservoirs with large R_{Dmin} values will produce pressure responses similar to that of a reservoir with a sharp front, for any front angle value.

5. Different patterns of layer mobilities and/or storativities may produce different pressure transient responses depending on the magnitude of the tilted front angle.

6. Different values of wellbore skin factors on each layer of a multilayer composite reservoir result in different pressure transient responses.

7. For equal swept volumes, pressure transient responses are not sensitive to the shape of the front, but to the value of R_{Dmin}.

8. The existence of true pseudosteady state is dependent on the shape of the front.

9. The shape of the Agarwal buildup slope is dependent on R_{Dmin}, front angle and producing (or injection) time.

6.2 Recommendations

Future studies in the area of composite reservoirs with a tilted front should be performed using a simulator, for comparison with results of this study, and to investigate further the effects of a tilted front and other front shapes on transient pressure responses. Such studies should include the effects of interlayer crossflow and the presense of a finite skin factor along the discontinuity.

REFERENCES

1. Earlougher, R.C., Jr.: "Advances in Well Test Analysis," Monograph Volume 5, Society of Petroleum Engineers of AIME, Dallas (1977) Ch. 2.

2. Matthews, C.S. and Russell, D.G.: "Pressure Buildup and Flow Tests," Monograph Series, Society of Petroleum Engineers of AIME, Dallas (1967) 1, Ch. 2.

3. Lefkovits, H.C., Hazebroek, P., Allen, E.E., Matthews, C.W.: "A study of the Behaviour of Bounded Reservoirs Composed of Stratified Layers," *SPEJ*. (March 1961), 43-58.

4. Tempelaar-Lietz, W.: "The Effect of the Rate of Oil Protection Upon the Performance of Wells Producing from more than One Horizon," *Trans*. AIME (1961), 222, 26.

5. Javandel, I., and Witherspoon, P.A.: "Analysis of Transient Fluid Flow in Multi-Layered Systems," Water Resources Center, Contribution No. 124, Dept. of Civil Eng., Univ. of California, Berkeley, Mar. 1968

6. Russell, D.G. and Prats, M.: "The Practical Aspects of Interlayer Crossflow," *JPT* (June 1962) 589-92.

7. Woods, E.G.: "Pulse-Test Response of a Two-Zone Reservoir," *SPEJ* (Sept 1970) 245-50; *Trans*., AIME, 249.

8. Cobb, W.W., Ramey, H.J. Jr., and Miller, F.G.: "Well-Test Analysis for Wells Producing Commingled Zones," *JPT* (Jan. 1972) 27-34; *Trans*., AIME, 253.

9. Earlougher, R.C. Jr., Kersch, K.M., and Kunzman, W.T.: "Some Characteristics of Pressure Buildup Behaviour in Bounded Multiple-Layer Reservoirs Without Crossflow," *JPT* (Oct. 1974) 1178-86; *Trans*., AIME, 257.

10. Raghavan, R.: "Behaviour of Wells Completed in Multiple Producing Zones," *SPEFE* (June 1989) 219-30.

11. Raghavan, R., Topaloglu, H.N., Cobb, W.M., and Ramey, H.J. Jr.: "Well-Test Analysis for Wells Producing from Two Commingled Zones of Unequal Thickness," *JPT* (Sept. 1974) 1035-43; *Trans*., AIME, 253.

12. Muskat, M.: "Use of Data on the Buildup of Bottom-Hole Pressures," *Trans.*, AIME (1937) 123, 44-48.

13. Miller, C.C., Dyes, A.B., and Hutchinson, C.A. Jr.: "Estimation of Permeability and Reservoir Pressure from Bottom-Hole Pressure Buildup Characteristics," *Trans.*, AIME (1950) 189, 91-104.

14. Horner D.R.: "Pressure Buildup in Wells," *Proc.*, Third World Pet. Cong., E.J. Brill (ed.), Leiden (1951) II, 502-23.

15. Matthews, C.S., Brons, F., and Hazebroek, P.: "A Method for determination of Average Pressure in a Bounded Reservoir," *JPT* (Aug. 1954) 35-44; *Trans.*, AIME, 201.

16. Tariq, S.M. and Ramey, H.J. Jr.: "Drawdown Behaviour of a Well with Storage and Skin Effect Communicating with Layers of Different Radii and Other Characteristics," paper SPE 7453 presented at the 1978 SPE Annual Technical Conference and Exhibition, Houston, Oct. 1-3.

17. Stehfest, H.: "Algorithm 368, Numerical Inversion of Laplace Transforms," D-5, *Communications of ACM*, (Jan. 1970), 13, No. 1, 49.

18. Larsen, L.: "Determination of Skin Factors and Flow Capacities of Individual Layers in Two-Layered Reservoirs," paper SPE 11138 presented at the 1982 SPE Annual Technical Conference and Exhibition, New Orleans, Sept. 26-29.

19. Kucuk, F., Karakas, M., and Ayestaran, L.: "Well Testing and Analysis Techniques for Layered Reservoirs," *SPEFE* (Aug. 1986) 342-54.

20. Ehlig-Economides, C.A., and Joseph, J.: "A New Test for Determination of Individual Layer properties in a Multilayered Reservoir," *SPEFE* (Sept. 1987) 261-83.

21. Kazemi, H.: "Locating a Burning Front by Pressure Transient Measurement," *JPT* (Feb. 1966) 227-32.

22. Eggenschwiler, M., Ramey, H.J., Jr., Satman, A., and Cinco-Ley, H.: "Interpretation of Injection Well Pressure Transient Data in Thermal Oil Recovery," paper SPE 8908 presented at the California Reg. Mtg., Los Angeles, CA (April 9-11, 1980).

23. Da Prat, G., Bockh, A., and Prado, L.: "Use of Pressure Falloff Tests to Locate the Burning Front in the Miga Field, Eastern Venezuela," paper SPE 13667 presented at the California Reg. Mtg., Bakersfield, CA (March 27-29, 1985).

24. Satman, A., Eggenschwiler, M., Tang, R. W-K., and Ramey, H.J., Jr.: "An Analytical Study of Transient Flow in Systems with Radial Discontinuities," paper SPE 9399 presented at the 55th Annual Mtg., Dallas, TX (Sept. 21-24, 1980).

25. Tang, R. W-K.: "Transient Pressure Analysis in a Composite Reservoir," DOE Topical Report (Aug. 1982).

26. Brown, L.P.: "Pressure Transient Behaviour of the Composite Reservoir," paper SPE 14316 presented at the Annual Technical Conference and Exhibition, Las Vegas, NV (Sept. 22-25, 1985).

27. Satman, A.: "An Analytical Study of Interference in Composite Reservoirs," *SPEJ.* (April 1985) 281-290.

28. Olarewaju, J.S., and Lee, W.J.: "A Comprehensive Application of a Composite Model to Pressure Transient Analysis," paper SPE 16345 presented at the California Regional Mtg., Ventura, CA (April 8-10) 1987.

29. Olarewaju, J.S., and Lee, W.J.: "An Analytical Model for Composite Reservoirs Produced at Either Constant Bottomhole Pressure or Constant Rate," paper SPE 16763 presented at the 62nd Annual Technical Conference and Exhibition, Dallas TX (Sept. 27-30) 1987.

30. Satman, A.: "An Analytical Study of Transient Flow in Stratified Systems with Fluid Banks," paper SPE 10264 presented at the 56th Annual Technical Conference and Exhibition, San Antonio, Texas, October 5-7, 1981.

31. Anbarci, K., Grader, A.S., and Ertekin, T.: "Determination of Front Locations in a Multilayer Composite Reservoir," paper SPE 19799 presented at the 64th Annual Technical Conference and Exhibition, San Antonio, TX, October 8-11, 1989.

32. Hatzignatiou, D.G., Ogbe, D.O., and Dehaghani, K.: "Interference Pressure Behaviour in Multilayered Composite Reservoirs," paper SPE 16766 presented at the 62nd Annual Technical Conference and Exhibition, Dallas, TX, Sept. 27-30, 1987.

33. Satman, A., and Oskay, M.M.: "Effect of a Tilted Front on Well Test Analysis," paper SPE 14701 available from SPE (1985).

34. Kazemi, H., Merrill, L.S., and Jargon, J.R.: "Problems in Interpretation of Pressure Fall-Off Tests in Reservoirs With and Without Fluid Banks," *JPT*. (Sept. 1972) 1147-56.

35. Kazemi, H.: "Pressure Buildup in Reservoir Limit Testing of Stratified Systems," *JPT*. (April 1970) 503-11.

36. Mangold, D.C., Tsang, C.F., Lippmann, M.J., and Witherspoon, P.A.: "A Study of a Thermal Discontinuity in Well Test Analysis," *JPT*. (June 1981) 1095-1105.

37. Horne, R.N., Satman, A., and Grant, M.A.: "Pressure Transient Analysis of Geothermal Wells with Phase Boundaries," paper SPE 9274 presented at the 55th Annual Meeting of SPE of AIME, Dallas, TX (Sept. 21 - 24, 1980).

38. Stanislav, J.F., Easwaran, C.V., and Kokal, S.L.: "Interpretation of Thermal Well Testing," *SPEFE* (June 1989) 181-186.

39. Onyekonwu, M.O., Ramey, H.J., Jr., Brigham, W.E., and Jenkins, R.: "Interpretation of Simulated Falloff Tests," paper SPE 12746 presented at the California Reg. Mtg. of SPE of AIME, Long Beach, CA (April 11-13, 1984).

40. Fassihi, M.R.: "Evaluation of an Analytical Technique for Estimating Swept Volume from Thermal Pressure Falloff Tests in Heterogeneous Systems," *SPEFE(*June 1988) 449-458.

41. Messner, G.L. and Williams, R.L.: "Application of Pressure Transient Analysis in Steam Injection Wells," paper SPE 10781 presented at California Reg. Mtg. of SPE of AIME, San Francisco, CA (March 24-26, 1982).

42. Barua, J. and Horne, R.N.: "Computerized Analysis of Thermal Recovery Well Test Data," *SPEFE* (Dec. 1987) 560-566.

43. Ambastha, A.K. and Ramey, H.J., Jr.,: "Injection Time Effects on Falloff Responses from Composite Reservoirs," *SPEFE* (Dec. 1990) 385-88.

44. Agarwal, R.G., Al-Hussainy, R., and Ramey, H.J., Jr.: "An Investigation of Wellbore Storage and Skin Effect in Unsteady Liquid Flow: I. Analytical Treatment," *SPEJ*. (Sept. 1970) 279-90.

45. Ambastha, A.K.: "Transient Pressure Analysis for Composite Systems," Ph.D. Thesis, Stanford University, Stanford, CA (Oct. 1988).

46. Ambastha, A.K., and Ramey, H.J., Jr.: "Thermal Recovery Well Test Design and Interpretation," *SPEFE* (June 1989) 173-180.

47. Bixel, H.C., and Van Poollen, H.K.: "Pressure Drawdown and Buildup in the Presence of Radial Disconfinuities," *SPEJ.* (Sept. 1967) 301-09.

48. Ramey, H.J., Jr. and Cobb, W.M.: "A General Pressure Buildup Theory for a Well in a Closed Drainage Area," *JPT.* (Dec. 1971) 1493-1505.

49. Earlougher, R.C., Jr., and Kersch, K.M.: "Analysis of Short-Time Transient Test Data by Type-Curve Matching," *JPT.* (July 1974) 793-800; *Trans.*, AIME, 257.

50. Gringarten, A.C., Bourdet, D., Landel, P.A., and Kniazeff, V.: "A Comparison Between Different Skin and Wellbore Storage Type Curves for Early-Time Transient Analysis," paper SPE 8205 presented at the 54th Annual Mtg. of SPE of AIME, Las Vegas (Sept. 23-26, 1979).

51. Vogel, J.V.: "Simplified Calculations for Steamfloods," *JPT.* (July 1984) 1127-36.

52. Agarwal, R.G.: "A New Method to Account for Producing Time Effects When Drawdown Type Curves are Used to Analyze Pressure Buildup and Other Test Data," paper SPE 9289 presented at the 55th Annual Meeting of SPE of AIME in Dallas, TX (Sept. 21-24, 1980).

APPENDIX A

Program #1: Pressure transient response for a two-region multilayered composite reservoir.

Program #2: Converting the base of t_D from R_{Dmin} to R_{Davg}.

Program #3: Calculation of the front radii values for the model.

```
C   PROGRAM #1
C
C   The purpose of this program is to generate the
C   pressure transient response for a well
C   in a two-region composite multilayered reservoir.
C   Wellbore storage and skin at the well are allowed.
C   The well produces at a constant rate.
C   The outer boundary condition can be either infinite,
C   constant-pressure or closed.
C   Both buildup and drawdown responses can be generated.
C   ************************************************************
C   VARIABLE IDENTIFICATION LIST
C   ****************************
C   CD --- WELLBORE STORAGE AT THE ACTIVE WELL
C   SKIN(J) --- SKIN AT THE ACTIVE WELL
C   RMOB1(J) --- RELATIVE MOBILITY OF REGION 1
C   RMOB2(J) --- RELATIVE MOBILITY OF REGION 2
C   RSTOR1(J) --- RELATIVE STORATIVITY OF REGION 1
C   RSTOR2(J) --- RELATIVE STORATIVITY OF REGION 2
C   RD----FRONT RADIUS
C   ************************************************************
      IMPLICIT REAL*8(A-H,O-Z)
      DIMENSION TD(20)
      COMMON M,JCODE,CD,SKIN(20),RMOB1(20),RMOB2(20),
     +RSTOR1(20),RSTOR2(20),RD(20),RED(20),JLAYER,NLAYER
C   ************************************************************
C           OPENING OUTPUT FILES
C   ************************************************************
C
C
C
      OPEN(UNIT=7,FILE='PD',STATUS='NEW')
      OPEN(UNIT=8,FILE='PDP',STATUS='NEW')
      OPEN(UNIT=9,FILE='PDC',STATUS='NEW')
      OPEN(UNIT=10,FILE='PDH',STATUS='NEW')
C
C   ************************************************************
C   ===Unformatted input section ===
C   ************************************************************
C
      PRINT*,'ENTER THE VALUE OF CD:'
      READ(5,*)CD
      PRINT*,'ENTER THE # OF LAYERS:'
      READ(5,*)NLAYER
      PRINT*,'ENTER RELATIVE MOBILITY FOR'
      PRINT*,' EACH LAYER, REGION 1 THEN 2:'
      READ(5,*)(RMOB1(J),RMOB2(J),J=1,NLAYER)
      PRINT*,'ENTER RELATIVE STORATIVITY '
      PRINT*,' FOR EACH LAYER, REGION 1 THEN 2:'
      READ(5,*)(RSTOR1(J),RSTOR2(J),J=1,NLAYER)
      PRINT *,'ENTER THE VALUES OF SKIN(J) AND FRONTAL '
      PRINT *,'RADIUS RD(J) FOR EACH LAYER RESPECTIVELY:'
      READ(5,*)(SKIN(J),RD(J), J=1,NLAYER)
```

```
      PRINT*,'NUMBER OF CYCLES OF DATA REQUIRED:'
      READ(5,*)NC
      PRINT*,'LAYER FOR WHICH WELLBORE PRESSURE IS REQUIRED:'
      READ(5,*)JLAYER
      PRINT*,'GIVE FIRST VALUE OF TD (BASED ON RW):'
      READ(5,*)TD1
      PRINT*,'NUMBER OF TERMS TO BE USED IN STEHFEST:'
      READ(5,*)NTERM
C
C   READ CODES FOR BOUNDARY CONDITIONS
C
      PRINT*,'SUPPLY RESPONSE FUNCTION CODE:'
      PRINT*,'1---DRAWDOWN'
      PRINT*,'2---BUILDUP'
      READ(5,*)ICODE
C
      PRINT*,'SUPPLY OUTER BOUNDARY CONDITION CODE:'
      PRINT*,'1---INFINITE'
      PRINT*,'2---CLOSED'
      PRINT*,'3---CONSTANT-PRESSURE'
      READ(5,*)JCODE
C
      IF(ICODE.EQ.2)THEN
      PRINT*,'DIMENSIONLESS PRODUCING TIME (BASED ON RW):'
      READ(5,*)TPD
      ENDIF
C
      IF(JCODE.NE.1)THEN
      PRINT*,'DIMENSIONLESS OUTER RADIUS FOR EACH LAYER'
      READ(5,*)(RED(J),J=1,NLAYER)
      ELSE
C
C   FOR INFINITE RESERVOIR, A FICTITIOUS RED IS SUPPLIED
C
      DO 3 J=1,NLAYER
    3 RED(J)=1.D30
      ENDIF
C
C   INPUT SECTION ENDS.
C ***************************************************************
C
      M=777
      PI=2.0*ASIN(1.0)
C
C  ****************************************************************
C     GENERATE THE FIRST SET OF TD VECTOR
C  ****************************************************************
C
      TD(1)=TD1
      TD(2)=1.5*TD1
      TD(3)=2.*TD1
      TD(4)=2.5*TD1
      TD(5)=3.*TD1
```

```
      TD(6)=3.5*TD1
      TD(7)=4.*TD1
      TD(8)=4.5*TD1
      TD(9)=5.*TD1
      TD(10)=6.*TD1
      TD(11)=7.*TD1
      TD(12)=8.*TD1
      TD(13)=9.*TD1
C
C
C     GENERATE AND PRINT THE PRESSURE TRANSIENT RESPONSE
C
      IF(ICODE.EQ.2)THEN
      CALL INVERT(TPD,NTERM,PD1,PDP1)
      ENDIF
C
      DO 1 I=1,NC
      DO 2 J=1,13
      SPC=TD(J)
      IF(ICODE.EQ.2)THEN
      SPC1=SPC+TPD
      CALL INVERT(SPC1,NTERM,PD2,PDP2)
      ENDIF
      CALL INVERT(SPC,NTERM,PD,PDP)
      IF(ICODE.EQ.1)PDC=PDP
      IF(ICODE.EQ.2)THEN
      PD=PD1+PD-PD2
      PDC=PDP-PDP2
      PDH=SPC1/TPD*SPC*PDC
      ENDIF
      PDP=SPC*PDC
C
C*********************************************************************
C
C     FIND THE MINIMUM DISCONTINUITY RADIUS
C
      CALL SORT(RD,NLAYER,RDMIN)
C
C
C*********************************************************************
C
C     CONVERT THE BASE OF 'SPC' FROM RW TO MINIMUM
C     DISCONTINUITY RADIUS
C
      SPC=SPC/RDMIN/RDMIN
C
C     REPORT THE RESULTS:
C
C
      WRITE(7,9)SPC,PD
      WRITE(8,9)SPC,PDP
      WRITE(9,9)SPC/PI,PDC*PI*RDMIN*RDMIN
      IF(ICODE.EQ.2) WRITE(10,9)SPC,PDH
```

```
    2   TD(J)=10.*TD(J)
    1   CONTINUE
    9   FORMAT(2X,F20.6,2X,F20.6)
        STOP
        END
C
C   ********************************************************************
C     THE SUBROUTINES
C   ********************************************************************
C
C
      SUBROUTINE LAP(S,PWDL,PDPL)
      IMPLICIT REAL*8(A-H,O-Z)
      DIMENSION ARG1(20),ARG2(20),ARG3(20),ARG4(20),A1(20),
     +A2(20),A3(20),A4(20),B1(20),B2(20),B3(20),B4(20),D1(20),
     +D2(20),D3(20),D4(20),E1(20),E2(20),E3(20),E4(20),F1(20),
     +F2(20),F3(20),F4(20),AL11(20),AL12(20),AL21(20),AL22(20),
     +AL23(20),AL24(20),AL31(20),AL32(20),AL33(20),AL34(20),
     +AL43(20),AL44(20),DELTA(20),GAMMA(20)
C
      COMMON M,JCODE,CD,SKIN(20),RMOB1(20),RMOB2(20),
     +RSTOR1(20),RSTOR2(20),RD(20),RED(20),JLAYER,NLAYER
C
C   COMPUTE THE ARGUMENTS OF BESSEL FUNCTIONS
C
      SUM=0.000
      DO 300 J=1,NLAYER
      ARG1(J)=DSQRT(S*RSTOR1(J)/RMOB1(J))
      ARG2(J)=RD(J)*ARG1(J)
        HI=DSQRT(S*RSTOR2(J)/RMOB2(J))
      ARG3(J)=RD(J)*HI
      IF(JCODE.NE.1)ARG4(J)=RED(J)*HI
C
C   COMPUTE NEEDED BESSEL FUNCTIONS (EXPONENTIALLY SCALED)
C
      A1(J)=DBSI0E(ARG1(J))
      A2(J)=DBSI0E(ARG2(J))
      A3(J)=DBSI0E(ARG3(J))
      IF(JCODE.EQ.3)A4(J)=DBSI0E(ARG4(J))
C
      B1(J)=DBSI1E(ARG1(J))
      B2(J)=DBSI1E(ARG2(J))
      B3(J)=DBSI1E(ARG3(J))
      IF(JCODE.EQ.2)B4(J)=DBSI1E(ARG4(J))
C
      D1(J)=DBSK0E(ARG1(J))
      D2(J)=DBSK0E(ARG2(J))
      D3(J)=DBSK0E(ARG3(J))
      IF(JCODE.EQ.3)D4(J)=DBSK0E(ARG4(J))
C
      E1(J)=DBSK1E(ARG1(J))
      E2(J)=DBSK1E(ARG2(J))
```

```
      E3(J)=DBSK1E(ARG3(J))
      IF(JCODE.EQ.2)E4(J)=DBSK1E(ARG4(J))
C
C
      IF(ARG1(J).GT.174.0)ARG1(J)=150.0
      IF(ARG2(J).GT.174.0)ARG2(J)=150.0
      IF(ARG3(J).GT.174.0)ARG3(J)=150.0
      IF(ARG4(J).GT.174.0)ARG4(J)=150.0
C
C   CALCULATION OF MULTIPLYING FACTORS
C
      F1(J)=DEXP(ARG1(J))
      F2(J)=DEXP(ARG2(J))
      F3(J)=DEXP(ARG3(J))
      IF(JCODE.NE.1)F4(J)=DEXP(ARG4(J))
C
C   CALCULATION OF COEFFICIENTS
C
        HI=ARG1(J)*E1(J)
      AL11(J)=CD*S*(D1(J)+SKIN(J)*HI)/F1(J)
        HI2=ARG1(J)*B1(J)
      AL12(J)=CD*S*(A1(J)-SKIN(J)*HI2)*F1(J)
      AL21(J)=D2(J)/F2(J)
      AL22(J)=A2(J)*F2(J)
      AL23(J)=-D3(J)/F3(J)
      AL31(J)=-RMOB1(J)*ARG1(J)*E2(J)/F2(J)
      AL32(J)=RMOB1(J)*ARG1(J)*B2(J)*F2(J)
        HI3=DSQRT(RSTOR2(J)*S/RMOB2(J))
      AL33(J)=RMOB2(J)*HI3*E3(J)/F3(J)
C
C
C   FOR CLOSED AND CONSTANT PRESSURE OUTER
C   BOUNDARY CASES, AL24(J) AND AL34(J) ARE:
C
      IF(JCODE.NE.1)THEN
      AL24(J)=-A3(J)*F3(J)
      AL34(J)=-RMOB2(J)*HI3*B3(J)*F3(J)
      ENDIF
C
C
C    CALCULATING REMAINING COEFFICIENTS FOR THE CASE OF A
     CLOSED BOUNDARY
C
      IF(JCODE.EQ.2) THEN
      AL43(J)=-E4(J)/F4(J)
      AL44(J)=B4(J)*F4(J)
      ENDIF
C
C
C   CALCULATING THE REMAINING COEFFICIENTS FOR CONSTANT
C   PRESSURE O.B. CASE.
C
      IF(JCODE.EQ.3) THEN
```

```
      AL43(J)=D4(J)/F4(J)
      AL44(J)=A4(J)*F4(J)
      ENDIF
C
C
      IF(JCODE.EQ.1) THEN
      DELTA(J)=(AL31(J)*AL23(J)-AL33(J)*AL21(J))/
     +(AL32(J)*AL23(J)-AL33(J)*AL22(J))
      ELSE
      HII1=AL23(J)*AL44(J)-AL24(J)*AL43(J)
      HII2=AL33(J)*AL44(J)-AL34(J)*AL43(J)
      DELTA(J)=(AL31(J)*HII1-AL21(J)*HII2)/
     +(AL32(J)*HII1-AL22(J)*HII2)
      ENDIF
C
C
      GAMMA(J)=-DELTA(J)*(A1(J)-SKIN(J)*ARG1(J)*B1(J))*F1(J)+
     +(D1(J)+SKIN(J)*ARG1(J)*E1(J))/F1(J)
C
C
      SUM=SUM+(RMOB1(J)*ARG1(J)/GAMMA(J))*(E1(J)/F1(J)+
     +DELTA(J)*B1(J)*F1(J))
C
  300 CONTINUE
C
C
C  CALCULATION OF TRANSFORMED SOLUTION PWDL.
C  PWDL REPRESENTS THE LAPLACE TRANSFORM OF PWD.
C  USE THE PROPERTIES OF ANY LAYER(J).
C
C
      PWDL=1.0/((S*(AL11(JLAYER)-AL12(JLAYER)*DELTA(JLAYER))/
     +GAMMA(JLAYER))+S*SUM)
C
C
      PDPL=PWDL*S
      RETURN
      END
C
C
C
C  ********************************************************************
C       SUBROUTINE SORT
C  ********************************************************************
C
      SUBROUTINE SORT(ARRAY,N,XMIN)
      IMPLICIT REAL*8(A-H,O-Z)
      DIMENSION ARRAY(100),XINCR(100)
C
C     ARRANGE THE ARRAY IN INCREASING ORDER
C
      DO 55 I=1,N
      IF(I.EQ.N)GO TO 111
```

```
      K=I+1
      DO 44 J=K,N
      IF(ARRAY(I).LE.ARRAY(J))GO TO 44
      R=ARRAY(I)
      ARRAY(I)=ARRAY(J)
      ARRAY(J)=R
   44 CONTINUE
  111 XINCR(I)=ARRAY(I)
   55 CONTINUE
C
C     OBTAIN THE MINIMUM VALUE OF THE ARRAY
C
      XMIN=XINCR(1)
      RETURN
      END
C
C     ******************************************************
C          THE STEHFEST ALGORITHM
C     ******************************************************
C
C       THIS FUNTION COMPUTES NUMERICALLY THE INVERSE LAPLACE
C       TRANSFORM
C       OF F(S).
C
      SUBROUTINE INVERT(TD,N,PD,PDP)
      IMPLICIT  REAL*8 (A-H,O-Z)
      COMMONM,JCODE,CD,SKIN(20),RMOB1(20),RMOB2(20),
     +RSTOR1(20),RSTOR2(20),RD(20),RED(20),JLAYER,NLAYER
      DIMENSION G(50),V(50),H(25)
C
C     NOW IF THE ARRAY V(I) WAS COMPUTED BEFORE THE PROGRAM
C     GOES DIRECTLY TO THE END OF THE SUBRUTINE TO CALCULATE
C     F(S).
C
      IF (N.EQ.M) GO TO 17
      M=N
      DLOGTW=0.6931471805599
      NH=N/2
C
C     THE FACTORIALS OF 1 TO N ARE CALCULATED INTO ARRAY G.
C
      G(1)=1
      DO 1 I=2,N
      G(I)=G(I-1)*I
    1 CONTINUE
C
C     TERMS WITH K ONLY ARE CALCULATED INTO ARRAY H.
C
      H(1)=2./G(NH-1)
      DO 6 I=2,NH
      FI=I
      IF(I-NH) 4,5,6
    4 H(I)=FI**NH*G(2*I)/(G(NH-I)*G(I)*G(I-1))
```

```
      GO TO 6
    5 H(I)=FI**NH*G(2*I)/(G(I)*G(I-1))
    6 CONTINUE
C
C   THE TERMS (-1)**NH+1 ARE CALCULATED.
C    FIRST THE TERM FOR I=1
C
      SN=2*(NH-NH/2*2)-1
C
C   THE REST OF THE SN'S ARE CALCULATED IN THE MAIN ROUTINE.
C
C
C   THE ARRAY V(I) IS CALCULATED.
      DO 7 I=1,N
C
C    FIRST SET V(I)=0
      V(I)=0.
C
C    THE LIMITS FOR K ARE ESTABLISHED.
C    THE LOWER LIMIT IS K1=INTEG((I+1/2))
      K1=(I+1)/2
C
C    THE UPPER LIMIT IS K2=MIN(I,N/2)
      K2=I
      IF (K2-NH) 8,8,9
    9 K2=NH
C
C   THE SUMMATION TERM IN V(I) IS CALCULATED.
    8 DO 10 K=K1,K2
      IF (2*K-I) 12,13,12
   12 IF (I-K) 11,14,11
   11 V(I)=V(I)+H(K)/(G(I-K)*G(2*K-I))
      GO TO 10
   13 V(I)=V(I)+H(K)/G(I-K)
      GO TO 10
   14 V(I)=V(I)+H(K)/G(2*K-I)
   10 CONTINUE
C
C    THE V(I) ARRAY IS FINALLY CALCULATED BY WEIGHTING
C    ACCORDING TO SN.
      V(I)=SN*V(I)
C
C    THE TERM SN CHANGES ITS SIGN EACH ITERATION.
      SN=-SN
    7 CONTINUE
C
C    THE NUMERICAL APPROXIMATION IS CALCULATED.
   17 PD=0.
      PDP=0.
      A=DLOGTW/TD
      DO 15 I=1,N
      ARG=A*I
      CALL LAP(ARG,PWDL,PDPL)
```

```
      PD=PD+V(I)*PWDL
      PDP=PDP+V(I)*PDPL
15    CONTINUE
      PD=PD*A
      PDP=PDP*A
18    RETURN
      END
```

```
C   PROGRAM #2
C
C   THIS PROGRAM CONVERTS (tD) BASED ON (RDMIN) TO
C   AN (RDAVG) BASIS.
C
C   PROGRAM CORRECT
C
        REAL NSET
        DOUBLE PRECISION PDC(200,2),RDMIN,RAVG,CONST1,CONST2,
       +BB(200,2)
        OPEN(UNIT=9,FILE='PDC',STATUS='OLD')
        OPEN(UNIT=7,FILE='BB',STATUS='OLD')
        PRINT *,'PROVIDE NUMBER OF SETS IN INPUT DATA'
        READ(5,*)NSET
        READ(9,100) ((PDC(I,J),J=1,2),I=1,NSET)
  100   FORMAT(2X,F20.6,2X,F20.6)
        PRINT *,'PROVIDE THE VALUE OF MIN. FRONTAL RADIUS'
        READ(5,*)RDMIN
        PRINT *,'PROVIDE THE VALUE OF AVERAGE RADIUS'
        READ(5,*)RAVG
C
C
        CONST1 = 0.0
        CONST2 = 0.0
C
        CONST1 = (RDMIN*RDMIN)/(RAVG*RAVG)
C
        CONST2 = 1/CONST1
C
        DO 200 I = 1,NSET
        BB(I,1) = PDC(I,1)*CONST1
        BB(I,2) = PDC(I,2)*CONST2
C
  200   CONTINUE
        WRITE(7,300) ((BB(I,J),J=1,2),I=1,NSET)
  300   FORMAT(2X,F20.6,2X,F20.6)
C
C
        STOP
        END
```

```
C       PROGRAM #3
C
C       THIS PROGRAM CALCULATES THE FRONT RADII FOR A
C       MULTILAYERED COMPOSITE RESERVOIR, GIVEN THE FRONT
C       ANGLE AND THE MINIMUM FRONT RADIUS.
C
C       ANGLE   = FRONT ANGLE
C       HEIGHT  = HEIGHT OF EACH LAYER
C       FRONT(M) = FRONT RADIUS OF LAYER M
C       N  = TOTAL NUMBER OF LAYERS
C       M  = LAYER NUMBER
C
C
        IMPLICIT REAL(A-H,O-Z)
        DIMENSION BOTTOMR(20),FRONT(20),TOPR(20)
C
C       UNFORMATTED INPUT SECTION
C
        M=1
        PRINT*,'ENTER THE NUMBER OF LAYERS,THE FRONT
        ANGLE(DEG)'
        PRINT*,'AND THE VALUE OF MINIMUM FRONT RADIUS:'
        READ(5,*)N,ANGLE,FRONT(M)
C
C       CALCULATE THE HEIGHT OF EACH LAYER
C
        HEIGHT=30.0/N
        PI=2.0*ASIN(1.0)
C
C       CONVERT DEGREES TO RADIANS
C
        THETA=PI*ANGLE/180.0
        STEP=HEIGHT/TAN(THETA)
        DELTVOL=FRONT(M)**2-STEP**2/3.0
        BOTTOMR(M)=(SQRT(DELTVOL*4.0+STEP**2)-STEP)/2.0
        TOPR(M)=BOTTOMR(M)+STEP
        WRITE(6,10) M,BOTTOMR(M),FRONT(M),TOPR(M)
   10   FORMAT(2X,I3,2X,F9.3,2X,F9.3,2X,F9.3)
C
C       CALCULATE OTHER FRONT RADII
C
C
        DO 20 M=2,N,1
           K=M-1
C       BOTTOMR(M)=TOPR(K)
C       TOPR(M)=BOTTOMR(M)+STEP
        IF(ANGLE.EQ.90.0)THEN
          BOTTOMR(M)=FRONT(K)
          FRONT(M)=FRONT(K)
          TOPR(M)=FRONT(K)
        ELSE
```

```
      BOTTOMR(M)=TOPR(K)
      TOPR(M)=BOTTOMR(M)+STEP
 FRONT(M)=SQRT((TOPR(M)**3-
+BOTTOMR(M)**3)*TAN(THETA) +/(HEIGHT*3.0))
 ENDIF
 WRITE(6,10)M,BOTTOMR(M),FRONT(M),TOPR(M)
20  CONTINUE
 STOP
 END
```

APPENDIX B

Table B1

Sample Input Values for the Computer Program ($\theta = 60°$, F = 100)

Front Angle = 60° M = 1000, F = 100 # Layers = 5	$R_{Dmin} = 200$ $R_{D2} = 203$ $R_{D3} = 207$	$R_{D4} = 210$ $R_{Dmax} = 214$
$\lambda_{j1} = 0.2$	$\lambda_{j2} = 0.0002$	j = 1, 2, . . . 5
$\omega_{j1} = 0.2$	$\omega_{j2} = 0.002$	j = 1, 2, . . . 5
$s_j = 0.0$ $C_D = 0.0$	$t_{D1} = 100$	# cycles = 9

Table B2

Sample Input Values for the Computer Program ($\theta = 30°$, F = 1000)

Front Angle = 30° M = 1000, F = 1000 # Layers = 5	$R_{Dmin} = 200$ $R_{D2} = 210$ $R_{D3} = 221$	$R_{D4} = 231$ $R_{Dmax} = 242$
$\lambda_{j1} = 0.2$	$\lambda_{j2} = 0.0002$	j = 1, 2, . . . 5
$\omega_{j1} = 0.2$	$\omega_{j1} = 0.0002$	j = 1, 2, . . . 5
$s_j = 0.0$ $C_D = 0.0$	$t_{D1} = 100$	# cycles = 9

Table B3: Front Radii for a 2-Layer System (h_{tD} = 30)

Front Angle (Degrees)	Dimensionless R_D			
	R_{start}	R_{Dmin}	R_{Dmax}	R_{end}
10	156	200	285	326
20	179	200	241	261
30	187	200	226	239
45	192	200	215	222
60	196	200	209	213
90	200	200	200	200

Table B4: Front Radii for a 3-Layer System (h_{tD} = 30)

Front Angle (Degrees)	Dimensionless R_D				
	R_{start}	R_{Dmin}	R_{D2}	R_{Dmax}	R_{end}
10	171	200	257	313	341
20	186	200	227	255	269
30	191	200	217	235	243
45	195	200	210	220	225
60	197	200	206	212	214
90	200	200	200	200	200

Table B5: Front Radii for a 6-Layer System (h_{tD} = 30)

Front Angle (Degrees)	Dimensionless R_D							
	R_{start}	R_{Dmin}	R_{D2}	R_{D3}	R_{D4}	R_{D5}	R_{Dmax}	R_{end}
10	186	200	228	257	285	313	342	356
20	193	200	214	227	241	255	269	276
30	196	200	209	217	226	235	243	248
45	197	200	205	210	215	220	225	227
60	199	200	203	206	209	212	214	216
90	200	200	200	200	200	200	200	200

Table B6 : Front Radii for a Ten-Layer System (h_{tD} = 30)

FRONT ANGLE (Degrees)	DIMENSIONLESS R_D											
	R_{start}	R_{Dmin}	R_{D_2}	R_{D_3}	R_{D_4}	R_{D_5}	R_{D_6}	R_{D_7}	R_{D_8}	R_{D_9}	R_{Dmax}	R_{end}
10	191	200	217	234	251	268	285	302	319	336	353	362
20	196	200	208	216	225	233	241	249	258	266	274	278
30	197	200	205	210	216	221	226	231	236	242	247	249
45	198	200	203	206	209	213	215	218	221	224	227	228
60	199	200	202	203	205	207	209	210	212	214	216	216
90	200	200	200	200	200	200	200	200	200	200	200	200